Rocketdyne
North American Rockwell

6633 Canoga Avenue,
Canoga Park, California 91304

R-8144

TRIDYNE ATTITUDE CONTROL THRUSTER INVESTIGATION, FINAL REPORT

Contract NAS7-719

PREPARED BY

H. E. Barber
C. H. Buell

APPROVED BY

J. Friedman
Manager
Advanced Technology Programs

NO. OF PAGES 120 & xii

REVISIONS

DATE 3 April 1970

DATE	REV. BY	PAGES AFFECTED	REMARKS

FORM R18-G REV. 5-69

FOREWORD

This document, the final report of the Tridyne Attitude Control Thruster Investigation Program, is submitted to the Jet Propulsion Laboratory, Pasadena, California, in compliance with Article II, Paragraph D, of NASA Contract NAS7-719.

Mr. P. Moynihan of the Jet Propulsion Laboratory was the Program Technical Manager, and Mr. J. Friedman, Rocketdyne Advanced Technology, was Program Manager for the subject contract.

ABSTRACT

The results of an experimental program to evaluate and demonstrate the feasibility of a Tridyne attitude control thruster are reported herein. Substantiating data are presented for catalyst selection and optimization. Criteria for the design of a Tridyne attitude control module with preconditioning heaters are described. The design, fabrication, and testing of a flightweight thruster is detailed.

ACKNOWLEDGEMENTS

Important contributions to the conduct of the program and the preparation of this technical report were made by the following personnel:

G. L. Falkenstein
J. P. Federer
G. C. French
R. N. Gurnitz
B. T. McDunn

CONTENTS

Foreword iii

Abstract iii

Acknowledgements v

Summary 1

Introduction 3

Thruster Design 5

Design Requirements 5

Phase I: Test Hardware 6

Phase II: Module Concept 6

Phase IV: Test Hardware 10

Thrust Chamber Assembly and Installation 13

Experimental Evaluations 23

Experimental Equipment and Procedures 23

Task I: Experimental Results 31

Task IV: Flightweight Thruster Tests 47

Analysis 71

Performance Analysis 71

Thermal Analysis 80

Test Conditions 85

Tridyne Module Performance 90

Projected Performance 97

Conclusions and Recommendations 99

References 101

Appendix A

Test Summaries for Tasks I and IV A-1

ILLUSTRATIONS

1. Tridyne Microthruster 1
2. Catalyst Evaluation Chamber Assembly 7
3. Lightweight Development Thruster 7
4. Flight-Type, Three-Engine Module Assembly 9
5. Thrust Chamber Assembly 11
6. Flightweight Test Configuration 12
7. Flow Calibrated Venturi Assembly 13
8. 347 Stainless-Steel Tube Sample Prior to Welding 15
9. 347 Stainless-Steel Tube Sample Following Laser-Beam Welding . 15
10. Assembled Flightweight Thrusters 16
11. Laser Beam-Welded Enclosures 17
12. Thermocouple Installation in Tridyne Thruster 19
13. Washer-Shaped Braze Materials 20
14. Thrust Chamber Assembly Fixture 21
15. Vacuum System 24
16. Kulite Model XTL-190-50 Pressure Transducer 25
17. Walter Kidde Valve and Test Fittings 26
18. Tridyne Thruster, 25-Millisecond Pulse 27
19. 0.150-Inch Stainless-Steel Thrust Chamber 29
20. Thermal Response of 0.1-Inch-ID Lavalite Chamber (30-Mesh MFSA Catalyst) 33
21. Thermal Response of 0.150- and 0.224-Inch-ID Stainless-Steel Chambers (MFSA Catalyst) 34
22. Thermal Response of 0.1-Inch-ID Lavalite Chamber (30-Mesh Shell-405 Catalyst) 35
23. Thermal Response of 0.150- and 0.224-Inch-ID Stainless-Steel Chambers (Shell-405 Catalyst) 36
24. Chamber Pressure and Temperature Versus Time (Tests 71 and 75) . 39
25. Chamber Pressure and Temperature Versus Time (Tests 73 and 76) . 40
26. Chamber Pressure and Temperature Versus Time (Tests 77 and 78) . 41
27. Chamber Pressure and Temperature Versus Time (Tests 79 and 80) . 42
28. Chamber Surface Temperature Versus Heater Power 43

29. Typical Temperature Response Characteristics for a Catalytic Reactor 46
30. Thermal Time Constant Parameter Versus Catalyst Mass 46
31. Flightweight Thruster Test Schematic 48
32. Temperature and Pressure Response (ΔT = 35 F/40 ms) 52
33. Temperature and Pressure Response (ΔT = 37 F/30 ms) 52
34. Temperature and Pressure Response (ΔT = 56 F/20 ms)
35. Thruster Temperature Decay Characteristics 55
36. Temperature Time Transient for Run 59 57
37. Thermal Time Constant Versus Chamber Pressure Parameter Flightweight Thrusters 59
38. Temperature and Pressure Response 61
39. Thermocouple Temperature Versus Time 62
40. Venturi Pressure Response (Minimum Venturi Mount Volume) . . . 65
41. Venturi Pressure Response (Excess Volume in Venturi) 65
42. Chamber Pressure Response (Excess Volume in Venturi) 66
43. Tridyne Chamber With Pressure Probe 66
44. Tridyne Thruster 25-Millisecond Pulse 67
45. Pressure Response (Minimum Volume Venturi) 68
46. Pressure Response at Venturi for 30-psia Chamber Pressure . . 68
47. Theoretical Specific Impulse vs Temperature 72
48. Thrust Coefficient Efficiency vs Chamber Temperature 73
49. Delivered Specific Impulse vs Temperature 74
50. Viscosity of Tridyne Combustion Products vs Temperature . . . 75
51. Predicted Values of Discharge Coefficient for Sonic Nozzles . . 77
52. Chamber Mass Flowrate vs Exit Temperature for Tridyne 78
53. Mass Flow Function vs Temperature 79
54. Sonic Static to Total Pressure Ratio vs Temperature 79
55. Thrust Variation With Temperature 81
56. Throat Reynolds Number vs Throat Diameter (Molecular Weight of Reacted Tridyne = 27.0) 82
57. Throat Reynolds Numbers vs Throat Diameter (Molecular Weight of Tridyne Gas = 25.61) 83

58. Throat Reynolds Number Variation With Temperature 84
59. Throat Discharge Coefficient vs Gas Temperature 84
60. Oscilloscope Recording of Thermocouple Transient 86
61. Rapid Thermal Transient (ΔT = 56 F/20 ms) 86
62. Tridyne Enthalpy Versus Temperature 88
63. Tridyne Thermal Model 91
64. Tridyne Module Thrust Chamber Forward Mount Heat Loss 92
65. Tridyne Module Thrust Chamber Rear Mount Heat Loss 93
66. Tridyne Thruster Module Propellant Line Heat Loss vs Line Length 94
67. Tridyne Module Thrust Chamber Radiation Heat Loss 95
68. Tridyne Module Thrust Chamber Total Heat Loss Conduction and Radiation 96
69. Projected Thermal Response for Advanced Tridyne Thruster . . . 97

TABLES

1. Effect of Temperature Change on $\Delta T/\Delta t$ 53
2. Summary of Task IV Thermal Response Data 58
3. Volume Percent of Tridyne 69

SUMMARY

Spacecraft and satellites for extended-duration space flights require attitude control systems that are simple, highly reliable, and capable of intermittent operation over long time periods. These features, commonly identified with cold gas systems, can be achieved in an improved specific impulse system through the use of a catalytically reactive gas (Tridyne) in place of an inert agent. The only system hardware change required is that of using reaction thrusters incorporating catalysts to replace the gas jets of a cold gas system.

Principal goal of the experimental program reported herein was the development of a design for a flight-type thruster using Tridyne and the evaluation of the thruster at vacuum conditions. The thruster (shown in actual size in Fig. 1) is configured for application to a three-chamber module as it would be used in a system, providing pitch, yaw, and roll control to a space vehicle.

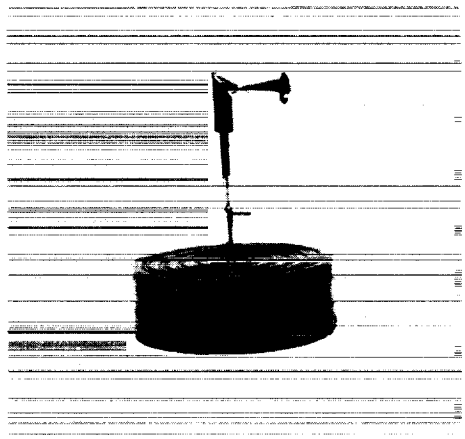

1XW32-2/11/70-C1C

Figure 1. Tridyne Microthruster

The program was successful in showing the feasibility of using Tridyne in microthrusters and in identifying the design criteria and thermal characteristics of spacecraft attitude control modules. Areas were also found where improvements in thruster operation are indicated and where new techniques in instrumentation installation are required. The efforts involved in creating a flightweight thruster design and in processing microminiature hardware were particularly successful. In these areas, it was possible to apply established advanced methods of fabrication to small-scale components. The resulting thruster is a precision assembly, dimensionally controllable to within 0.0001 inch at the throat, 0.0002 inch on wall thickness, and to 0.001 inch on noncritical surfaces. Assembly weight is 0.18 grams.

The thruster development sequence was initiated by selecting and optimizing the catalyst to be used in the chamber. These tests resulted in the selection of Engelhard Industries' 30-mesh MFSA catalyst in preference to Shell-405 catalyst from the Shell Development Company. Secondly, thermal losses from the catalyst reactor were determined and heater requirements to maintain a minimum thruster temperature were analytically established. In the three-chamber module in a space environment, the heat losses were computed to be 1.6 watts at a chamber temperature of 1000 F.

The flightweight thruster design (Fig. 1) was then established to be compatible with a three-chamber modular installation. The final effort consisted of fabricating and testing the flightweight thruster. The constant-pressure engine mass flowrate at maximum temperature was determined to be about one-half that of the cold-flow value. Thrust produced by the thruster, however, varies only slightly (less than 5 percent) over the operational temperature range. Pressure and temperature transients were also documented to show pulse-mode operational characteristics.

Operation and performance of the thruster may be improved by using a smaller-mesh catalyst and by a general reduction in the effective thermal mass. If required, higher combustion temperatures can be provided by increasing the Tridyne reactant concentration slightly. Additional effort with Tridyne chambers should include the construction of a complete three-chamber module for evaluation of operation over a real-time long-duration space mission duty cycle. In this operation, integration of the module with a set of valves to provide proper mission simulation would be required. The data provided on possible valve leakage effects would also be of interest.

INTRODUCTION

Spacecraft, such as earth orbital satellites and interplanetary probes, are normally volume- and weight-limited, and require relatively efficient attitude control systems. Frequently, it is also possible to increase the impulsive energy of such systems by use of electrical heaters. Prior exploratory work at Rocketdyne with catalytically reacting gases (Tridyne) shows them to be potentially very suitable for use in the spacecraft types requiring high-performance propulsion systems at the microthrust level. The investigation of Tridyne in flightweight thrusters at 0.01 pound thrust is reported herein. The requirements for heaters were also evaluated at various temperatures.

Experimental work at Rocketdyne with catalysts and various reactive gases shows that a chemical reaction can be promoted over a wide range of temperatures and pressures in a predictable and repeatable manner. In the Tridyne concept small fractions of reactive gases are combined with an inert diluent to form a nondetonable mixture that may be safely stored at high pressure in a vessel. Energy release is accomplished by passing the mixture through a catalyst which combines the reactants and creates a hot gaseous mixture. Mixture temperature is controlled by varying the reactant concentration. The basic gas composition, 1500 F design operational temperature, used in the Tridyne thruster tests consists of mole fractions of 0.85 nitrogen, 0.10 hydrogen, and 0.05 oxygen.

Data on Tridyne storability and the uses of various gas mixtures for pressurization were obtained on an advanced pressurization system technology program under Air Force contract (Ref. 1). Numerous experiments with catalysts as potential ignition devices are reported under a J-2 Engine ignition development program (Ref. 2). The characteristics of catalysts with cryogenic oxygen and hydrogen propellants in reaction control systems are reported in Ref. 3 and 4. Tridyne was also recently evaluated as an agent for clearing gases from tank guns (Ref. 5). The program consisted of applying the accumulated Rocketdyne technologies with Tridyne to

operation in the microthrust regime. Five tasks were conducted in the Tridyne evaluation: Task I consisted of catalyst selection, Task II was assigned to thermal analysis and heater design, Task III included the design and fabrication of flightweight thrusters that were tested in Task IV, and Task V consisted of documenting and reporting the results.

The information of the report is oriented in the sequence of thruster design requirements, hardware design details, experimental evaluations, and test results. Test summaries are included in the Appendix.

THRUSTER DESIGN

DESIGN REQUIREMENTS

The design effort of the program consisted of providing the test configurations for the experimental evaluations and the flight-type concepts for detailed studies. The initial task involved the test hardware for the evaluation and selection of the catalyst and for the determination of the amount of catalyst for a complete Tridyne reaction. A flightweight module concept also was improvised to illustrate the use of Tridyne thrusters for pitch, yaw, and roll control of a spacecraft. The concept included provisions for temperature maintenance above a minimum level by the use of heaters. A flightweight thruster design was then created based on the module geometry. This design was fabricated and used for the flightweight thruster tests of the program.

Requirements for the flightweight design were established by the performance specification prepared for the program by the Jet Propulsion Laboratory. The principal parameters listed below are compared to the performance attained during the program.

Parameter	Specified Value	Program Value
Vacuum Thrust, pounds (calculated)	0.01 ±0.002	0.01 ±0.0004
Expansion Area Ratio	100:1	100:1
Chamber Pressure Range, psia	15 to 30	30 selected
Impulse Bit, lb-sec x 10^4	2.4 ±0.4	2.0 ±0.2
Valve Excitation Time, milliseconds	20	20
Thrust Response Time, milliseconds		
From Signal to 2-Percent P_c	6	6
From Signal to 90-Percent P_c	8	8
Nominal Pulse Width	20	20
Thrust Decay Times, milliseconds		
Off Signal to 10-Percent P_c	8	18

Provisions were made for heating the catalyst during tests. The thruster designs were established to be consistent with spacecraft construction practices.

PHASE I: TEST HARDWARE

The test configuration shown in Fig. 2 was used in the first test series for the selection of a catalyst and in the sizing of the catalyst bed. It consists of a machined, stainless-steel thrust chamber configured for assembly to a standard, flared-tube fitting and includes provisions for varying the catalyst bed length. The large mass of material at the injector end prohibited a precise evaluation of the catalyst, but the ease of disassembly and the flexibility in changing or modifying the catalyst bed geometry made this design very convenient for test changes in the early catalyst evaluation.

To verify and further evaluate the catalyst and its bed geometry, a more nearly optimum chamber configuration was devised by eliminating the large injector-end fitting. A selected length and diameter of chamber was fitted to a small, low mass injector (Fig. 3). This assembly was readily fabricated except for the installation of the small thermocouple. The thermocouple is very sensitive and can be easily damaged. This is possible not only during the brazing operation but also in subsequent handling of the unit. The chamber was tested with an outer wall surface thermocouple to record temperatures since the internal thermocouple was found to be inoperative.

PHASE II: MODULE CONCEPT

The second principal design task consisted of the formulation of a three-chamber module concept for providing pitch, yaw, and roll control of a spacecraft. This task was a progressive effort and consisted of several

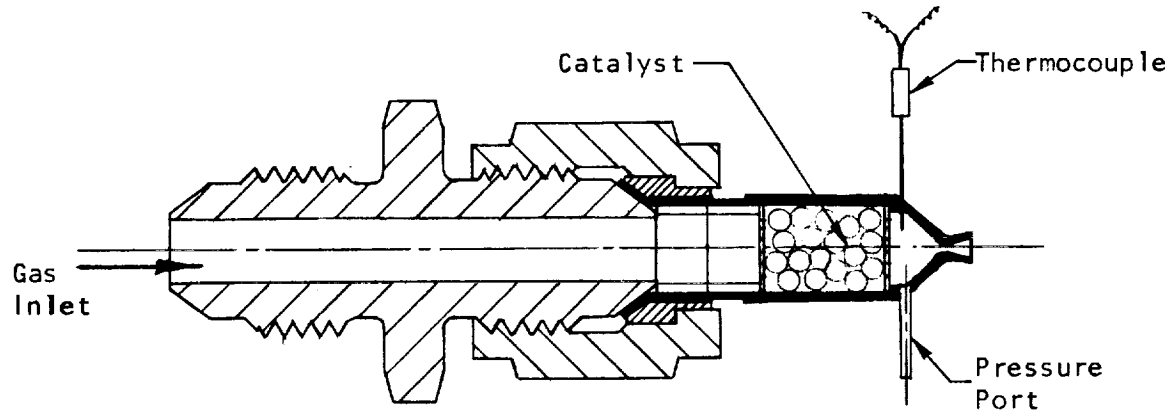

Figure 2. Catalyst Evaluation Chamber Assembly

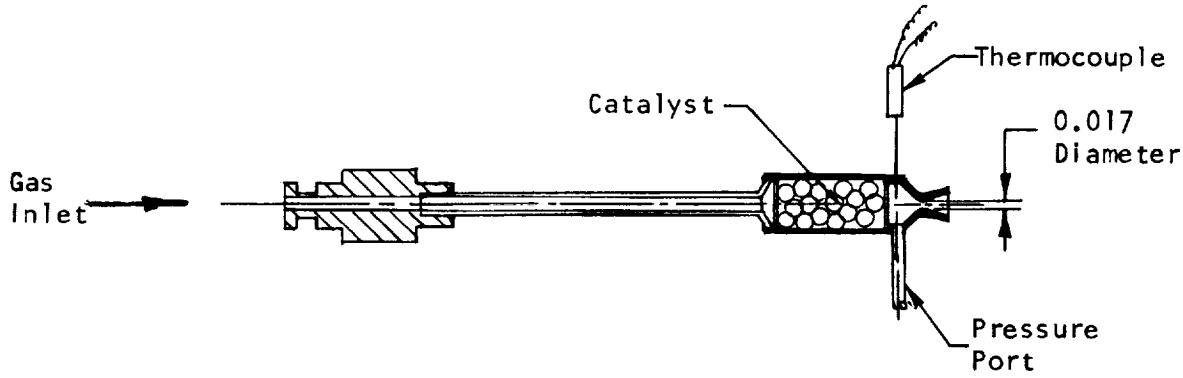

Figure 3. Lightweight Development Thruster

preliminary design layouts to resolve the best geometric shape of the chamber, nozzle, and temperature-conditioning heater. Periodically, as test data were acquired on the thruster, the designs were modified to incorporate indicated improvements. Informal design reviews also were held to ensure design consistency with conventional flight hardware standards.

The flightweight module resulting from the study is shown in Fig. 4. Two opposing chambers are oriented for pitch and yaw control in a vertical plane with a roll chamber at a right angle to the vertical chambers. The thrusters are configured for ease of assembly into a thermally efficient, three-chamber cluster and heater module. The concept provided a basis for a realistic flightweight thruster configuration and, additionally, was a useful tool in determining the probable thruster heat loss rates as they would occur on a spacecraft installation.

The principal module materials used in the thermal analysis were selected to control the heat flux from the chambers into the valves to a tolerable level and to minimize radiation losses. The inlet lines are stainless steel of reference size: 0.030-inch ID, 0.002-inch wall thickness, and 1.25-inch length. The module shell is titanium with the inner surfaces gold plated to reflect radiant heat from the thrusters. The thruster supports are shown as stabilized zirconia, although minimum surface contact supports of titanium are thermally comparable and were used in the thermal analysis. The thrusters are made from electroformed nickel and are gold plated to reduce radiation losses.

The module is large enough to enclose three 0.5-watt heaters, which would permit maintaining the module above 600 F with 60 percent of the heat energy being contained within the module. The thermal loss characteristics are shown in the Thermal Analysis section.

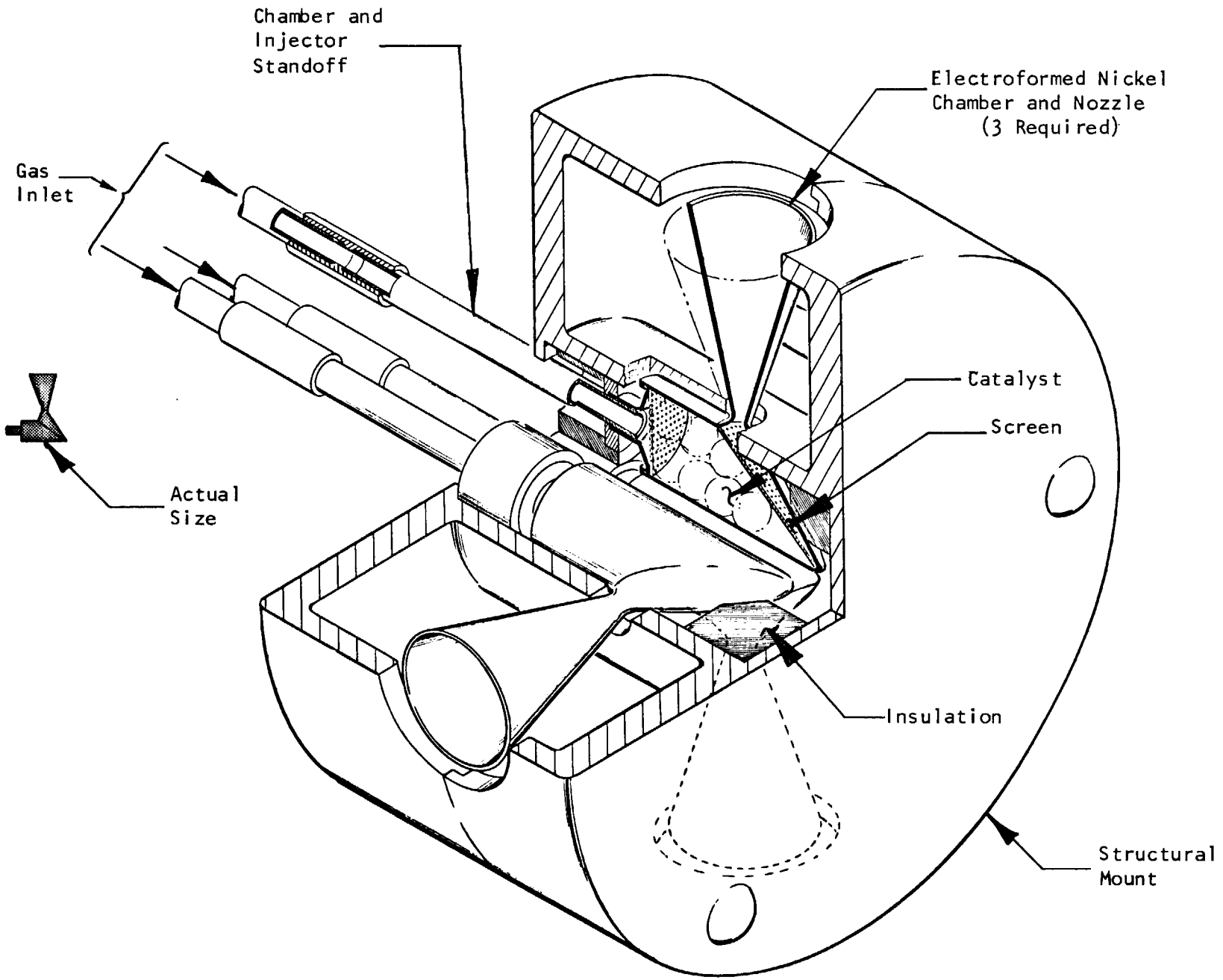

Figure 4. Flight-Type, Three-Engine Module Assembly

PHASE IV: TEST HARDWARE

A flightweight thruster design was established based on the thruster configuration in the modular concept shown in Fig. 4. Considerable effort was devoted to the refinement of the test flighweight thrust design to achieve reproducibility. As shown in Fig. 5, the chamber body is a cylindrical section with an injector and screen at the inlet to provide a uniform distribution of Tridyne through the catalyst bed. The catalyst bed also has a screen at the downstream face which is positioned 40 degrees from the chamber axis. The screen is elliptical in shape and configured to match the chamber and nozzle section truncations. The exit nozzle and throat section is formed by joining two cones (nozzle section with 16-degree half-angle and convergent section with 33-degree half-angle) by a wall radius three times the throat radius. The convergent section is cut at a complementary angle (50 degrees from the nozzle centerline) to form an elliptical face matching the chamber section. By use of this design approach, the chamber is easily constructed by electrodepositing nickel over two simple mandrels with a screen interface. The single critical dimension is the throat diameter, which is controlled to a tolerance of ±0.0001 inch.

A test configuration (Fig. 6) was assembled for evaluation of the flightweight thrusters. It consists of an electroformed chamber and nozzle assembly, an electroformed injector that is laser beam welded to the chamber, nickel screens at the chamber inlet and at the convergent section of the nozzle, a calibrated venturi flow-measurement device, a Kulite transducer for measuring pulse performance, a Walter Kidde Corporation solenoid valve assembly, and a thermocouple in the chamber assembly. The greatest technical problem was encountered in installing the pressure transducer and thermocouple. The best technique for installing thermocouples was found to be that of electroforming the thermocouple in place during the chamber fabrication.

ACTUAL SIZE

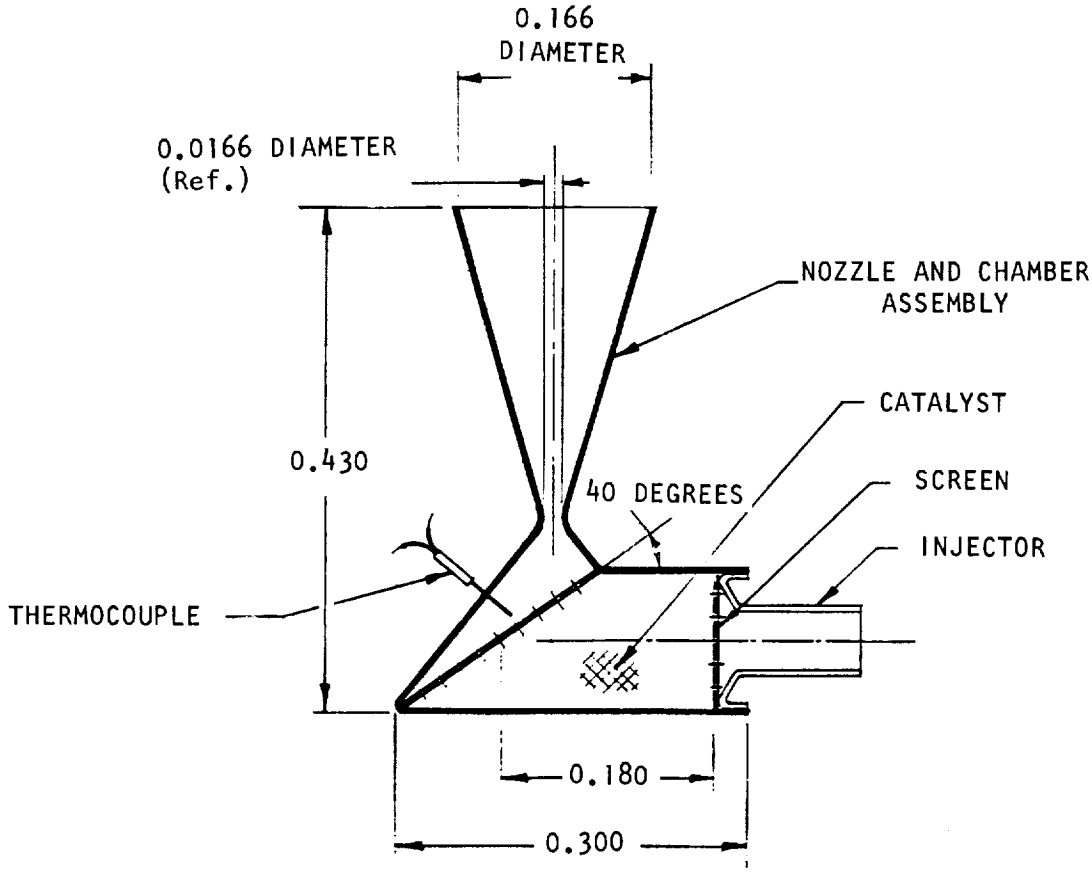

Figure 5. Thrust Chamber Assembly (0.01-Pound Thrust)

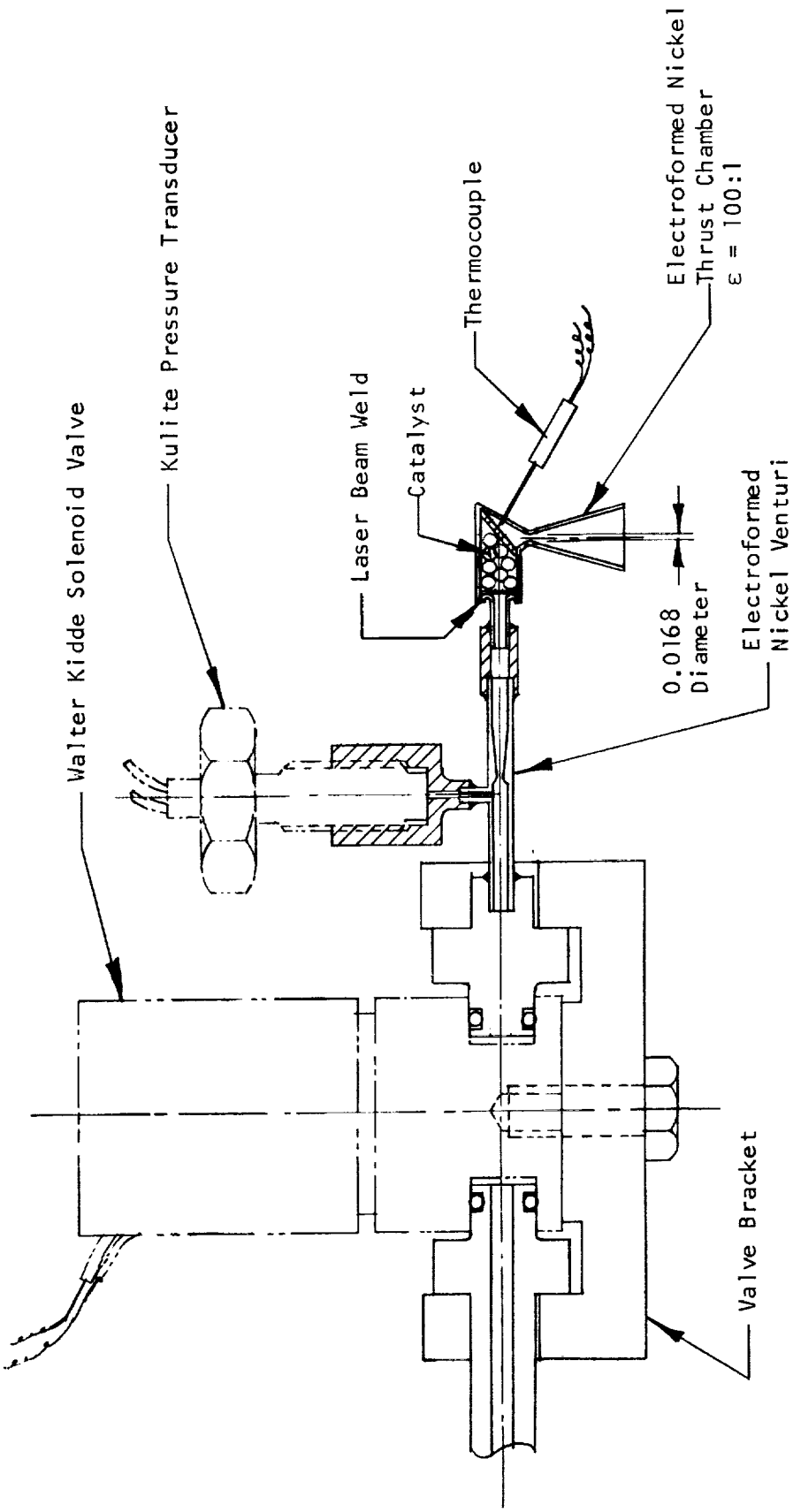

Figure 6. Flightweight Test Configuration

The sonic venturi (Fig. 7) used for flow measurements during pulse operation is a dimensionally precise device fabricated by electroforming nickel over an aluminum mandrel followed by chemically leaching the aluminum. The wall/throat radius ratio is 3:1 and the duct flow area at the transducer probe has an A/A* ratio of 8.2:1 with a static to total pressure ratio of 0.9965:1. The throat dimension was fabricated to a tolerance of 0.0001 inch.

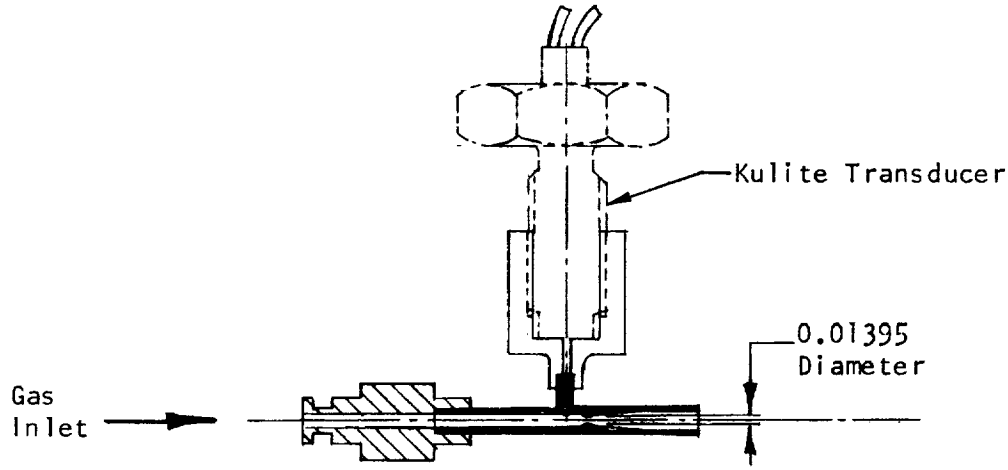

Figure 7. Flow Calibrated Venturi Assembly

THRUST CHAMBER ASSEMBLY AND INSTALLATION

Chamber Assembly

In the various steps of assembling hardware and improvising test installations, it was frequently necessary to explore unconventional methods and processes and, as is normally encountered, with varying degrees of success. Some of the more fruitful of these merit comment.

A critical step in the thrust chamber assembly process is that of sealing the chamber with the catalyst in place. The catalyst should not be heated above the range of 400 F unless immersed in an inert gas to prevent catalyst oxidation. The thruster also must be capable of an unlimited number of thermal cycles from ambient temperatures to 1400 F. Three methods of chamber enclosure were investigated.

Induction brazing was found to be unsatisfactory from the viewpoint of quality control and possible catalyst contamination. However, induction brazing was shown to be a logical method for the assembly of components into a test installation. Electron-beam welding was explored and has the potential of precise control and repeatability. It is performed in an inert atmosphere which would prevent catalyst damage. However, the machines readily available were too large for use on the thrusters. A centrally positioned, 0.115-inch-diameter chamber rotating at maximum spindle speed has a peripheral speed substantially below the minimum permitted. Use of beam deflection to create a circular electron discharge path also was tried but was found to cause excessive heating. This work was performed on a Hamilton-Standard welder rated at 6 kilowatts power and 150,000 volts. A small electron-beam welder of proper size for the thrusters would probably be the most suitable approach for welding a large number of chambers.

Consultation with welding specialists resulted in the evaluation of laser beam welding. A 347 stainless-steel weld sample is shown in Fig. 8 . The sample consists of a sleeve inserted within a cylinder. Wall thicknesses are 0.004 inch and the contact surface diameter is 0.100 inch. The geometry closely approximates the chamber weldment. The sample following welding is shown in Fig. 9, illustrating the effectiveness of the laser weld method. Nickel 200 samples also were satisfactorily welded.

Flightweight thrusters assembled by laser beam welds at the injector face are shown in Fig. 10. The central chamber has a pressure probe installation to document pressure transient characteristics. The chamber discoloration is from brazing flux used to attach the inlet line for testing.

The final two chambers to be laser beam welded are presented in Fig. 11. As shown, the weld beads are uniform and the discharge point overlap is reasonably symmetrical. It was noted that the general weld quality progressively improved as the operator gained experience in positioning the discharge point. The final weld time was on the order of 2.5 minutes.

1XZ82-12/8/69-C1

Figure 8. 347 Stainless-Steel Tube Sample Prior to Welding

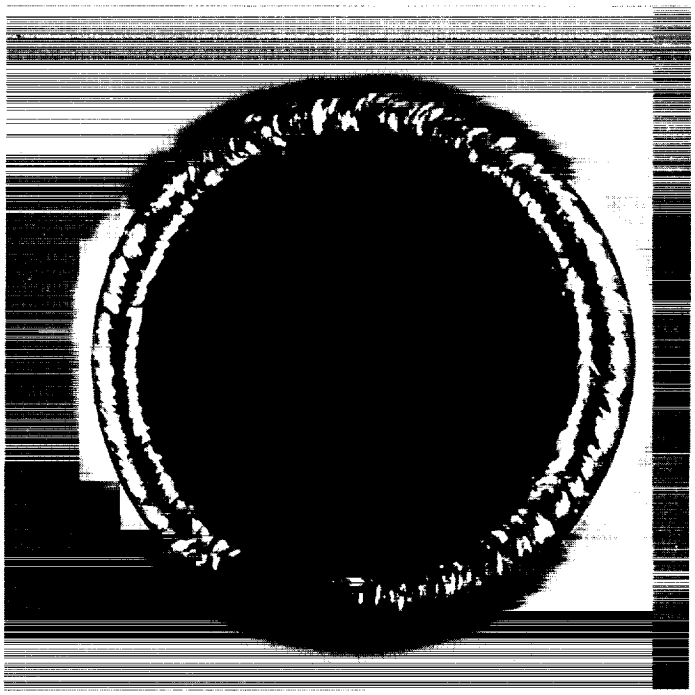

1XW32-1/7/70-C1C

Figure 9. 347 Stainless-Steel Tube Sample Following Laser-Beam Welding

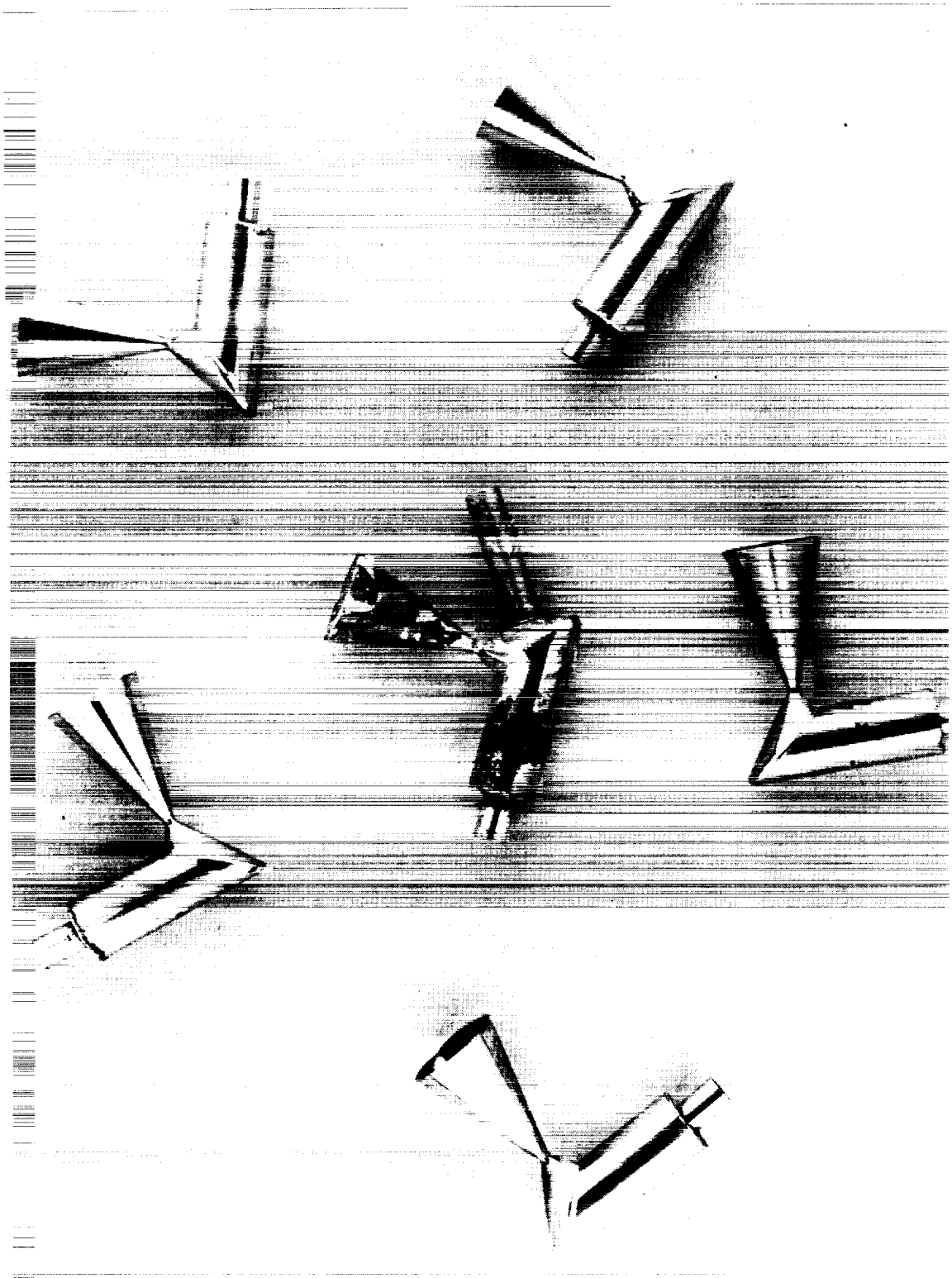

Figure 10. Assembled Flightweight Thrusters

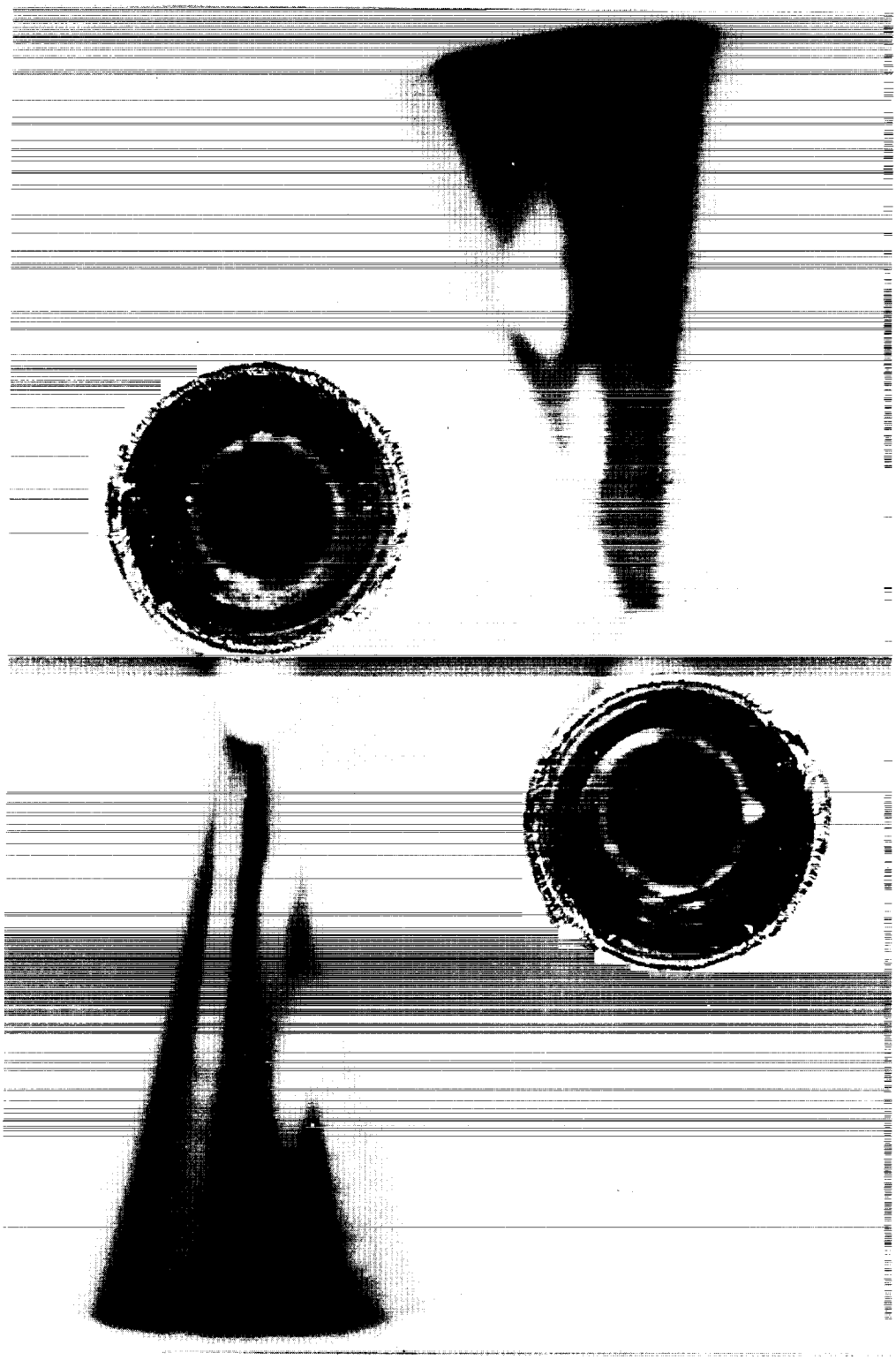

Figure 11. Laser Beam-Welded Enclosures

The thermal cycling accomplished to date on the welded chambers has had no evident effect on the weld integrity. The maximum recorded chamber operational temperature was 1331 F. It was also necessary to heat the weld area to a temperature of about 1700 F when assembling the test chambers to the inlet line. Here, again, no adverse effect from the heating is shown.

Laser weld technology is an interesting development and is relatively new. There is still a great deal of information yet to be obtained on optimum weld methods. Clealiness is obviously important, and normal degreasing of parts should be performed. No open cracks at the weld face are permitted as the beam will penetrate the crack, causing erosion and a larger aperture. The weld consists of a series of overlapping spot discharges placed progressively along the weld seam, and causes virtually no increase in metal temperature since the highly focused, small impact energy is readily dissipated into the adjacent metal. An argon jet shield is used to blanket the weld area to avoid local surface oxidation.

Component Assembly

The test instrumentation required unusual design features to avoid excessively large weld bosses and fittings. Experiments with test devices showed that induction brazing can be successfully used to place miniaturized thermocouples and pressure taps on the chamber. A thermocouple installation is shown in Fig. 12. The braze materials were formed into washers (Fig. 13) and held in place during the induction heating. The Task IV test chamber with a pressure probe has the same fitting as in Fig. 12 without the thermocouple and button.

Proper alignment and positioning of the chamber were achieved by use of the fixtures shown in Fig. 14. Pressure probe and thermocouple installations were made with the same fittings.

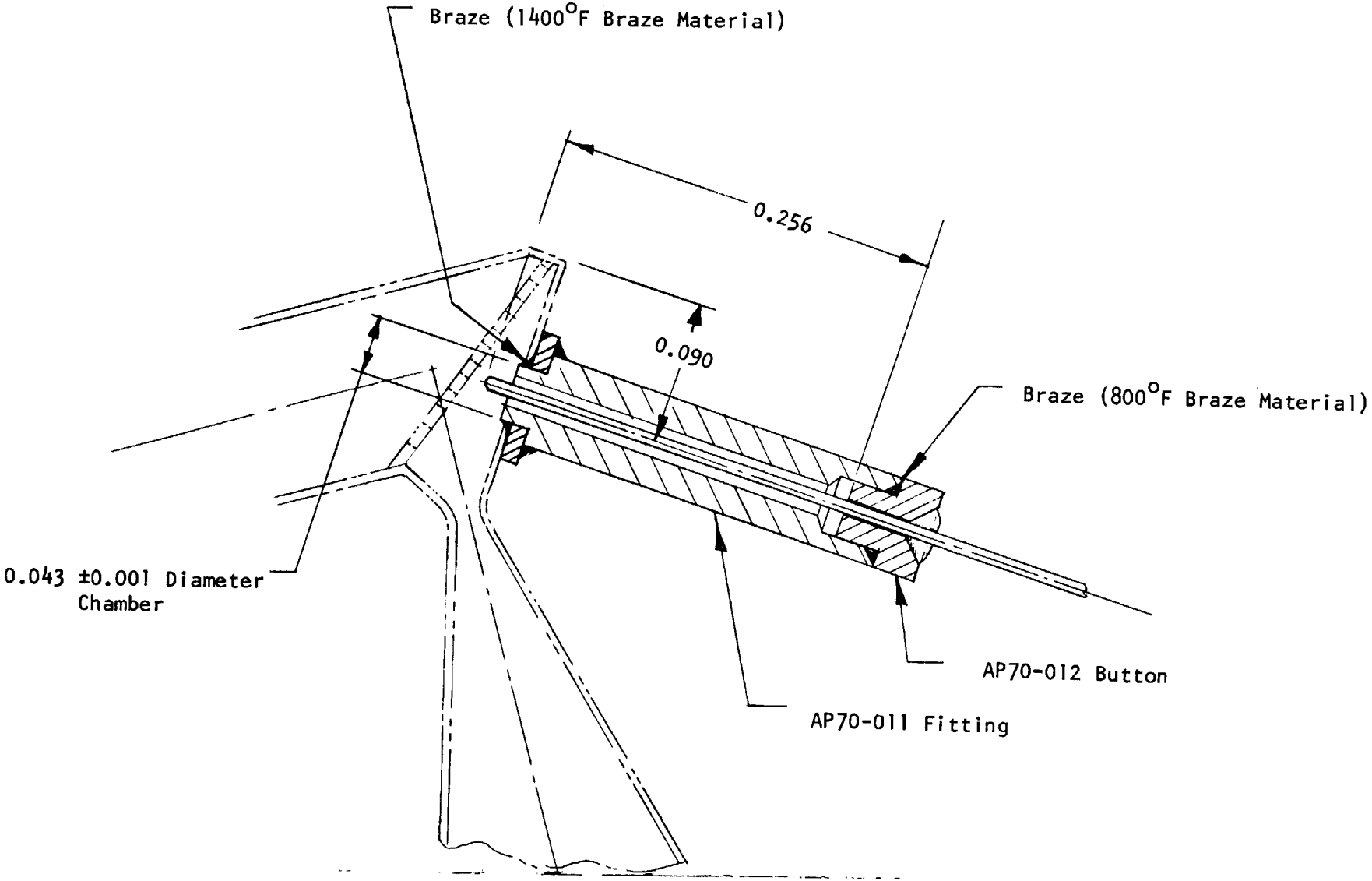

Figure 12. Thermocouple Installation in Tridyne Thruster (Scale 10:1)

1XW32-2/4/70-C1E

Figure 13. Washer-Shaped Braze Materials

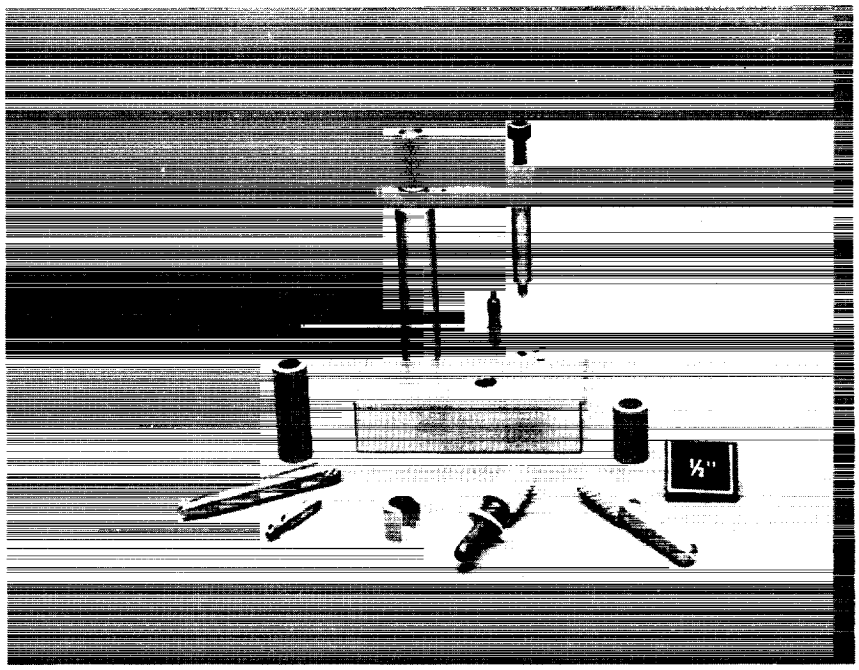

Figure 14. Thrust Chamber Assembly Fixture

The installation of thermocouples was a major implementation problem. A limited number were installed by brazing and found to be extremely fragile. Near the program completion, a chamber was supplied by Servometer Corporation with a thermocouple positioned to extend through the chamber wall during the electroforming process. The forming technique involved in integrating the thermocouple is a special process developed by the vendor and is considered proprietary by them. Four thermocouples and two chamber shells were expended as development items to obtain a functioning thermocouple installation. A major advantage in this type of construction results from the very small change in chamber mass due to the thermocouple attachment. The thermocouple has an 8-mil shell enclosing two 0.5-mil leads forming the thermal juncture. The leads are encased in an insulating compound, which appears to be magnesium oxide. Consequently, addition of the thermocouple causes no significant change in the thruster thermal response (the mass change is in the order of 0.001 gm per inch of thermocouple). The assembled flightweight thruster weighs 0.18 gm, including 0.02 gm of catalyst.

EXPERIMENTAL EVALUATIONS

The program's experimental effort consisted of catalyst evaluation in Phase I and tests of flightweight thrusters in Phase IV. The Phase I tests were conducted to select the minimum mass of catalyst that will still effect a complete reaction of Tridyne at a flowrate of 1.8 sci/sec and at 15- and 30-psia chamber pressures. The effectiveness of Engelhard MFSA catalyst was compared with Shell-405 catalyst and found to be nearly twice as reactive per unit mass. Thirty-mesh MFSA catalyst was also found to be approximately twice as effective per unit mass as 16-mesh MFSA pellets, indicating the Tridyne reaction to be contact surface-controlled. About 0.015 and 0.030 grams of 30-mesh MFSA catalyst are required to 30- and 15-psia chamber pressure, respectively.

Based on Phase I data, flightweight thrusters for Phase IV tests were fabricated for operation at 30-psia chamber pressure with 0.02 grams of 30-mesh MFSA catalyst. Tests of the thrusters showed thrust response at engine start to be within the design requirement of 8 milliseconds from Command On to 90-percent chamber pressure. The thrust decay time was about 18 milliseconds rather than the required 8 milliseconds to 10-percent chamber pressure. Thermal analyses of the Phase IV thruster tests indicate that the selected catalyst quantity is sufficient to complete the Tridyne reaction. However, the maximum recorded gas temperature was 1331 F, which occurred with an insulated chamber.

The experimental test runs are summarized in the Appendix.

EXPERIMENTAL EQUIPMENT AND PROCEDURES

Facilities

The experimental effort of the program was conducted in the Transducer Laboratory of the Rocketdyne Research Division. This allowed an efficient and effective coupling of the instrumentation and testing efforts. Phase I

and Phase IV thruster testing was performed in a high-altitude simulator stand (Fig.15) which consists of a bell jar connected to a 6-inch CVC oil-type diffusion pump and a 1397 Welch forepump. With no thruster flow, the forepump is capable of reducing the pressure to 5 x 10^{-3} mm Hg, making it possible to demonstrate vacuum starts. It is estimated that during steady-state operation of the thruster with a gas flowrate of 1.75 sci/sec, the forepump is capable of maintaining a system pressure below 1 psia.

5AH23-1/23/68-S1

Figure 15. Vacuum System

Test operations and data acquisition were conducted through a central control and recording center. All measurements were recorded on a CEC direct-reading oscillograph with six input channels. A CRT oscilloscope with two-channel input and storage capabilities was used to display the response characteristics during many of the tests.

Test Instrumentation

Commercially available microminiature regime instrumentation was used in the experimental evaluations. The critical parameters measured during the 20-millisecond pulses were pressure and temperature. A Kulite Model XTL-190-50 transducer (Fig. 16) was used for pressure measurements. The transducer, featuring a 0.070-inch-diameter diaphragm sensor enclosed within a 0.135-inch-OD threaded casing, is rated for 50 psia and has a natural frequency of 100 kHz or a time constant less than 0.1 millisecond.

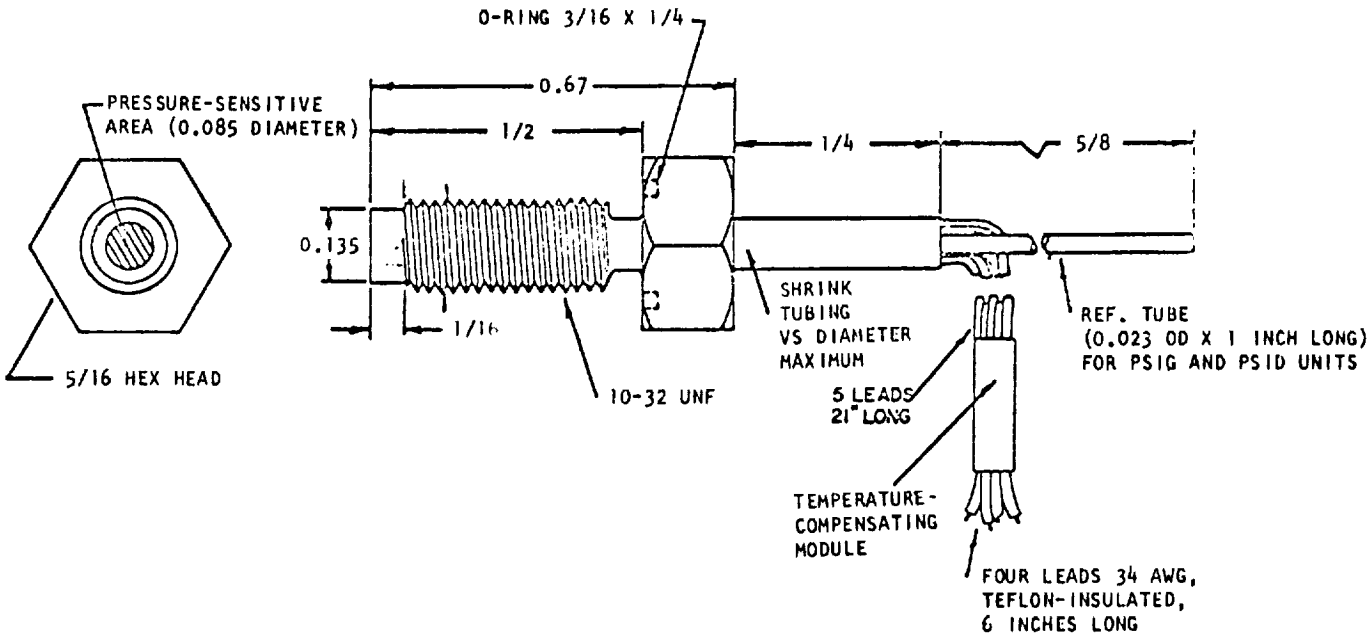

Figure 16. Kulite Model XTL-190-50 Pressure Transducer

For the temperature measurement, ultra-miniature thermocouples were employed. These thermocouples were of the platinel-platinel variety rather than chromel-alumel because platinel resists brittleness at high temperatures (1500 F). The thermocouple is constructed by joining two 0.5-mil wires to form a 1-mil exposed tip. The body of the thermocouple is contained in an 8-mil-OD stainless-steel sheath packed with insulating material. An ultra-miniature thermocouple installed in a microthruster and operated under the subject program conditions was computed to have a thermal time constant of less than 10 milliseconds.

Thruster pulsing operation was controlled with a Walter Kidde valve. The valve and valve bracket are shown in Fig. 17. The motion of the valve was monitored by measuring a voltage signal from an induction coil wrapped around the valve solenoid coil. The induction coil is energized by magnetic flux from both the solenoid coil when it is actuated and the

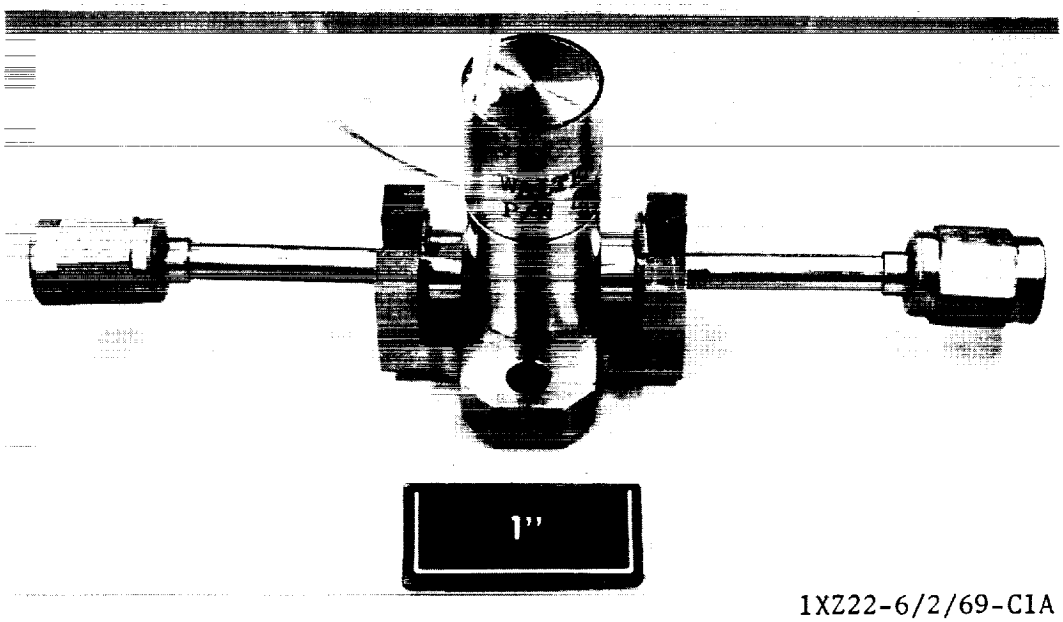

Figure 17. Walter Kidde Valve and Test Fittings

armature motion due to its effect on the magnetic field. An oscilloscope trace of the valve being opened and closed is shown in Fig.18. The first peak shows that when the solenoid is energized, the voltage across the monitoring coil instantaneously rises to a maximum and then begins to decay because the energizing current is no longer changing. The movement of the armature changes the strength of the magnetic field and induces an additional voltage across the monitored coil during motion as shown by the second peak on the trace. The lag time required for the valve to open or close from signal initiation is between 3 and 4 milliseconds.

A pressure-time trace for a 0.15-inch-OD chamber filled with MFSA catalyst is also shown in Fig. 18. It should be noted that although the trace is for a Phase I prototype chamber, only about 6 milliseconds are required for the pressure to reach a steady value after the valve opens. This is sufficient to meet specification requirements.

Steady-state flow measurements, which are thought to be within ±4 percent of actual flowrate, were obtained by the use of a rotameter. A sonic venturi was used as a flowmeter in the pulse-mode operation of Phase IV.

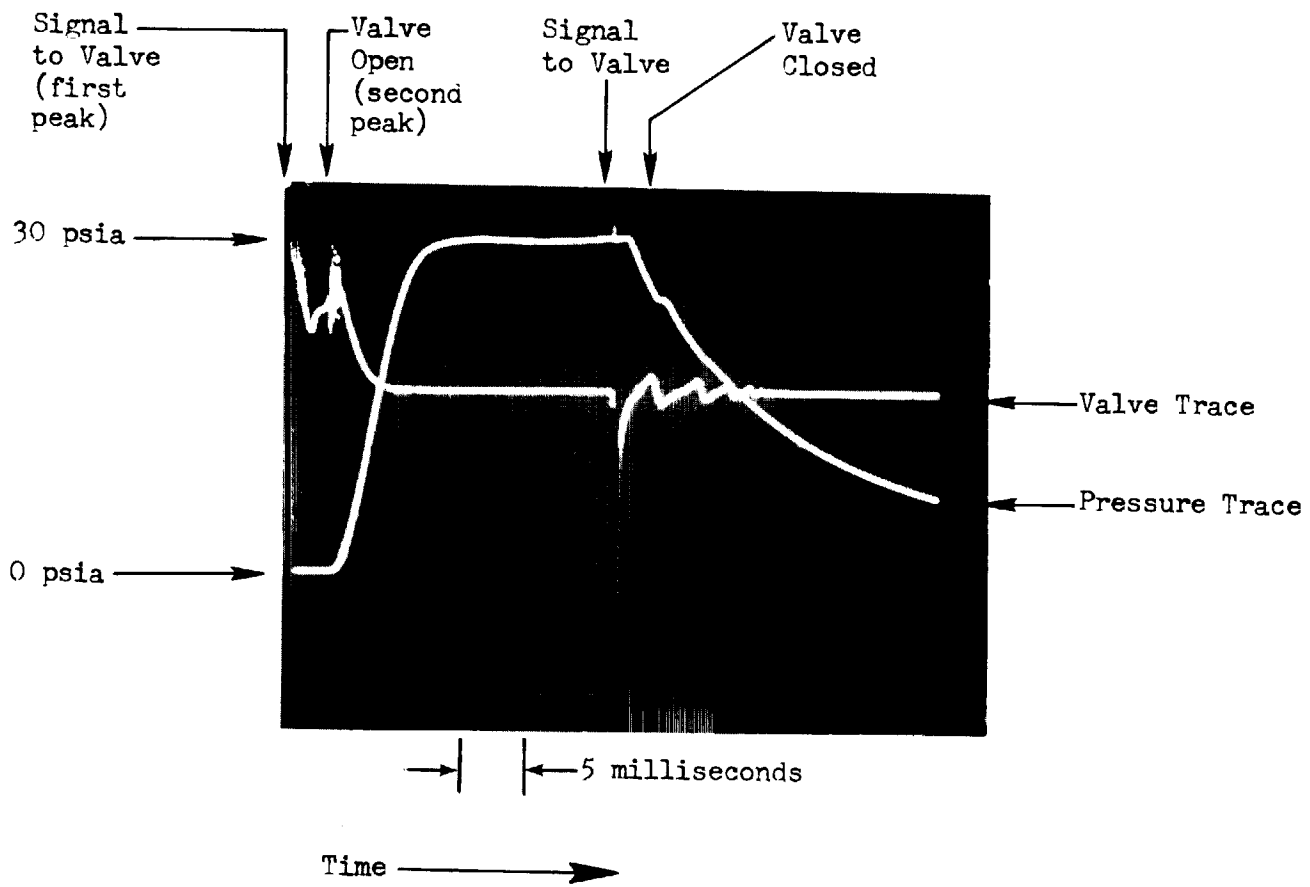

Figure 18. Tridyne Thruster, 25-Millisecond Pulse

Calibration Procedures

Pressure transducers were calibrated by recording the output on an oscillograph. The procedure consisted of first evacuating the vacuum system to obtain zero pressure and then making a recording. The system was next allowed to reach ambient pressure and another recording was made. Barometric pressure was also tabulated. A 200-psig Heise gage was used to calibrate the transducers from ambient to 35 psig.

The accuracy of the first thermocouples to be received was checked by measuring the temperature output of the thermocouples when submerged in boiling water. The readings obtained were found to be within ±1 F of the boiling point of water. Thermocouples from subsequent shipments were merely checked for continuity.

Thrust Chambers

The principal test effort of Phase I consisted of comparing and evaluating catalyst reactors suitable for use at pressures of 15 to 30 psia, with flowrates in the range of 1.8 sci/sec. Several chambers were constructed and tested with various amounts of catalyst at the above conditions. The first two chambers tested were 0.150 inch and 0.224 inch ID. The 0.150-inch chamber is shown in Fig. 19.

Both chambers constructed of stainless steel had a common B-nut attachment at the injector which created considerable heat loss. It was calculated that approximately 15 percent of the heat is lost at the injector end of the 0.150-inch chamber during operation. When the heat losses from the pressure and thermocouple ports are included, a maximum chamber temperature of 1100 F is obtained. Experimental results reveal this to be a realistic value. The calculations neglect radiation and conduction heat losses from the chamber to the insulation material used in some of the tests.

In an attempt to reduce the heat loss, a 0.10-inch-ID chamber was constructed from Lavalite, a non-metallic composite that has a thermal

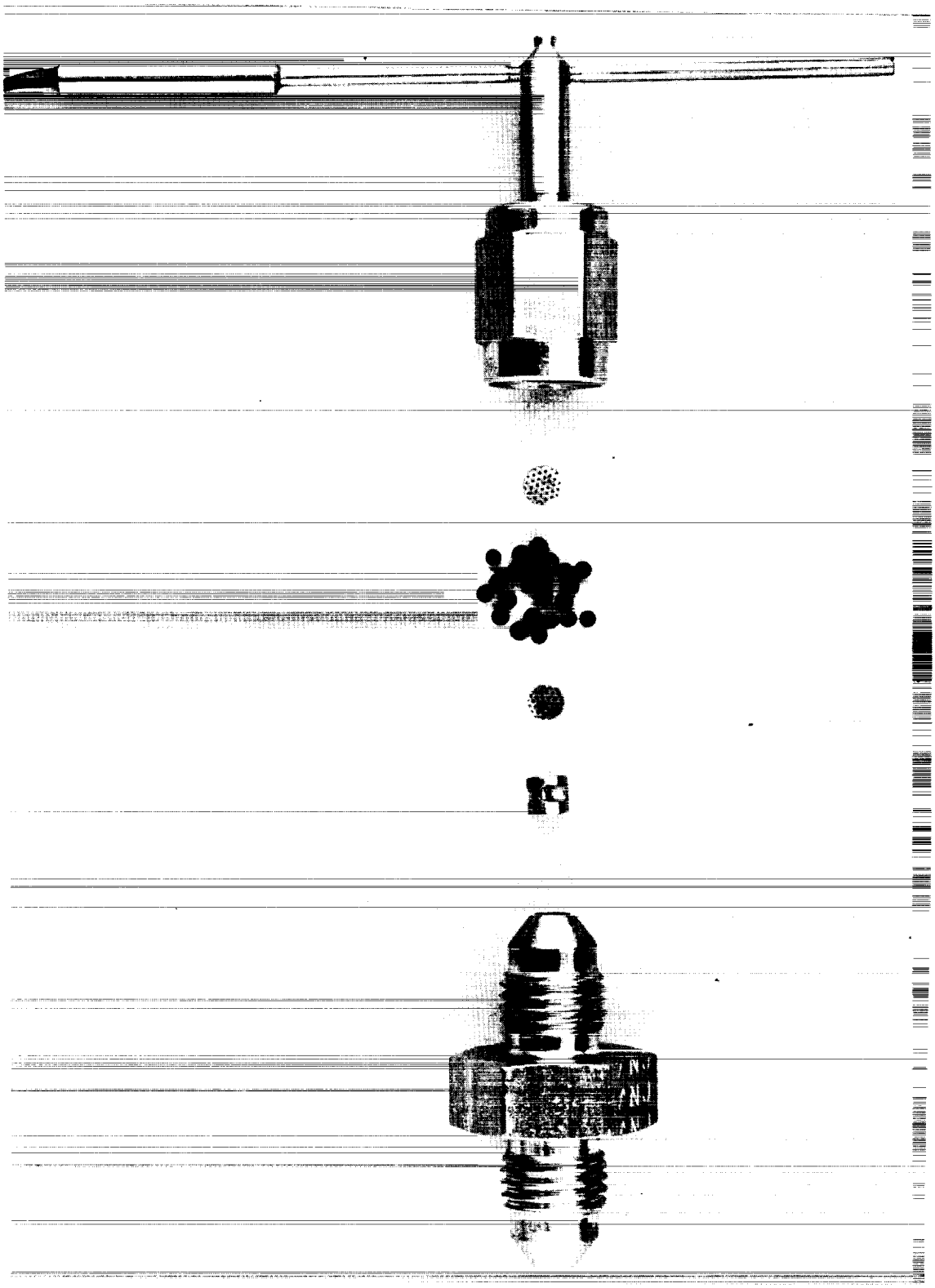

Figure 19. 0.150-Inch Stainless-Steel Thrust Chamber

conductivity about 9.5 percent that of stainless steel. However, the steady-state chamber temperature was approximately the same as in the 0.150-inch chamber. This is attributable to the heavy walls of the Lavalite chamber, which were about 12 times as thick as the walls of the steel chambers. The thicker walls, which were necessary for structural integrity, produced a similar heat loss.

A modified 0.150-inch stainless-steel chamber with a flange replacing the B-nut and union combination at the injector was also tested. In these tests, a phenolic insulator was placed between the support flange and the chamber flange. The experimental results show that the heat losses were similar to those observed in the other chambers; however, the heat loss in this chamber could probably have been reduced by increasing the insulation thickness between the flanges. An improved chamber design incorporating a small-diameter inlet line was also fabricated and tested. The test results were inconclusive since the chamber thermocouple was found to be open after test installation. However, test temperatures were measured by a thermocouple placed on the chamber external wall surface. Electrical heaters were also used with the chamber to provide data on catalyst characteristics at high temperatures.

Test Procedure

After the thrust chamber, valve, and pressure transducers were installed in the test facility, the vacuum cell was reduced to a pressure of 5×10^{-3} mm Hg to verify the zero readings of the pressure transducers. The line between the valve and the Tridyne supply bottle was then pressurized to the desired value. Steady-state readings were obtained by flowing Tridyne through the thrust chamber for 30 seconds. Oscillograph readings were usually taken for the first 5 seconds and the last 5 seconds of a test. Pulses of approximately 20-millisecond durations were usually made after a steady-state test was completed. The system was operated at nominal line pressure of 16 and 32 psia.

TASK I: EXPERIMENTAL RESULTS

Shell-405 and MFSA catalysts were tested in various sizes and geometrical arrangements to determine optimum catalyst quantities. It was found that the Engelhard MFSA catalyst is about twice as active per unit mass as the Shell-405, and the 30-mesh MFSA catalyst is about twice as active per unit mass as the 16-mesh MFSA. For a flowrate of 1.8 sci/sec, about 0.015 and 0.030 grams of 30-mesh MFSA catalyst are required at 30 and 15 psia, respectively.

In previous experimental programs using 1/16-inch MFSA catalyst with Tridyne, it was found the minimum amount of catalyst required to completely react the Tridyne could be computed by the following empirical relationship:

$$M_c = K \frac{\dot{\nu}}{P_c}$$

where

M_c = catalyst mass, grams

P_c = chamber pressure, psia

$\dot{\nu}$ = chamber flowrate, sci/sec

K = experimental constant for the catalyst formulation and size

This equation has been found applicable in the pressure range between 10 and 1000 psia. The units within the equation may be varied by adjusting the K value as required. Rearranged in the form $K = M_c (P_c/\dot{\nu})$ and plotting the steady-state chamber temperature as a function of $M_c (P_c/\dot{\nu})$, it was found that as M_c is increased while the flow conditions $(P_c/\dot{\nu})$ are held constant, the temperature will increase to a point where all the gas is reacting. Adding more catalyst beyond this point will produce no additional increase in temperature. In practice, the use of more catalyst than necessary may cause a decrease in temperature because more catalyst will be in contact with the chamber walls thus increasing heat transfer from the gas to the chamber. Additional catalyst also increases the thermal mass.

The experimental results for the Lavalite chamber with 30-mesh MFSA catalyst are shown in Fig. 20. The steady-state chamber temperature is plotted as a function of M_c $(P_c/\dot{\nu})$. A break in the temperature curve occurs at K = 0.20; therefore, this point corresponds to the optimum amount of catalyst. It should be noted that the temperature is independent of pressure for a given value of K.

Figure 21 illustrates the experimental results for the 0.224- and 0.150-inch stainless-steel chambers with 16- and 30-mesh MFSA catalyst at 32 psia. Although the quantity of data is limited in the low K value range, the optimum K values for the 30- and 16-mesh catalysts are about 0.2 and 0.6, respectively. These results can be compared with trends predicted theoretically. If the Tridyne reaction is surface catalyzed, then the reactivity should be proportional to the outer surface area. Because the surface area per unit mass in inversely proportional to the diameter, as theorized, the 30-mesh catalyst should have approximately twice the surface area and twice the reactivity of the 16-mesh catalyst. Therefore, the optimum K values for 30- and 16-mesh catalysts indicate that the reaction is surface catalyzed.

Several factors were found that influenced the maximum temperature reached during a test run. Some of these were difficult to control because the small chamber diameter caused varying catalyst packaging densities and, in non-optimum geometries, flow striation. Heat loss rates were affected by the spacers used to position the catalyst-retaining screens and also by the degree of component compression attained at assembly. At low values of the K parameter, the number of pellets was significant in determining the catalyst geometry and the variable mass increment; i.e., in some tests as few as three or four 16-mesh pellets were used or six to eight 30-mesh pellets. As a result of these considerations, the tests produced considerable data scatter. However, the Lavalite chamber data appear reasonably consistent and are used for the flightweight thruster design.

Experimental results for the Shell-405 catalyst are shown in Fig. 22 and 23. The most important of these is that the optimum K value for 30-mesh Shell-405 is about 0.5 as compared with about 0.24 for the equivalent sized MFSA catalyst.

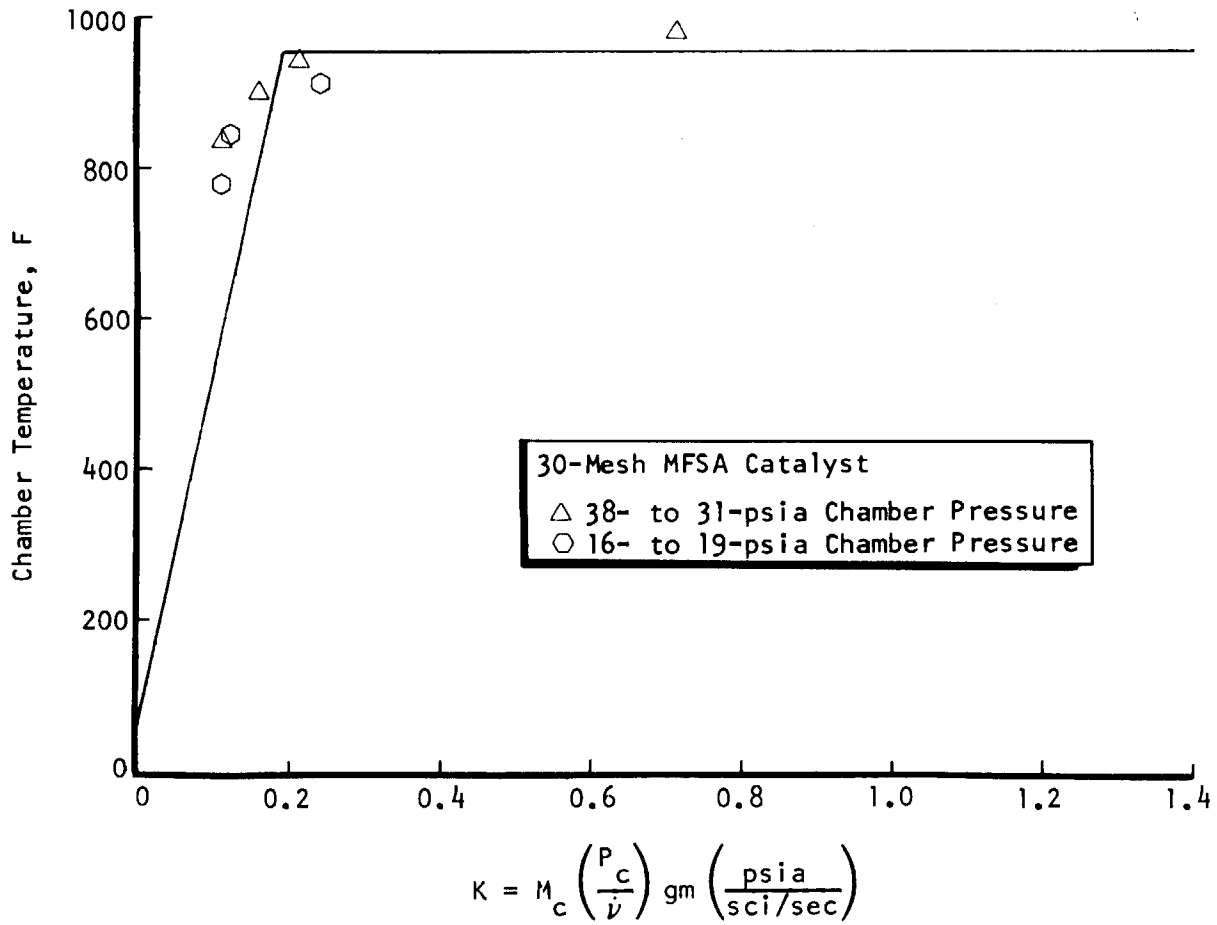

Figure 20. Thermal Response of 0.1-Inch-ID Lavalite Chamber (30-Mesh MFSA Catalyst)

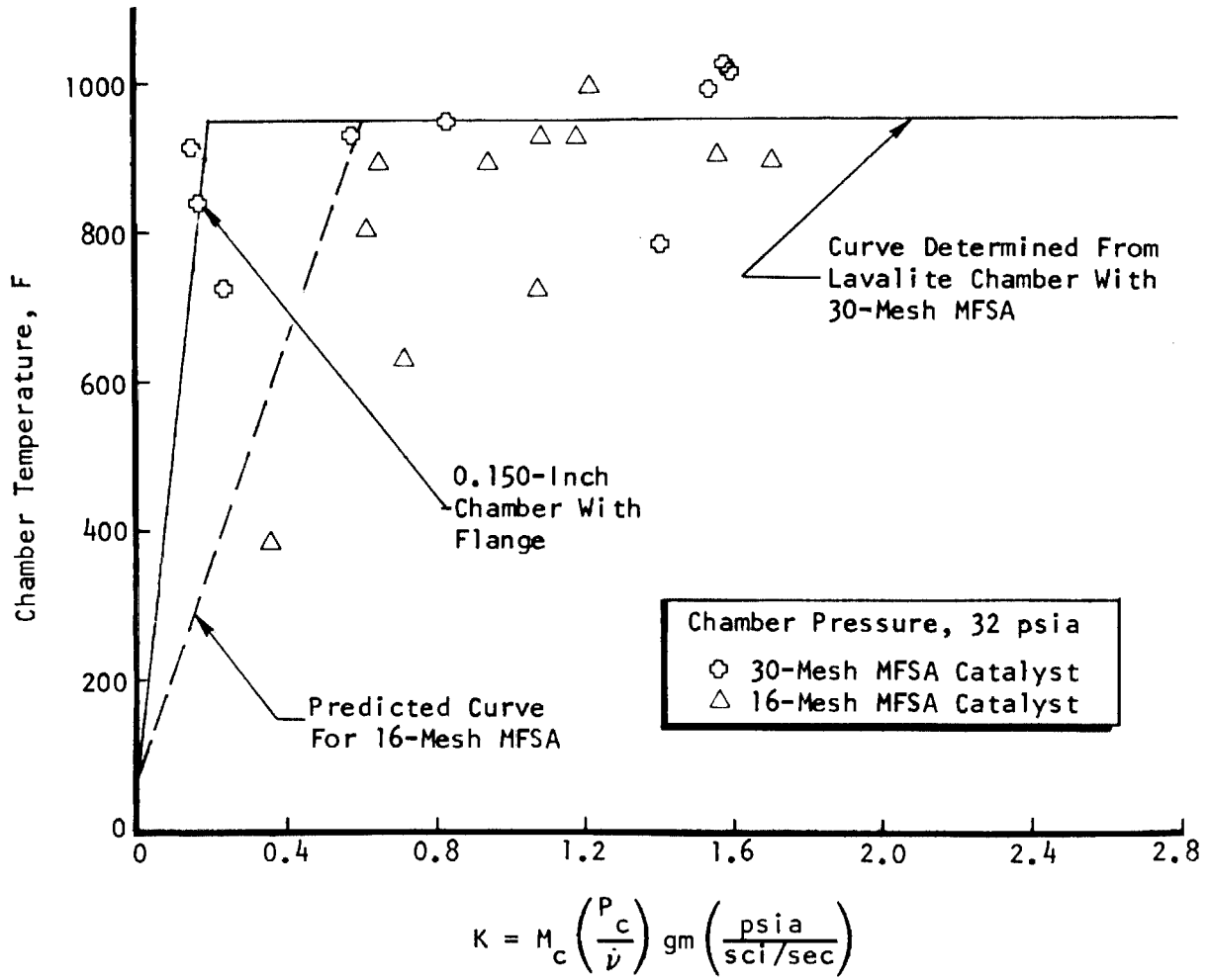

Figure 21. Thermal Response of 0.150- and 0.224-Inch-ID Stainless-Steel Chambers (MFSA Catalyst)

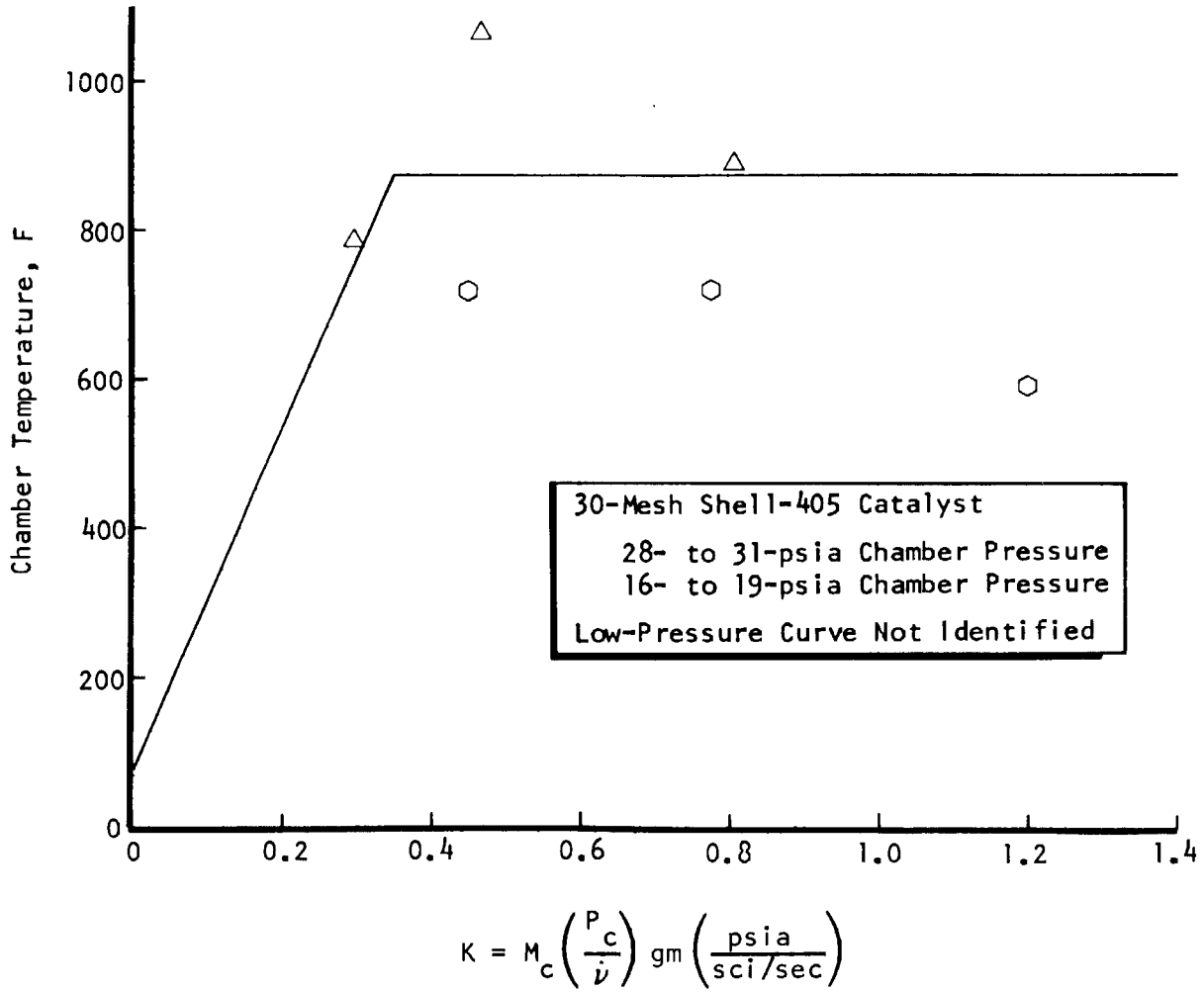

Figure 22. Thermal Response of 0.1-Inch-ID Lavalite Chamber (30-Mesh Shell-405 Catalyst)

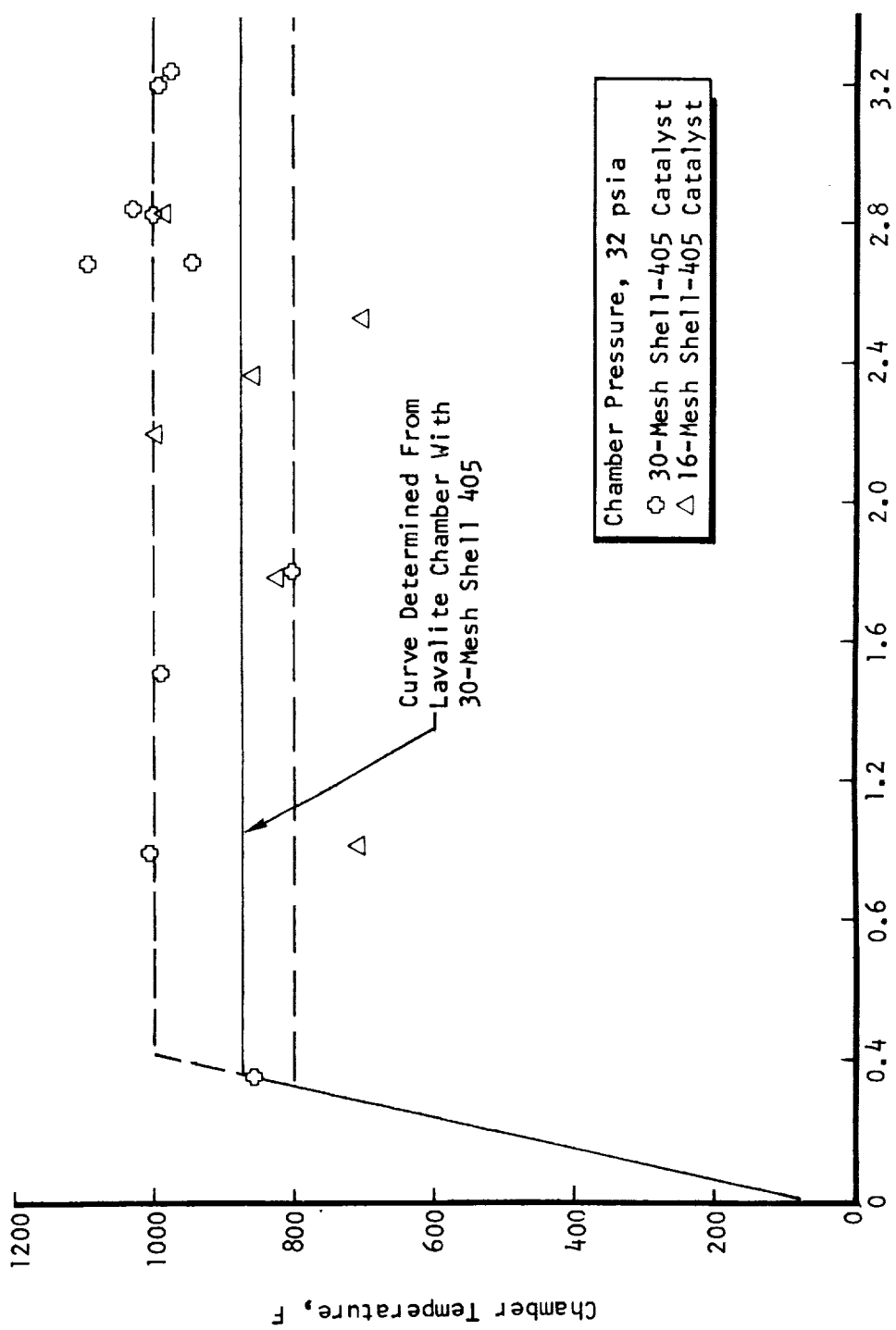

Figure 23. Thermal Response of 0.150- and 0.224-Inch-ID Stainless-Steel Chambers (Shell-405 Catalyst)

In conclusion, it appears that the MFSA is more reactive per unit mass than the Shell-405, and the smaller catalyst pellets are about twice as reactive per unit mass as the larger catalyst pellets. For the 30-mesh MFSA catalyst the optimum K value is 0.24. This implies that with a flowrate of 1.8 sci/sec, 0.015 and 0.03 grams of catalyst are needed at 30 and 15 psia, respectively.

Test results of platinum and platinum-rhodium wires evaluated as potential catalyst retainers show that the platinum-rhodium combination is catalytically inactive with Tridyne. There was no attempt to try to activate the wire by applying heat or special cleaning processes. The use of 0.5-mil wire as a retainer at the injector end of the chamber may be advantageous. This wire is lighter than the screens presently in use and possibly could more effectively prevent the catalyst from moving around the chamber than the screens. Since the platinum-rhodium wire was catalytically inactive, nickel wire, which is less expensive, would be preferable as a retainer material.

Thermal preconditioning tests were conducted with a Tridyne flowrate of 1.8 sci/sec at chamber pressures of 15 and 30 psia and at catalyst bed temperatures of 70, 500, 1000, and 1500 F. A 0.150-inch chamber, modified to incorporate a flange mounting, was wound with 3-mil insulated chromel wire, which was used as a heater. The chamber was filled with 0.0214 grams of 30-mesh MFSA catalyst and operated at 16 psia. The heater operated satisfactorily at 500 F; however, when it was heated to 1000 F in a vacuum, the wire developed a hot spot and burned out, necessitating rewinding. Tests were then conducted in a vacuum at initial catalyst bed temperatures as high as 966 F before the tests were terminated when heater wire insulation began breaking down. Results of tests 60 through 71 are tabulated in the Appendix, which includes initial and steady-state temperatures, chamber pressure, and thermal time constant.

On the average, the thermal time constants for chamber pressures of 29 and 17 psia are about 1 and 2 seconds, respectively. The depressurization time constants were found to be about 11 milliseconds.

It is not clear why test 62 has such an unusually large thermal time constant as compared to the other tests. It may be attributed in some way to system startup, although this same phenomenon did not occur in test 66 after the chamber was rewound. There is a possibility that some grease or oil, which may have been accidentally left on the chamber during fabrication, was vaporized during test run 61.

Transient temperature and pressure characteristics for these tests are shown in Fig. 24 through 27. It can be seen that for approximately equivalent initial bed temperatures, the high-pressure tests have faster temperature responses than the low-pressure tests. Also, as would be expected, higher initial bed temperatures produce higher steady-state temperatures.

Tests were also conducted with a heated steel chamber containing 0.053 grams of 30-mesh Shell-405 catalyst. The maximum catalyst bed temperature attained was 1600 F. Chamber temperatures were recorded by means of an external surface thermocouple. Since the chamber internal thermocouple was open, temperature response data were not obtained. The recorded results did show that the catalyst was active after eight 30-second tests with catalyst bed temperatures at least 1600 F and possibly higher.

A preliminary analysis of heater power was performed for a 0.225-inch-ID lightweight chamber with a 0.045-inch-OD supply tube. The power requirements calculated for the lightweight model are compared in Fig. 28 with the experimental results obtained from a 0.150-inch lightweight chamber with a 0.062-inch-OD fuel inlet tube. The 0.150-inch chamber had greater heat losses than the 0.225-inch model. This can be attributed to more heat being dissipated through the larger fuel inlet tube in the experimental 0.150-inch chamber.

At the completion of Task I tests, calculations were performed to estimate the surface and gas temperature for the lightweight model without external heating. It was found that with a complete Tridyne reaction the chamber surface temperature should be about 980 F and the exit gas temperature about 1400 F. Total heat loss was computed to be about 3.2 watts.

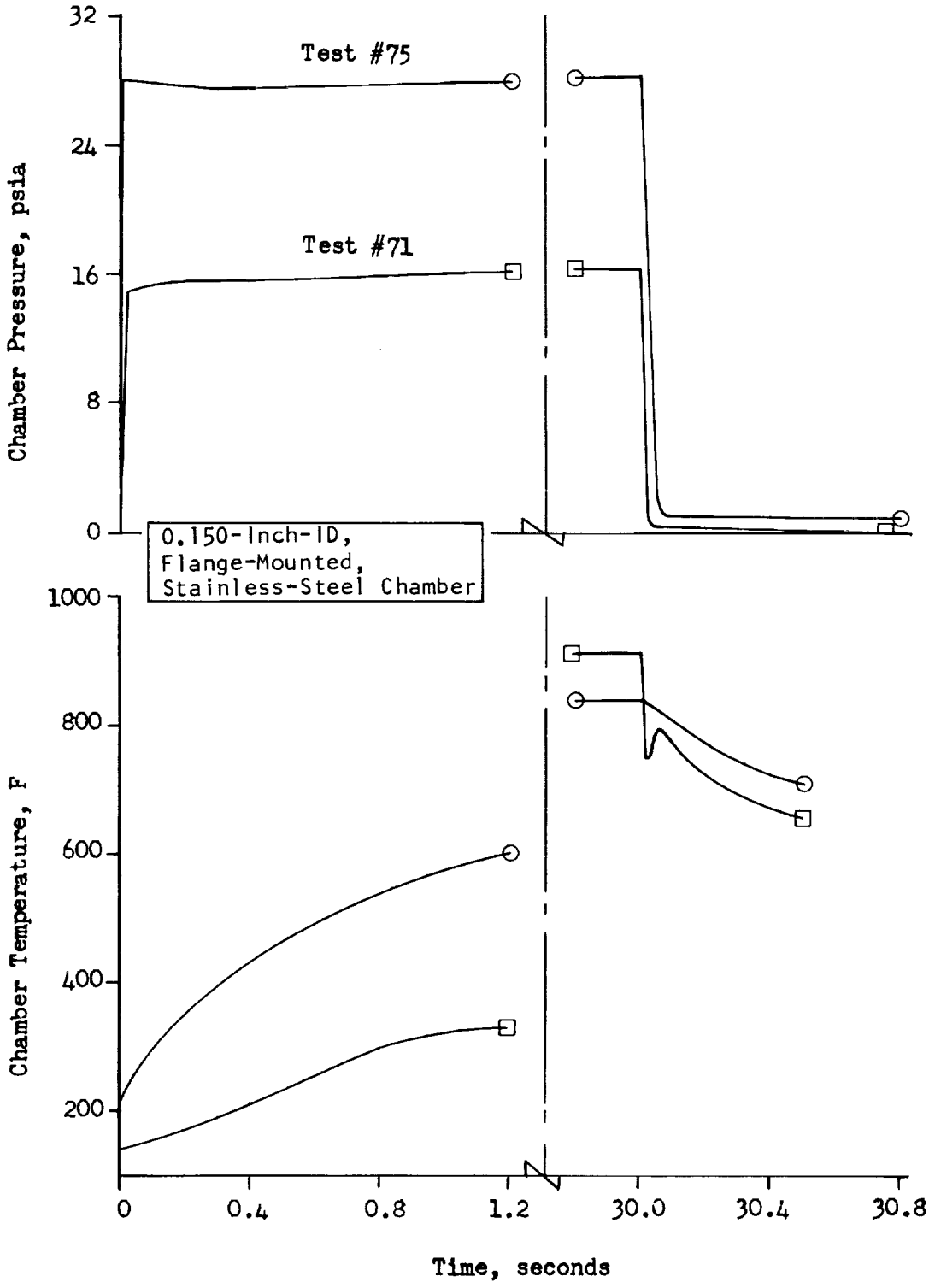

Figure 24. Chamber Pressure and Temperature Versus Time (Tests 71 and 75)

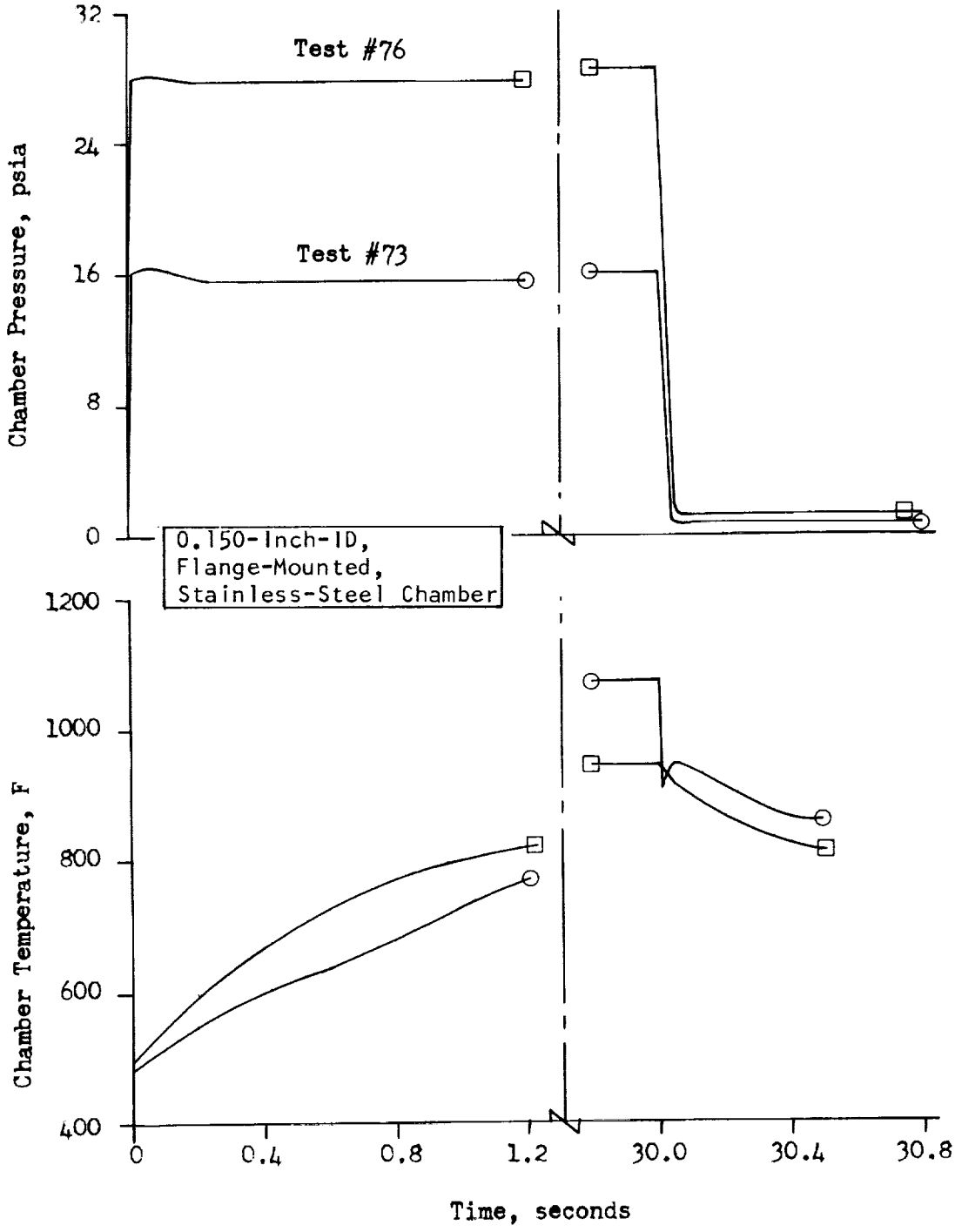

Figure 25. Chamber Pressure and Temperature Versus Time (Tests 73 and 76)

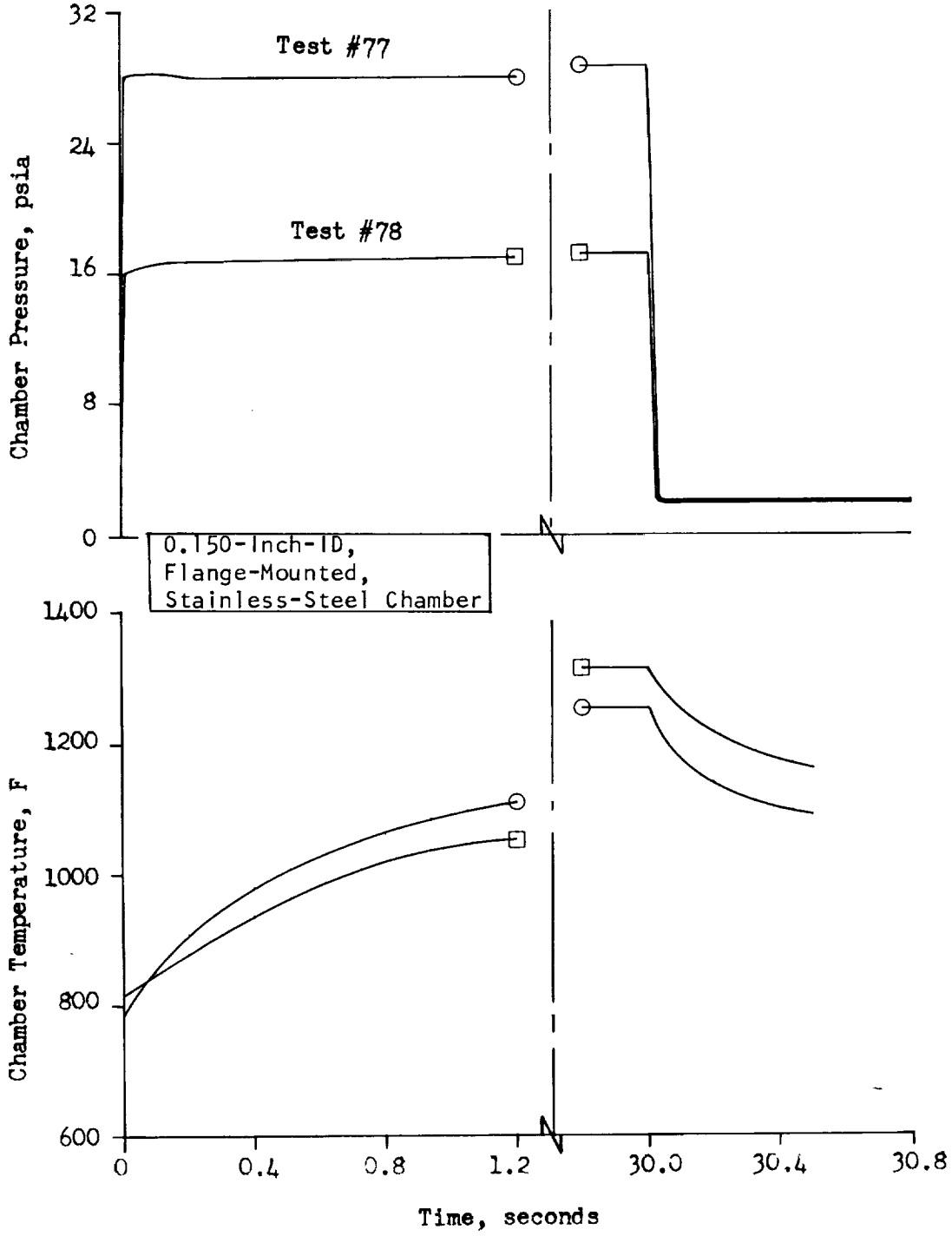

Figure 26. Chamber Pressure and Temperature Versus Time (Tests 77 and 78)

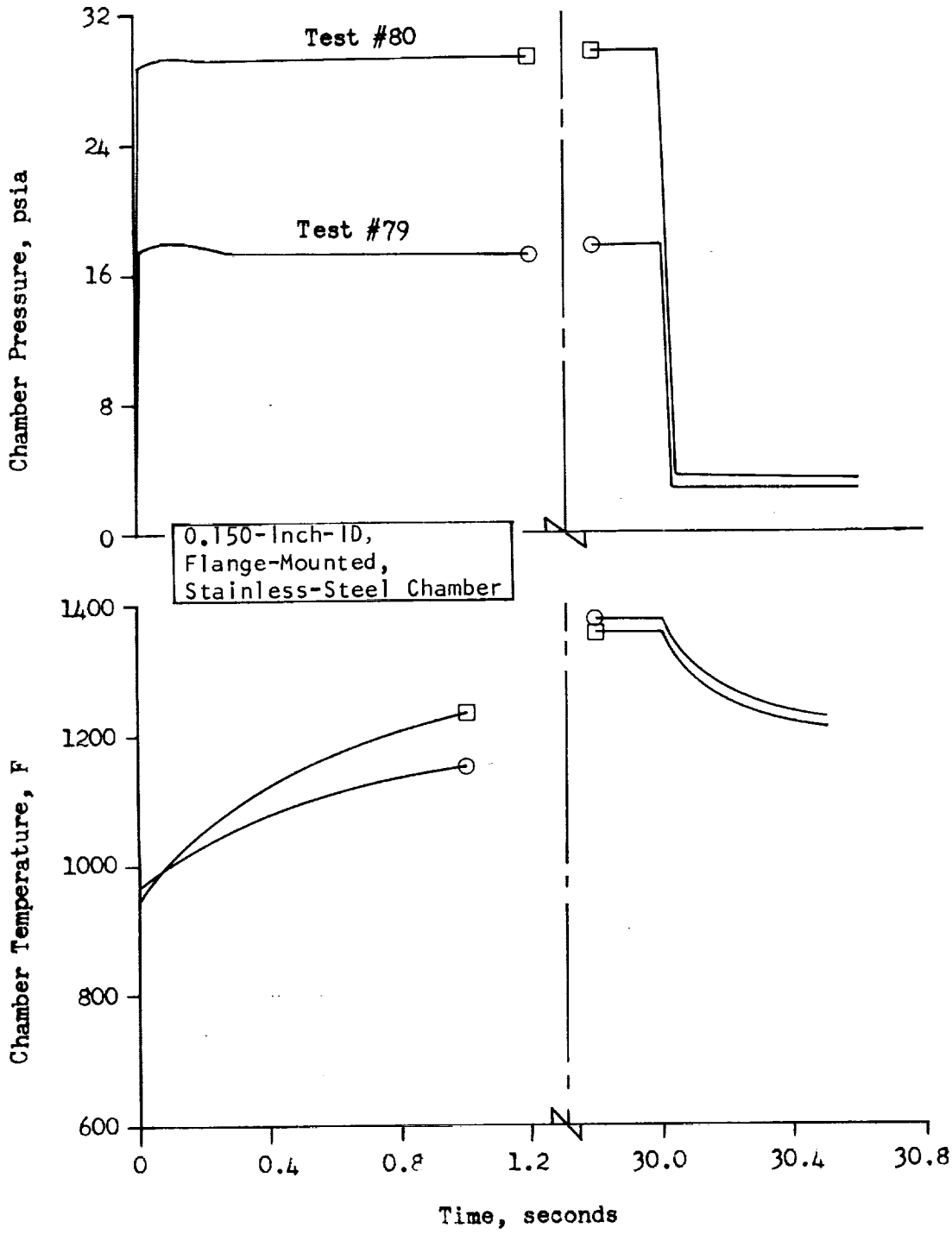

Figure 27. Chamber Pressure and Temperature Versus Time (Tests 79 and 80)

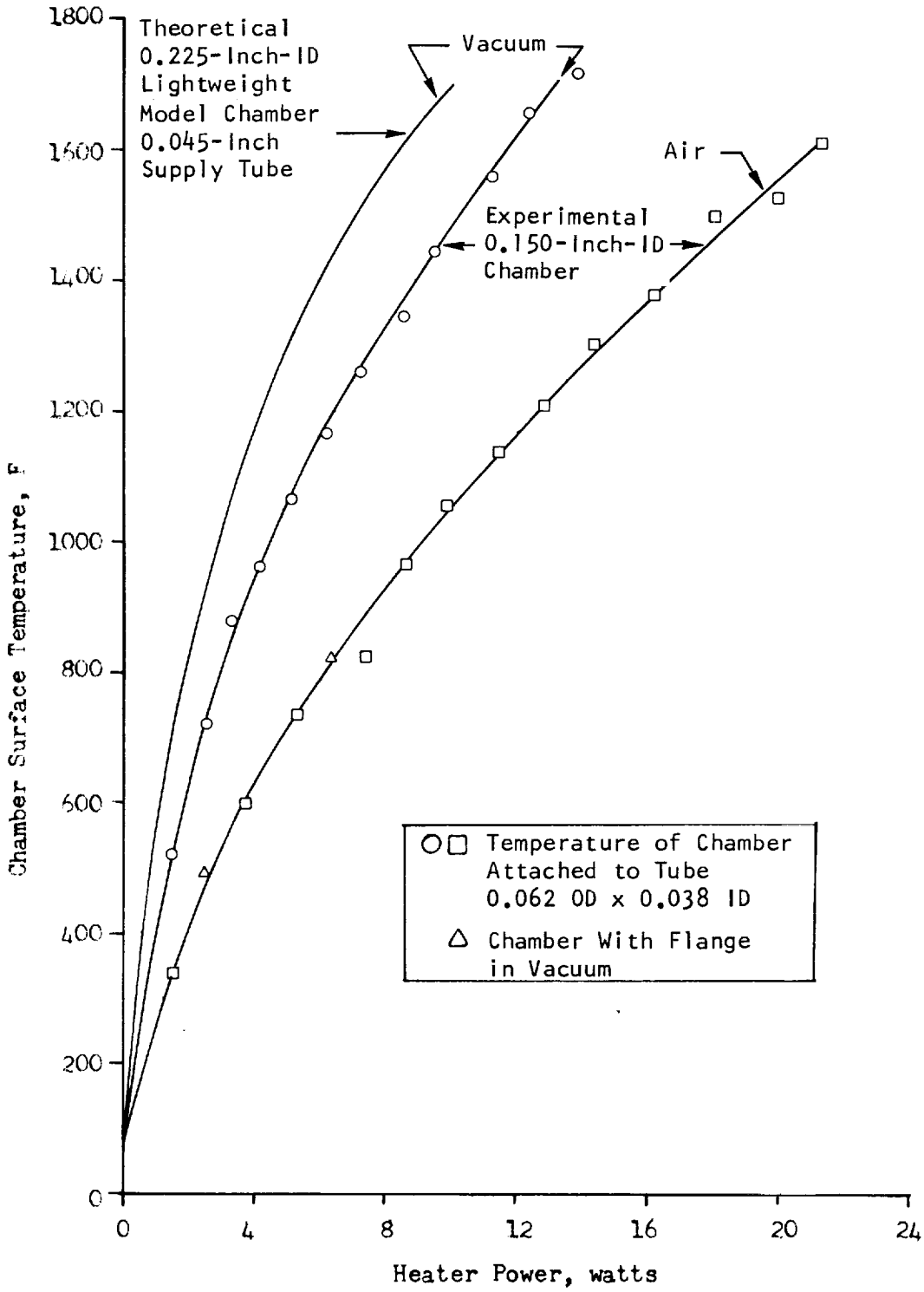

Figure 28. Chamber Surface Temperature Versus Heater Power

Pressure dynamics were also analytically investigated for the chamber design in Task IV. None of the chambers fired in Task I had a small enough depressurization time constant to satisfy the performance specifications. The flightweight chamber preliminary design was shown to have a void volume less than one-half that of the Task I chamber and was predicted to provide improved pressure-response characteristics.

System geometry iterations were performed to provide ΔP data for Task IV. Chambers with 0.255-, 0.150-, and 0.100-inch ID's and containing 0.02 to 0.03 grams of catalyst were tested. Approximate pressure drops of 1 psi were observed across the catalyst beds at 30-psia chamber pressure. Therefore, the Task IV design criteria were based on minimizing chamber heat losses since catalyst bed pressure drops were shown to be insignificant.

The instrumentation and techniques for data measurements in Task IV were developed. Microminiature thermocouples with 1-mil beads and thermal time constants of less than 1.0 millisecond were used in both Tasks I and IV. A 50-psia pressure transducer was used to measure chamber pressure. The time constant for the transducer was calculated to be less than 0.1 millisecond. A rotameter accurate to within ±4 percent measured steady-state flowrates, and a sonic venturi was used as a flowmeter in the pulse-mode operation of Task IV.

Temperature Response Analysis

Temperature data were correlated by means of thermal time constants to facilitate configuration comparisons and to establish the temperature-time curve form for analytical performance projections. The time constant is defined as the time required for the temperature to increase from the initial value to 63 percent of the final steady-state temperature.

The theoretical temperature response can be estimated by means of a heat balance for the catalyst bed. The catalyst bed was assumed to be in thermal equilibrium with the gas, and the gas was assumed to react instantaneously

on the catalyst's surface. If an incremental mass for the screens and chamber is included in the heat balance, the equation becomes:

$$\bar{\omega}\ (-\Delta H_r)\ dt = \bar{\omega}\ C_p\ (T-T_o)\ dt + M_c\ C_{p_c}\ dT + M_e C_{p_e}\ dT$$

where

$\bar{\omega}$ = average Tridyne flowrate, lb/sec

ΔH_r = Tridyne heat of reaction = $C_p\ (T_f - T_i)$, Btu/lb

M_c = catalyst mass, pounds

M_e = mass due to the screens and chamber, pounds

C_p = heat capacity of Tridyne, Btu/lb-R

C_{p_c} = catalyst heat capacity, Btu/lb-R

C_{p_e} = effective heat capacity of the M_e increment, Btu/lb-R

T = outlet temperature of Tridyne,R;also assumed equal to catalyst bed temperature under assumption of thermal equilibration

T_i = initial temperature of Tridyne, R

T_f = adiabatic flame temperature of Tridyne, R

T_o = initial temperature of catalyst, R

Integrating the above equation from T_o to T and rearranging, the Tridyne outlet temperature is:

$$T = T_f - (T_f - T_o)\ e^{-t/\tau} \qquad (1)$$

where the time constant term is $\tau = (M_c\ C_{p_c} + M_e\ C_{p_e})/\bar{\omega}\ C_p$. (The curve form is illustrated in Fig. 29). The equation neglects both the effects of a temperature gradient within the catalyst and the heat losses.

Heat losses reduce the steady-state chamber temperature to a value below the flame temperature. By replacing the flame temperature in Eq. 1 with

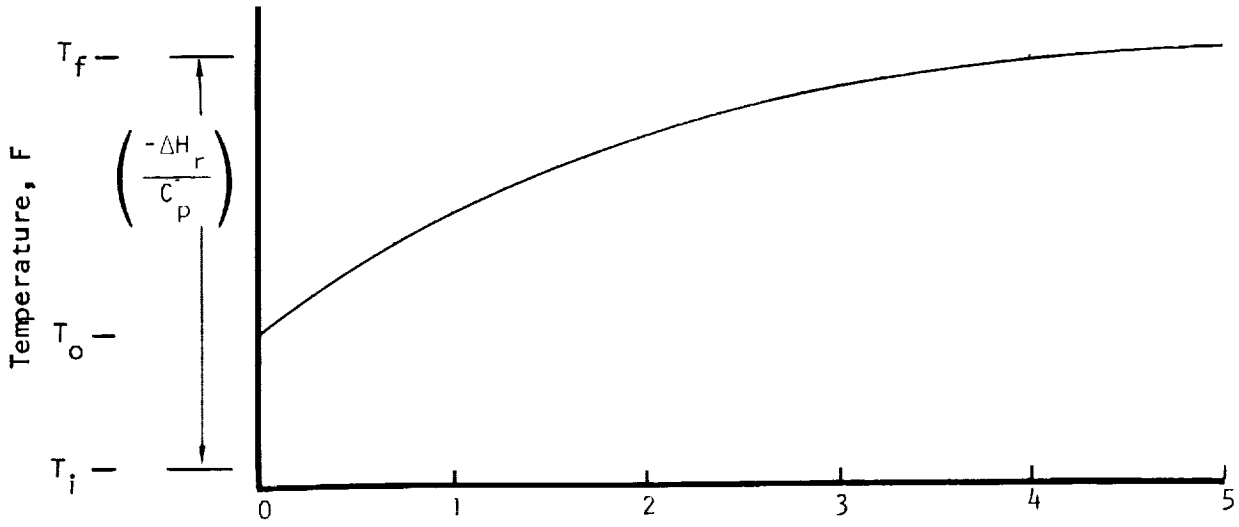

Figure 29. Typical Temperature Response Characteristics for a Catalytic Reactor

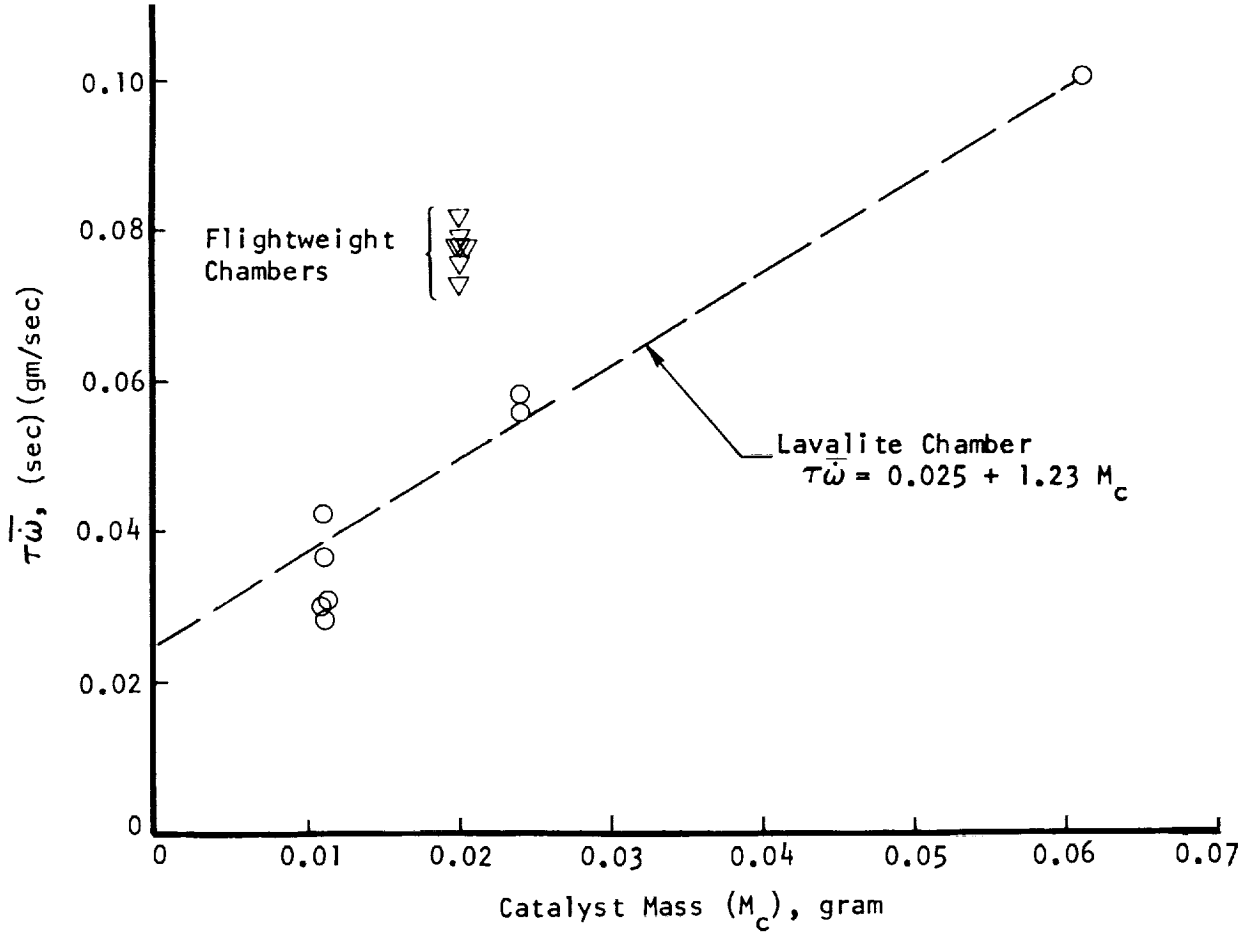

Figure 30. Thermal Time Constant Parameter Versus Catalyst Mass

the steady-state temperature, an estimate of the temperature response allowing for nonideal effects can be obtained. Equation 1 then becomes

$$T = T_{ss} - (T_{ss} - T_o)\, e^{-t/\tau} \qquad (2)$$

The time constant τ can be determined experimentally since $\tau = t$ when the temperature reaches $T = T_{ss} - 0.37\,(T_{ss} - T_o)$.

To investigate the validity of this analysis, the experimental value of $\overline{\tau\dot{\omega}}$ was plotted as a function of M_c in Fig. 30 for the Lavalite chamber. The resulting curve appears to be a linear function of catalyst mass as predicted. The intercept at $M_c = 0$ indicates that $M_e(C_{pe}/C_p) = 0.025$ gm. If the extra mass has the same heat capacity as the Tridyne, then $M_e = 0.025$ gm, which may be optimistic for a flightweight chamber but appears to be reasonable for the low thermal capacitance Lavalite material. Computed time constants for the major test configurations are shown in the run summary (Appendix).

TASK IV: FLIGHTWEIGHT THRUSTER TESTS

The objective of Task IV was to evaluate the characteristics of flightweight Tridyne thrusters in both pulse-mode and steady-state operation. The tests were to provide performance data and information on thermal- and pressure-response characteristics and to demonstrate the feasibility of flightweight thrusters.

Equipment

The test system (shown schematically in Fig. 31) consists of a rotameter, a sonic venturi flowmeter, a flightweight chamber, and a thermocouple placed in the exit nozzle. Chamber details are presented in the Design section.

Two engine configurations were employed in the tests. One was instrumented with a thermocouple in the chamber wall; the other had a pressure probe installed in the chamber upstream of the nozzle throat. Instrumentation

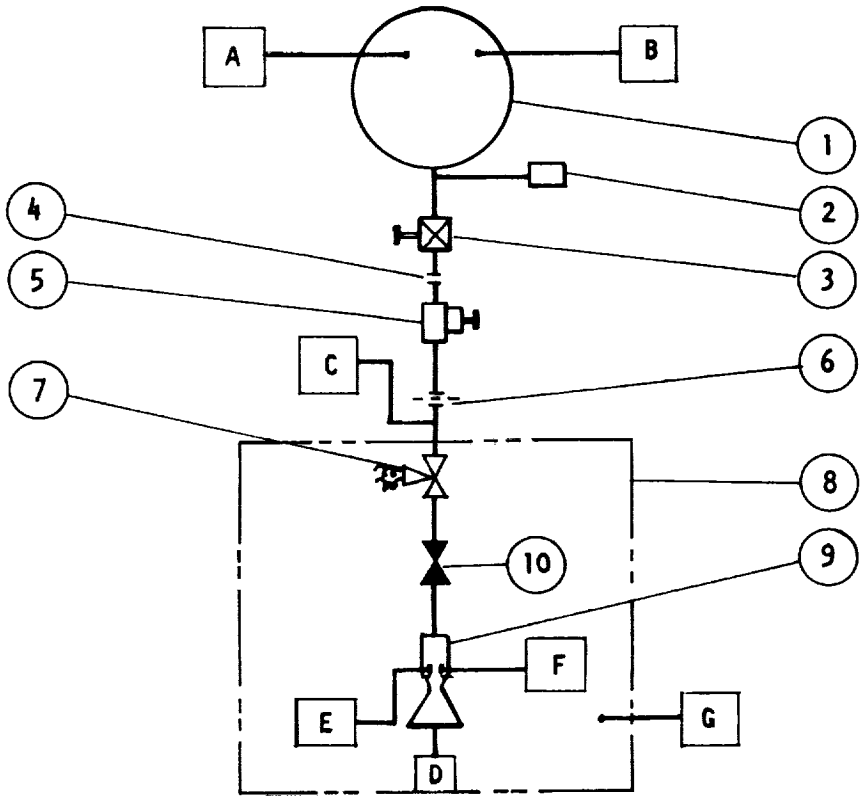

1. 500-PSI PRESSURE VESSEL
2. FILL VALVE
3. SHUTOFF VALVE
4. DISCONNECT
5. HAND-OPERATED PRESSURE REGULATOR
6. ROTAMETER
7. SOLENOID VALVE
8. VACUUM TANK
9. REACTOR OR THRUSTER
10. SONIC VENTURI

A. PRESSURE TRANSDUCER (0 TO 1000 PSI)
B. THERMOCOUPLE (0 TO 100 F)
C. PRESSURE TRANSDUCER (0 TO 50 PSI)
D. THERMOCOUPLE (0 TO 1500 F)
E. THERMOCOUPLE (0 TO 1500 F)
F. PRESSURE TRANSDUCER (0 TO 50 PSI)
G. PRESSURE TRANSDUCER (0.1 TO 1000 MILLIMETERS)

Figure 31. Flightweight Thruster Test Schematic

mounts were designed to record representative transient response rates but were only partially successful as demonstrated by test data. The area of the base of the pressure transducer is 132 percent of the thruster cross-sectional area and the pressure probe volume caused substantial delays in thrust rise and decay times. The thermocouple provided reasonably exact wall temperature transients but was of questionable value for evaluating gas temperatures. Further details of the operational characteristics are presented with the test data.

Experimental results showed that the exit nozzle thermocouple always read lower than the chamber thermocouple when the chamber was hot. This was attributed to the low gas density in the nozzle. The thermocouple also produced generally inconsistent readings and was quite sensitive to its orientation in the nozzle; therefore, these data are not presented.

The venturi shown in the schematic diagram was flow calibrated and used to record flowrates during pulse-mode operation. The venturi flow is sonic at low chamber temperatures as the chamber exit throat area is larger than the venturi throat area (area ratio 1.43:1) permitting an approximate chamber/venturi total pressure ratio of 0.70 with ambient temperatures throughout the system. This value includes a molecular weight adjustment for the Tridyne reaction.

The venturi will maintain sonic flow to a total pressure ratio (P_{T_1}/P_{T_2}) across the throat of 1.3:1. This means that the venturi mass flow is constant and a direct function of the inlet pressure. However, at constant mass flow, the chamber pressure increases as temperature is increased. This may be illustrated by the compressible flow equation:

$$\dot{\omega} = \frac{P_T(P/P_T)\dot{m}A}{\sqrt{T}}$$

where

$\dot{\omega}$ = mass flow, lbm/sec

P_T = total pressure, psia

P = static pressure, psia

$\dot{m} = g\sqrt{\gamma/R}\, M\left[1 + \frac{\gamma-1}{2} M^2\right]^{0.5}$; g = 32.174, M = 1,

$R = 1545 \frac{32.174}{\text{molecular weight}}$

A = geometric throat and discharge coefficient, $in.^2$

T = total temperature, R

At a known inlet temperature and gas composition, the mass flow equation reduces to the expression:

$$\dot{\omega} = \text{constant} \times P_T$$

This permits the mass flow to be measured very precisely by recording the total pressure at the venturi. In the tests, the venturi pressure was established by a wall static measurement at a station with an A/A^* ratio of 8.2:1, resulting in a static/total pressure ratio at the station of 0.9965. However, as the chamber gas becomes hot during combustion, it is seen from the mass flow equation that the chamber pressure will increase by the approximate ratio of $1/T^{0.5}$. The parameters P/P_T and $\dot{m}$ vary only a small amount with temperature. Values of $\dot{m}$ and P/P_T versus temperature are shown in the Performance Analysis section. Consequently, the engine chamber pressure increases to the point at which the venturi unchokes (chamber pressure/venturi pressure ratio of 0.77). The chamber then functions as a conventionally supplied thruster, and mass flow varies as a function of chamber temperature. At this condition, thrust changes very little over the temperature range as discussed in the Performance Analysis section. The advantage of the venturi is in being able to record mass flow at the chamber inlet and thus identify, with reasonable accuracy,

the pulse performance of the chamber by mass continuity relationships. A flight system would not include venturis but would be designed as a low ΔP system with a nearly constant chamber pressure.

Steady-State Performance

Steady-state tests were conducted with gaseous nitrogen and Tridyne, the nitrogen tests providing a baseline for the Tridyne tests. They also made it possible to check the system calibration for constant temperature flow conditions. The long-duration Tridyne tests were conducted to determine the thermal time constant and to record the steady-state temperature. The steady-state Tridyne tests were conducted at line pressures between 23.8 and 48.1 psia, with the sonic venturi unchoked. The results of the long-duration tests are presented in the following sections.

Temperature Response

A flightweight thruster with an integral thermocouple was used to evaluate the thermal response of the chamber. The installation was intended to permit the thermocouple tip to approach free stream temperature and thus permit characterization of the thruster thermal transients. After several test runs and data analyses, it was determined that the thermocouple would provide excellent chamber wall temperature measurements but would not approach true gas temperatures. This is illustrated by the recorded thermocouple output (millivolts) during a pulse interval (Fig. 32). The temperature trace increases from 129 to 164 F during the 40-millisecond on time (measured rate 1000 deg/sec). The rate of decrease is also extremely fast at the pulse termination, indicating a rapid energy loss from the thermocouple juncture. The indicated rate of temperature change is shown to have an increasingly greater slope ($\Delta T/\Delta t$) as the thruster temperature increases (Fig. 32 through 34). These values are listed in Table 1. The slope increase is consistent with the assumption that the maximum gas-chamber temperature difference occurs at peak chamber temperatures; i.e., at low chamber temperature more of the available Tridyne energy is absorbed by the catalyst and chamber, at high chamber temperatures very little is absorbed (steady-state chamber heat loss).

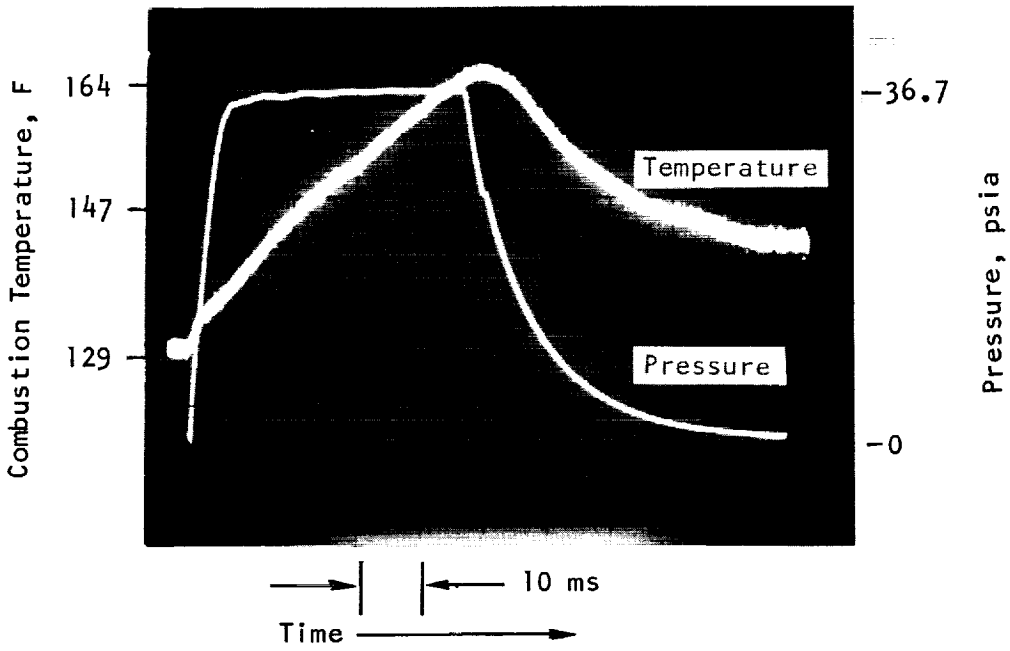

Figure 32. Temperature and Pressure Response (ΔT = 35 F/40 ms)

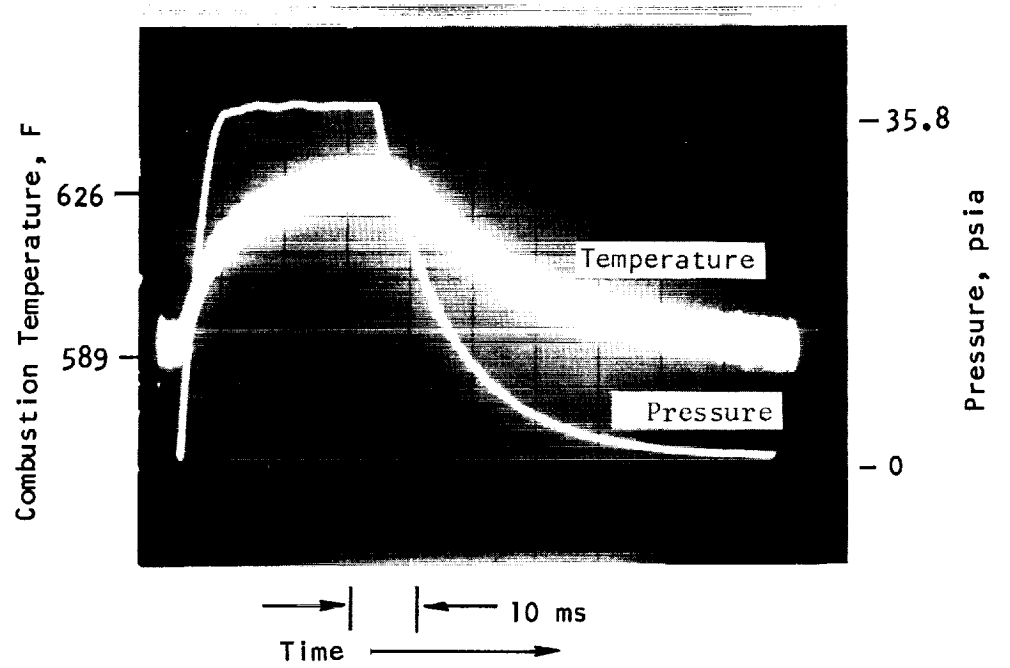

Figure 33. Temperature and Pressure Response (ΔT = 37 F/30 ms)

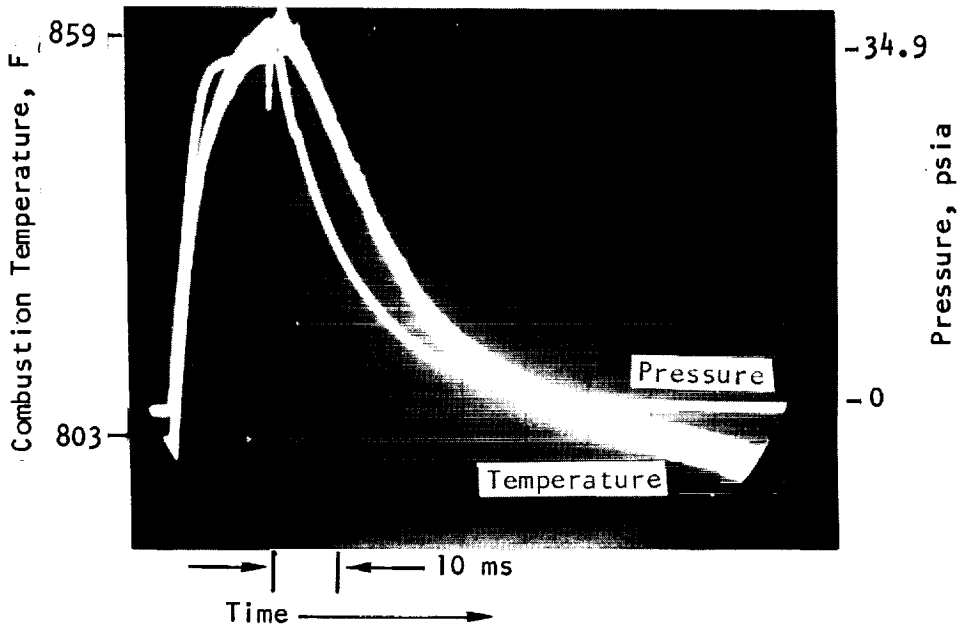

Figure 34. Temperature and Pressure Response (ΔT = 56 F/20 ms)

TABLE 1

EFFECT OF TEMPERATURE CHANGE ON ΔT/Δt

P_v, psia	$T_{initial}$, F	T_{final}, F	Run Duration, milliseconds	ΔT/Δt, F/ms	Rate of Change, degrees/second
36.7	129	164	40	20/20	1000
35.8	589	626	30	24/20	1200
36.7	126	161	40	21/20	1050*
34.9	803	859	20	56/20	2800

*Insulated

Long-duration runs, presented later in this section, show that the Tridyne temperature varies only a small amount over a 40-millisecond period (possibly 2 F) near maximum temperature. The chamber wall temperature change is also shown to be negligible over this interval. Referring again to Fig. 33 and 34, which are short pulses following relatively long-duration operations, it is a logical deduction that the indicated $\Delta T/\Delta t$ rate is the thermocouple transient response at nearly steady-state gas temperatures and not a reflection of gas temperature changes. The maximum temperature differential measured between the chamber steady-state value and the thermocouple-indicated temperature is about 65 F. This is considered to be substantially less than the actual difference because of the rapid thermocouple temperature decay at shutdown. An analytical determination of the probable true gas temperature is presented in the Thermal Analysis section.

Long-duration thermal transients were recorded to evaluate heat loss rates from the thrust chamber. Following a period of steady-state operation, the thermocouple trace was recorded from thrust termination over a 5-second period to determine the heat loss rate (Fig. 35). The initial drop at peak temperature is the equilibration of the thermocouple tip with the chamber wall followed by a gradual temperature decay at the initial rate of about 98 deg/sec. This rate coupled with the thruster thermal capacitance shows an energy decrease of 54×10^{-4} Btu/sec, which is 17.7 percent of the Tridyne reaction enthalpy. A similar temperature-decay recording shown in the Thermal Analysis section is used for predicting flight-type thruster module performance.

Thermal Characterization

Long-duration tests were conducted to determine the thermal time constant for the thruster. In these tests, the Tridyne gas was allowed to flow through the chamber for about 10 seconds, which is the time required for the chamber to heat up to a constant temperature. The thermal time constant is defined as the time required for the temperature to increase from

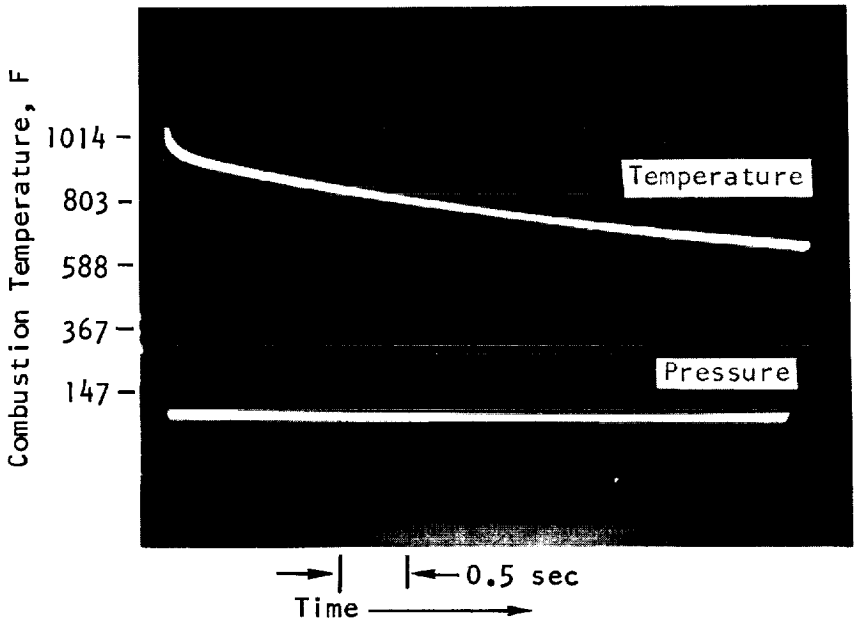

Figure 35. Thruster Temperature Decay Characteristics

its initial value to 63 percent of its steady-state value. If the system is first order with respect to temperature, the temperature will reach 86 percent of its steady-state value at two time constants and 95 percent of its steady-state value at three time constants.

Thrust chamber temperature changes with time were recorded with the chamber initial temperature near ambient. A typical test is presented in Fig. 36. The temperatures are thermocouple-recorded temperatures and are above the actual thruster wall temperature. The curve illustrates the temperature increase with time to approximately steady state. Since the inlet venturi becomes unchoked at a chamber temperature of 136 F, the data are with an unchoked venturi, and chamber mass flow decreases from 3.80 sci/sec at 136 F to 2.85 sci/sec as the chamber reaches 991 F. These flowrates are about 10 percent above the target flowrate of 3.40 sci/sec at 136 F and 30 psia, but are representative of design-point operation. The curve form is used in predicting thruster gas temperatures over the design operational temperature range.

Thermal time constants were computed from the temperature-response data of the long-duration runs listed in Table 2. The values were found to vary from 1.46 to 2.94 seconds, depending on the venturi pressure. The time constant (τ) was plotted in Fig. 37 as a function of the venturi pressure (P_v) in the form $100/P_v$.

The time constant equation previously presented is:

$$\tau = (M_c C_{p_c} + M_e C_{p_e})/\dot{\bar{\omega}}\, C_p$$

where all terms except the flowrate are constant. As can be seen from Fig. 37, the experimental data are described by:

$$\tau = 67.5/P_v$$

since

$$\dot{\omega} = k\, P_v$$

where k is a constant, the experimental data are in agreement with the theoretical prediction.

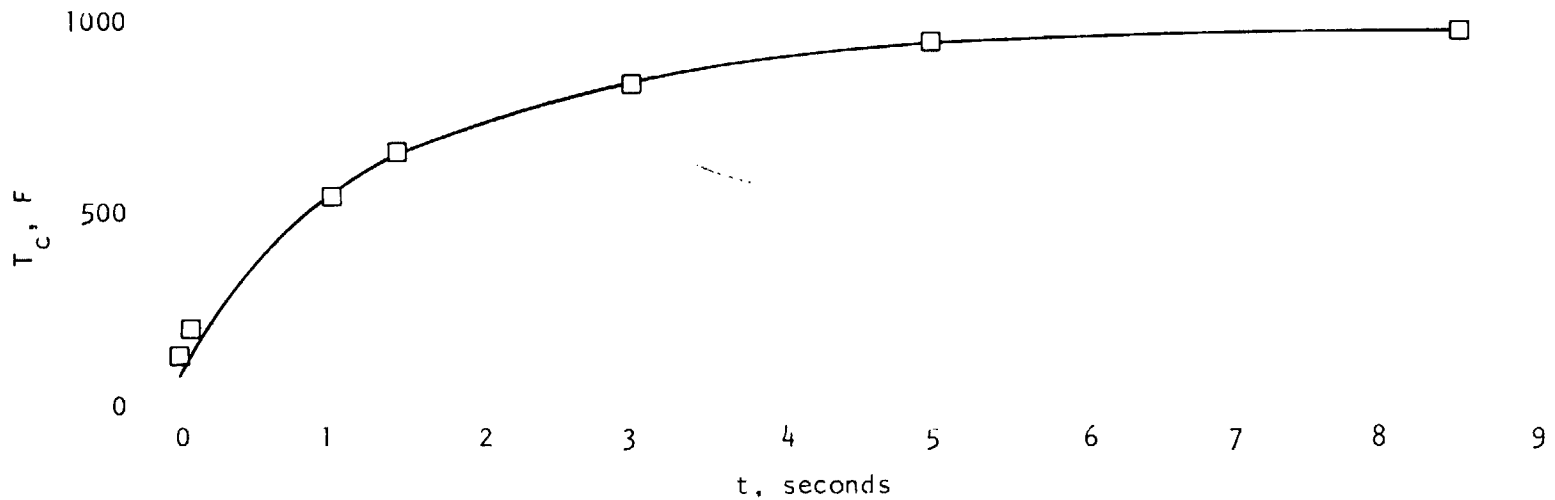

t	=	0.1	t	=	10.1 sec
$\dot{\omega}_v$	~	3.80 sci/sec	$\dot{\omega}_r$	=	2.85 sci/sec
P_v	~	47.7 psia	P_v	=	47.7 psia
P_c	~	38.5 psia	P_c	~	43.2 psia
T_c	~	136 F	T_c	=	991 F
P_v/P_c	~	1.30			

Figure 36. Temperature Time Transient for Run 59

TABLE 2

SUMMARY OF TASK IV THERMAL RESPONSE DATA

Run Number	P_v, psia	$\dot{\omega}_r$, sci/sec	$T_{initial}$, F	T_{final}, F	Run Duration, seconds	τ_t, seconds	Insulation	Remarks
57	23.1	1.32	93	955	9.8	2.94		
58	33.1	2.01	114	987	12.0	2.07		
59	47.7	2.85	136	991	12.0	1.46		
60	47.6	2.82	136	1012	~15.0	1.46		
108	37.5	--	402	1289	20.0	1.74	Yes	Venturi and chamber hot initially
109	37.9	2.35	93	1021	17.0	1.85	Yes	
110	37.5	2.35	134	1027	12.3	1.74	Yes	

NOTES: P_v = venturi pressure, psia

$T_{initial}$ = initial chamber temperature, F

T_{final} = final chamber temperature, F

τ_t = thermal time constant, seconds

$\dot{\omega}_r$ = rotameter flowrate, sci/sec

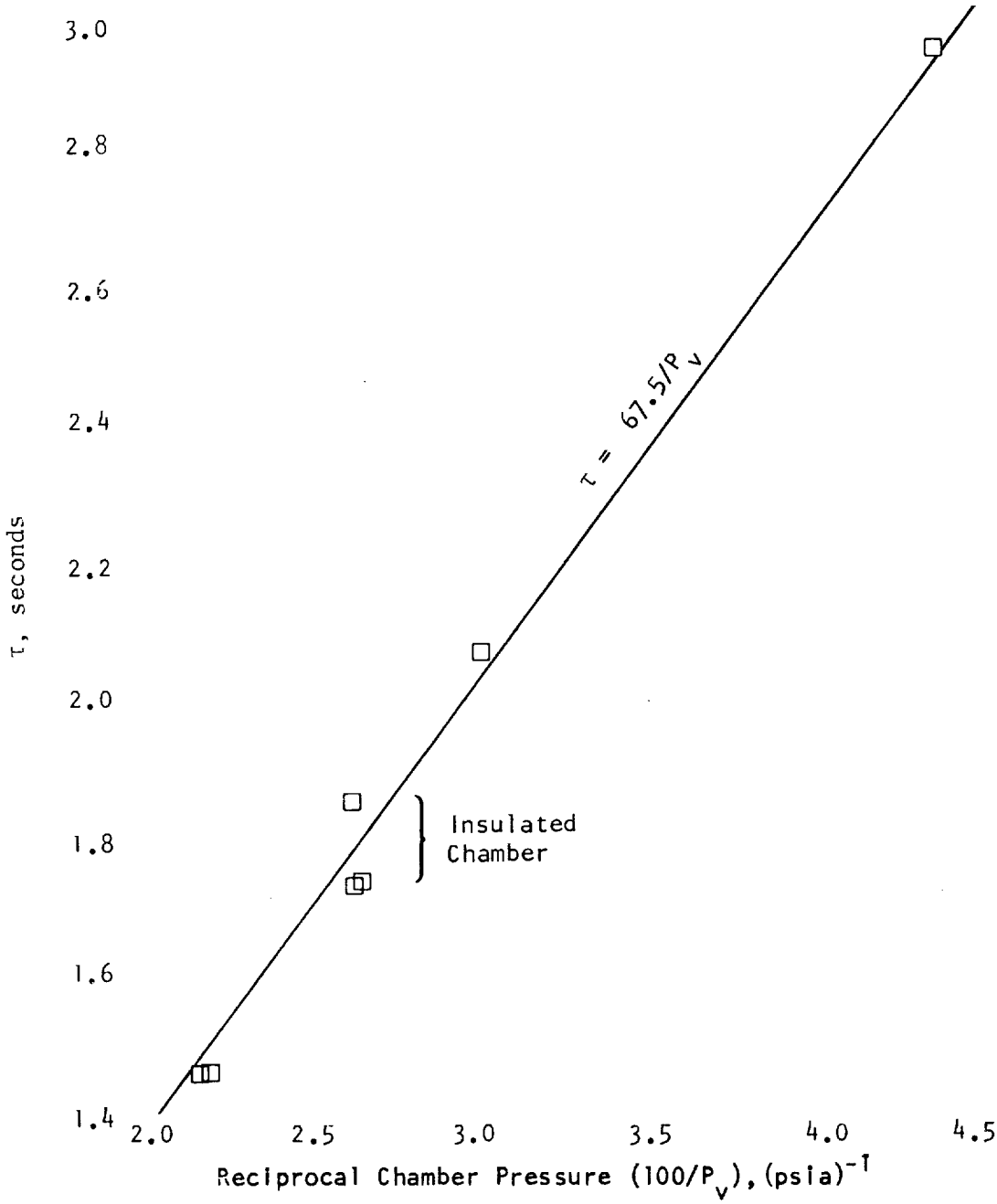

Figure 37. Thermal Time Constant Versus Chamber Pressure Parameter Flightweight Thrusters

To compare the thermal characteristics of the flightweight chamber with the Lavalite test configuration, the term $\tau\dot{\omega}$ is plotted in Fig. 30 as a function of the catalyst mass (0.020 gram). It can be seen that the $\tau\dot{\omega}$ data for the Task IV chambers are about 50 percent higher than for the Task I Lavalite chamber. The higher time constant is attributed to an increase in the effective mass (M_e). This is possibly due to the higher thermal capacitance of the nickel in the flightweight chambers as compared to that of Lavalite.

Insulation Effects. A chamber was embedded in an insulating blanket to evaluate the effects of insulation on the chamber thermal behavior. Figure 38 illustrates the temperature response with the chamber initially at room temperature and wrapped with insulation. Because the results are identical to those of Fig. 32, it may be concluded that the insulation does not influence the temperature-response characteristics with the chamber initially at room temperature. These data substantiate the long-duration tests which revealed that the insulation did not increase the thermal time constant or the extra thermal mass (M_e) of the system. This implies that the heat transferred from the chamber by radiation and conduction to the insulation is negligible in comparison to the heat absorbed by the chamber and the inlet line.

Some data on the thermal behavior of the chamber at high temperatures were provided during the insulation tests by run number 108 (Table 2). The temperature-time history is shown in Fig. 39 together with runs 109 and 110. A series of pretest checkout and instrumentation calibration firings were made prior to run 108, which caused the chamber and inlet venturi to reach near equilibration at a 400 F temperature. The run was then conducted at an initial temperature of 402 F, which increased to 1331 F at the run termination. Subsequently recorded temperature traces indicate that the thermocouple tip does not attain actual gas temperatures because of its close proximity to the wall because its shield is integral with the wall structure. Consequently, the free stream gas temperature may have approached the design operational temperature of the Tridyne, i.e., 1500 F.

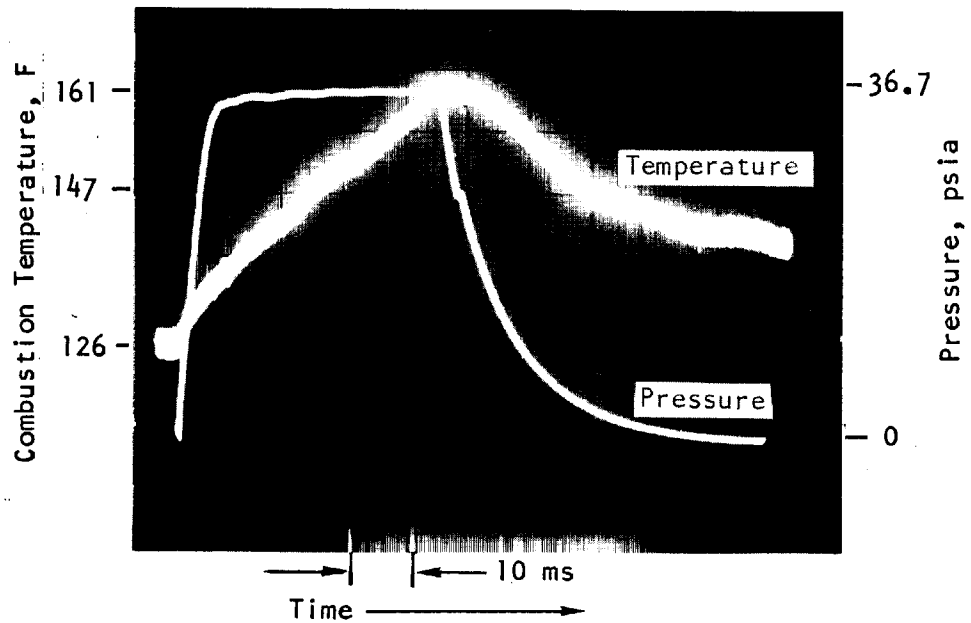

Figure 38. Temperature and Pressure Response (Heater and Insulation, Minimum Volume Data; ΔT = 35 F/40 ms)

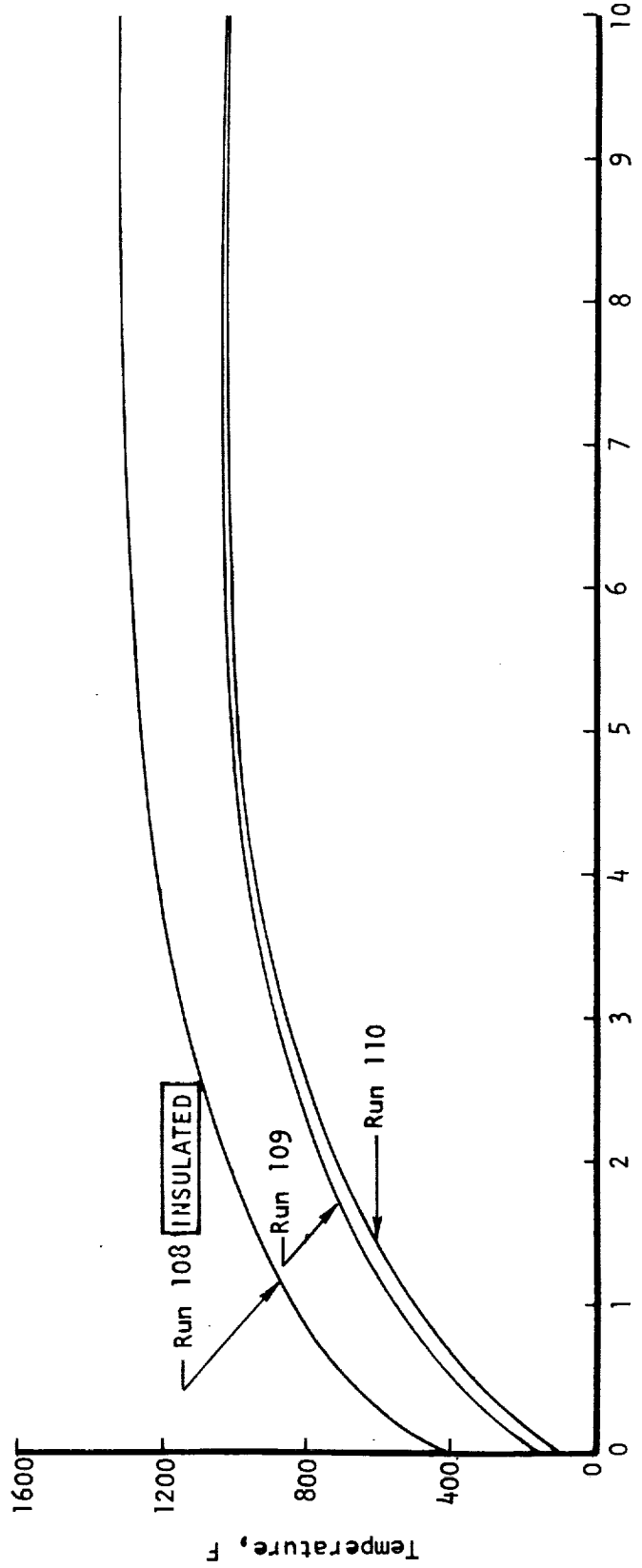

Figure 39. Thermocouple Temperature Versus Time (Tridyne Gas Flightweight Thruster)

In such conditions, the possible thermocouple error would be limited to the difference between 1331 and 1500 F or 169 F. At a 1331 F thermocouple reading, the chamber wall temperature is computed to be about 1250 F by using the temperature ratios and characteristics shown in Fig. 35. These values are later used in a performance projection presented following the Thermal Analysis section.

Typically, in a catalyst reactor there is a large axial temperature gradient from the front to the back of the bed because of the progressive combustion process. There is also a large degree of interegenerative heating, i.e., thermal conduction of heat from the back of the chamber to the front via the chamber wall. Under the conditons of run 108, much of the thermal equilibration preceded the run, substantially reducing the heat loss at the inlet. The insulation also contained the thermal radiation loss to a very low value. With no insulation the computed thermal loss caused by radiation would be about 8 percent of the Tridyne enthalpy. The run results stress the importance of using a thermally effective installation for Tridyne thrusters with low-conductance inlet supply lines. Also demonstrated were the operational characteristics of a thruster with small conductive and radiative heat losses.

Heater Test. A 36-ohm heater was attached to the flightweight chamber and the assembly was wrapped with insulation. The heater was capable of heating the chamber in a vacuum from 95 to 168 F with 0.36 watt of power. A maximum temperature of 224 F was produced with 0.81 watt of power. The 1/2-watt heater burned out when the current input was intentionally increased above its rated power level. The steady-state power requirements for thermal preconditioning of a thruster module are presented in the Thermal Analysis section.

This demonstration showed the feasibility of heating the Tridyne thrusters by using auxiliary electrical heaters. Although heating is unnecessary for chamber operation, an appreciably higher specific impulse is attained during pulse-mode operation by preconditioning the chambers to an intermediate temperature range, i.e., 400 to 600 F.

Pressure Response

Pressure transient characteristics of the thruster were evaluated by a fast-response Kulite transducer mounted directly on the chamber and then on the sonic venturi in the inlet line. A high degree of sensitivity to the volumes of the lines and transducer mounts was noted during these tests. By reducing the void volume in the Kulite mount to a practical minimum amount, it was possible to achieve a pressure transient (Fig. 40) of 5 milliseconds from valve-open to full chamber pressure. These traces were made with the transducer mounted on the inlet venturi (Fig. 6) and reflected the pressure buildup at the sensor element through a 0.010-inch-ID inlet line. The mount void volume was estimated to be in the range of 25 percent of the chamber void volume.

Previously, a test with the Kulite transducer mounted in the same position but with a larger cavity volume showed a 10-millisecond interval from valve-open to full chamber pressure (Fig. 41). In this case, the transducer mount cavity was larger (0.050 inch long) due to the use of O-ring seals rather than flat seals under the transducer adapter. These data provided some insight into the effects of relatively small geometry variations.

A pressure trace with the Kulite transducer mounted directly on the chamber (Fig. 42) shows a 15-millisecond pressure buildup interval, which included comparatively large instrumentation volumes. The transducer was mounted on the chamber as shown in Fig. 43 and an inactive Kulite was positioned at the venturi as a sealing device. These added volumes prevented an accurate appraisal of the pressure transients for an unencumbered chamber.

The close-coupled Kulite trace (Fig. 44) when compared with earlier chamber response recordings on the Task I development hardware (Fig. 18) was found to have nearly the same pressure buildup interval. As a result, the thrust response rate on the flightweight chamber is assumed to be represented by the venturi pressure buildup rate with potential improvement by further reductions in the instrumentation line and mount volumes. The criteria for more exact pressure transient measurements were also identified.

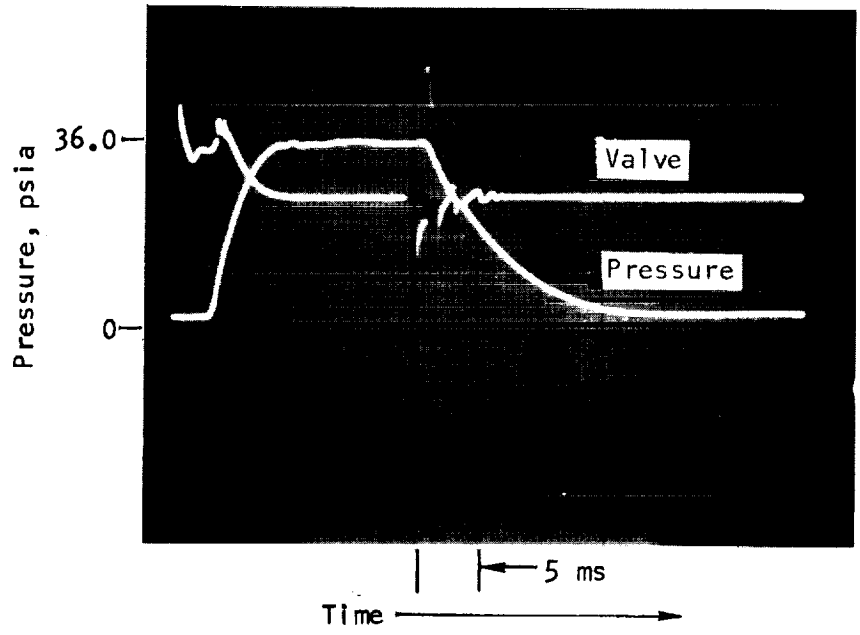

Figure 40. Venturi Pressure Response (Minimum Venturi Mount Volume)

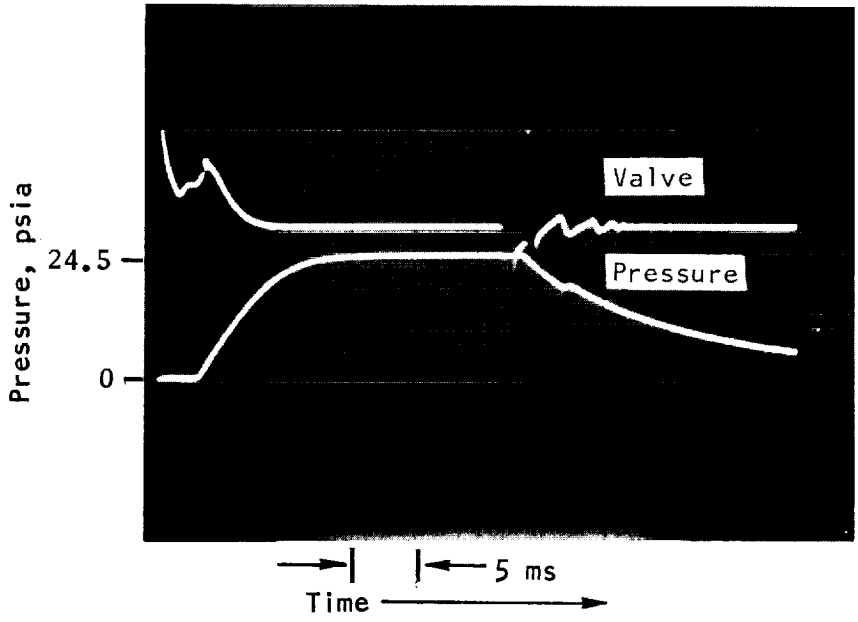

Figure 41. Venturi Pressure Response (Excess Volume in Venturi)

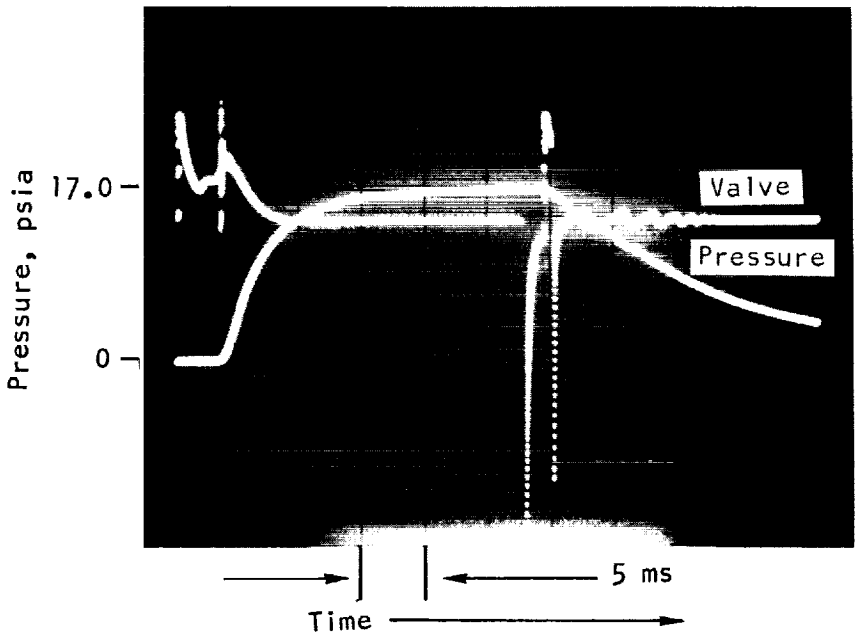

Figure 42. Chamber Pressure Response (Excess Volume in Venturi)

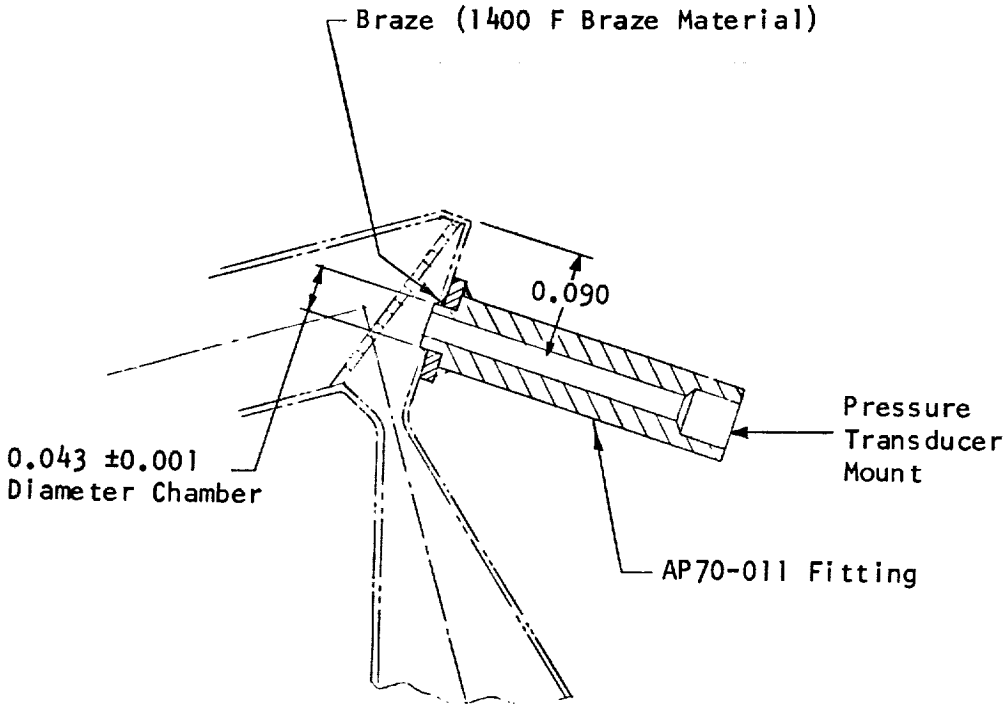

Figure 43. Tridyne Chamber With Pressure Probe

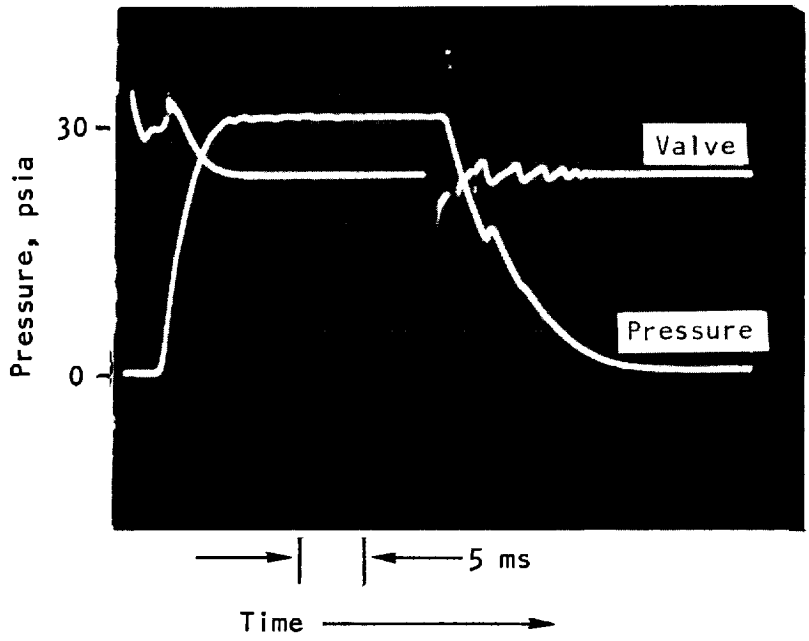

Figure 44. Tridyne Thruster 25-Millisecond Pulse

The required thrust buildup rate of 8 milliseconds from the Command On signal to 90-percent thrust on a flight-type installation is readily achieved by employing a valve, such as the test valve, with an approximate 3-millisecond interval from signal initiation to open. A flight-type installation would have smaller-diameter supply lines than those of the test installation and these would be only slightly longer than those tested, thus providing a response improvement over that shown by tests. The pressure buildup transients at various pressure levels are shown in detail in Fig. 45 with a greatly expanded time scale in 1-millisecond increments. Shown in Fig. 46 is a representative pressure trace at a venturi pressure of 38.8 psia to provide 30-psia chamber pressure. The total impuse per pulse is easily measured by integrating the pressure-time trace over the required interval. In Fig. 46, time from on to off is 46 milliseconds. Some of the traces presented in other sections show typical pulse widths varying from 10 to 50 milliseconds. Thrust variance with temperature is discussed in the Performance Analysis section.

The pressure decay time (Fig. 40) of 18 milliseconds from the off signal to 10 percent of maximum pressure is a conservative estimate of the actual

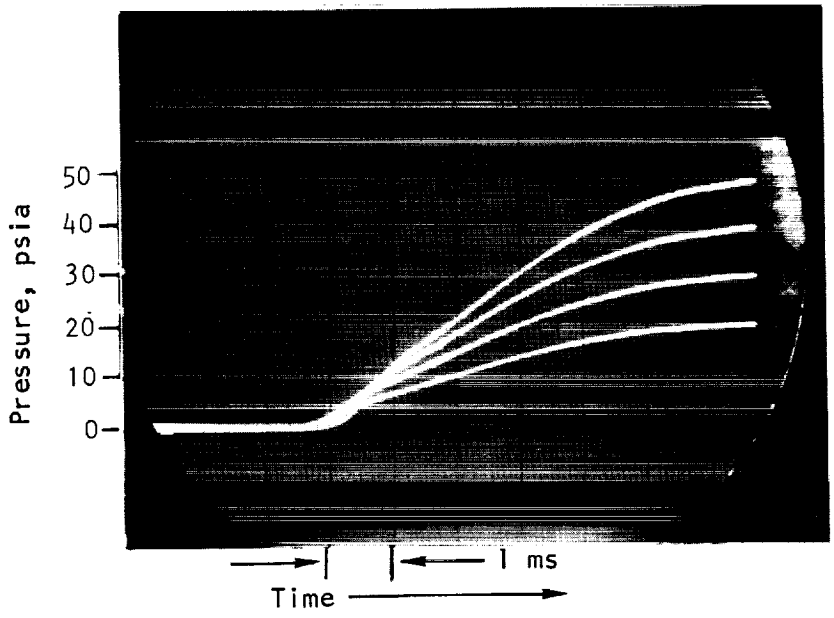

Figure 45. Pressure Response (Minimum Volume Venturi)

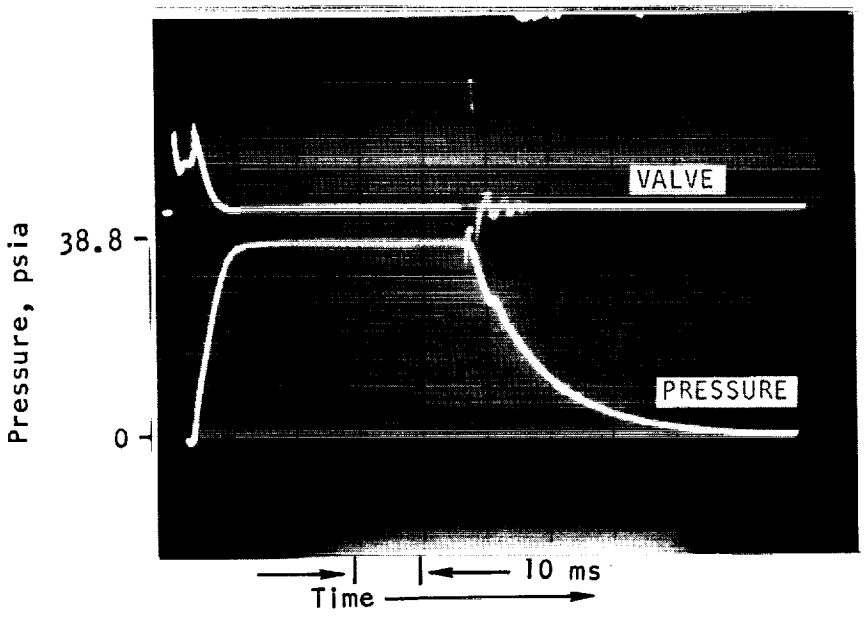

Figure 46. Pressure Response at Venturi for 30-psia Chamber Pressure

chamber thrust decay as the chamber pressure is always slightly less than the venturi pressure. A minor improvement could be effected by eliminating instrumentation lines and minimizing valve downstream volumes, but the program objective of 8 milliseconds from the off signal to 10-percent chamber pressure is probably unattainable.

Tridyne Test Composition

The volume percentages of the reactants in the test Tridyne is shown in Table 3.

TABLE 3

VOLUME PERCENT OF TRIDYNE

Gas	Volume Percent
Nitrogen	85.21
Oxygen	5.02
Hydrogen	9.77

Ideal reaction temperature 1470 F with an inlet gas temperature of 70 F.

Error Analysis

Task IV errors were limited to those produced by the instrumentation. The errors produced by zero shifts were corrected by checking the pressure transducer zeros before each test sequence. The exit nozzle thermocouple oscillograph output was nonlinear below 4 millivolts and the zero seemed to fluctuate. Therefore, the exit nozzle temperature data were not reported or used in the calculations. No problems were encountered with the chamber thermocouple and only one incident occurred in which a leak developed in the chamber. The leak was caused by the pressure probe attachment in Configuration I. Another source of error exists in evaluating the oscillograph and oscilloscope traces. The values can be read to about ±0.005 inch, which is equivalent to about ±0.01 psia for the pressure transducer and about ±0.10 millivolt (or ±4 F) for the thermocouple.

Microminiature thermocouples with 1-mil beads and thermal time constants of less than 1.0 millisecond were used in both Tasks I and IV. A 50-psia pressure transducer was used to measure chamber pressure. The time constant for the transducer was calculated to be less than 0.1 millisecond. A rotameter accurate to within ±4 percent was used to measure steady-state flowrates. In the pulse-mode operation of Task IV, a sonic venturi was used as a flowmeter.

ANALYSIS

PERFORMANCE ANALYSIS

Thrust chamber performance is presented at conditions established during program development. These include a chamber pressure of 30 psia, an expansion ratio of 100:1, and an exit nozzle throat nominal diameter of 0.017 inch. Parameters used in evaluating thruster operation and for correlating data are discussed in the following paragraphs.

Theoretical Performance

The performance characteristics of Tridyne (molar fractions of 0.85 nitrogen, 0.10 hydrogen, and 0.05 oxygen) were evaluated to determine specific impulse, thrust, and mass flow variances with temperature. The theoretical specific impulse of Tridyne at 30 psia pressure and 100:1 expansion ratio is shown in Fig. 47 as a function of the gas total temperature at the nozzle throat. Flow loss factors are evaluated by means of a Rocketdyne-developed analytical model that utilizes the integral momentum and energy equations with a finite difference solution. The loss terms, potential flow at the throat, nozzle divergence, and boundary layer effects are combined as a thrust coefficient efficiency term presented in Fig. 48. These efficiencies are applied to establish the delivered specific impulse curve of Fig. 49. The thrust chamber effective throat area is thus determined by the flowrate required to deliver the rated thrust of 0.01 pounds.

The efficiency terms of Fig. 48 are slightly lower (about 4 percent) than those predicted at the start of the program, primarily because of a more complete evaluation of gas viscosity effects. The gas viscosity-temperature variation is shown in Fig. 50. The only significant effects from the efficiency change are a slight increase in throat diameter (from 0.0166 to 0.0172 inch) and an increase in engine mass flow (from 6.9×10^{-5} to 7.3×10^{-5} lbm/sec at 1500 F) to produce 0.01 pound thrust. Chamber thrust is virtually

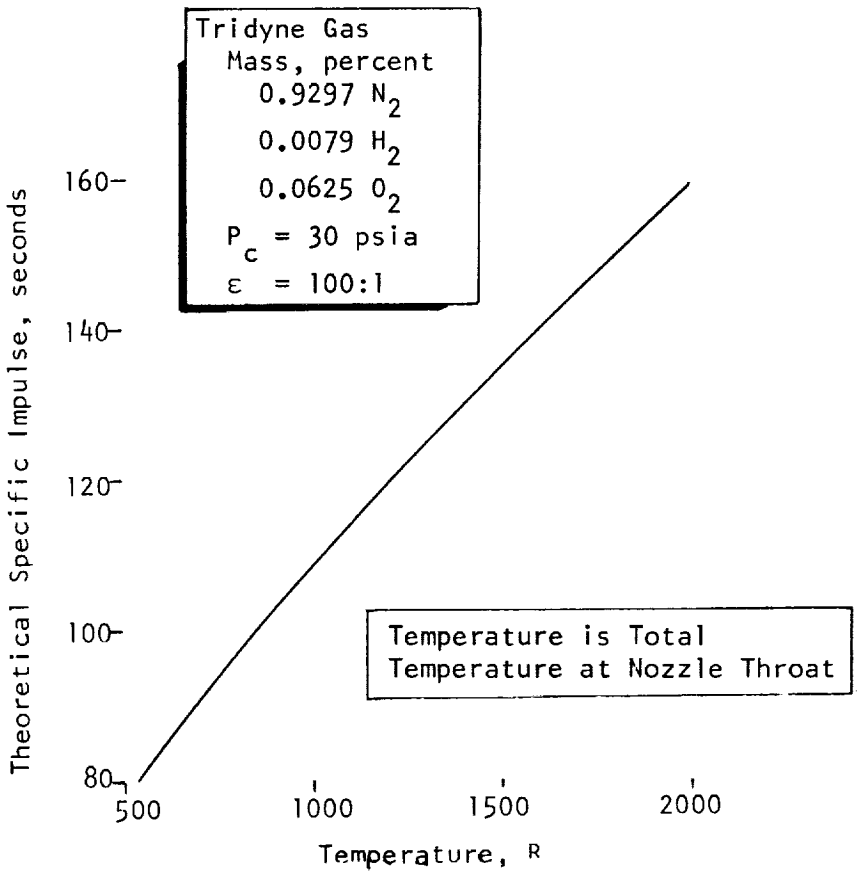

Figure 47. Theoretical Specific Impulse vs Temperature

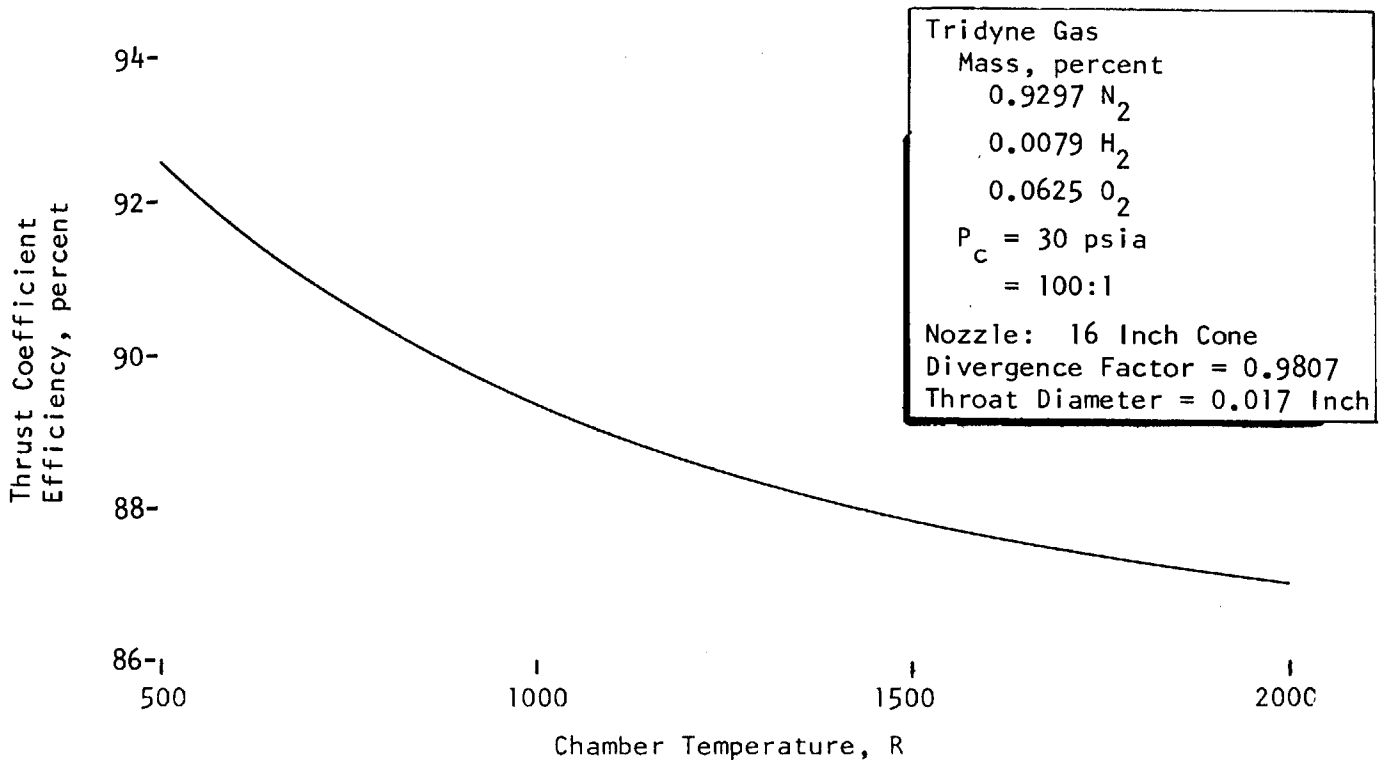

Figure 48. Thrust Coefficient Efficiency vs Chamber Temperature

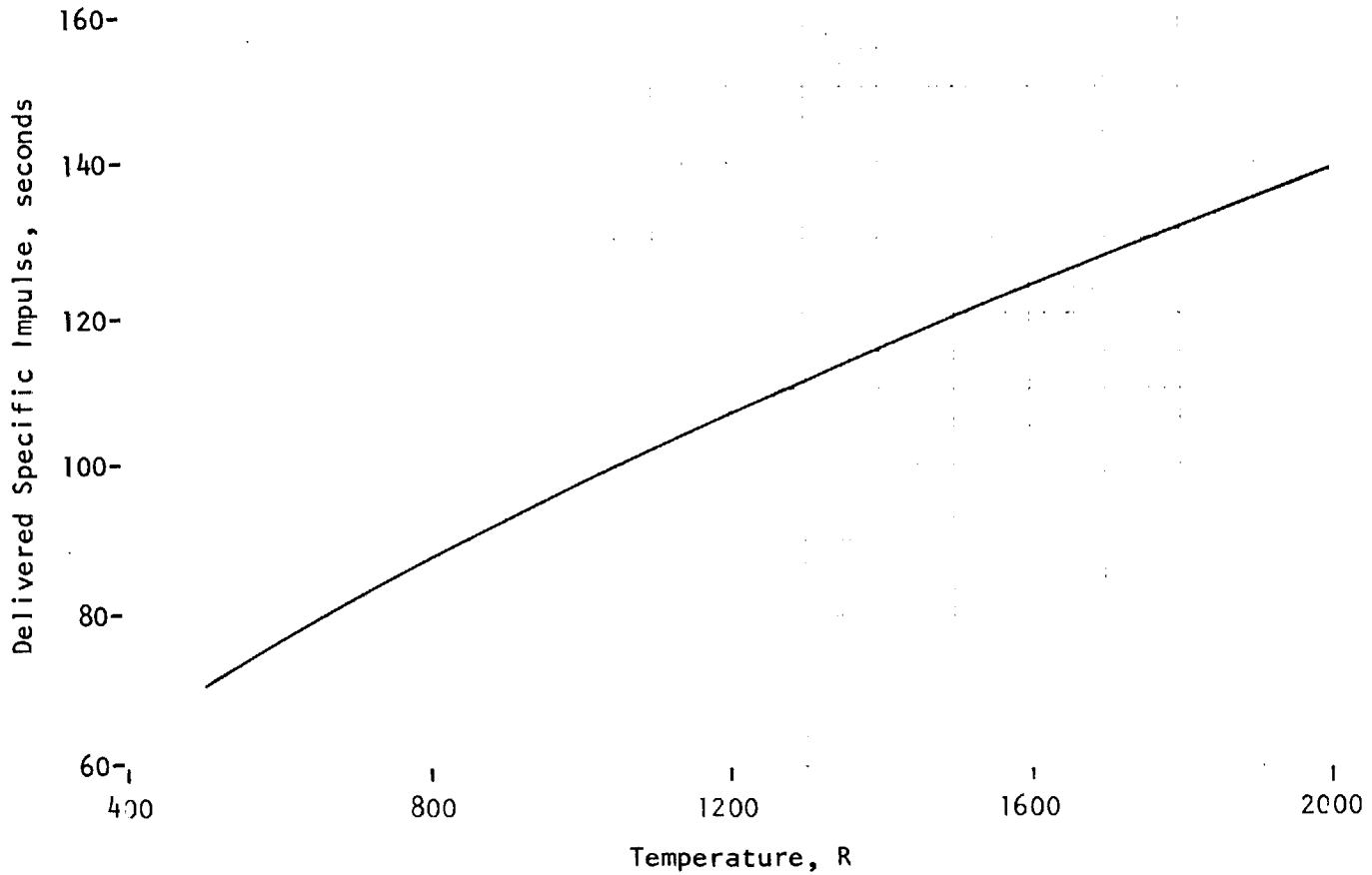

Figure 49. Delivered Specific Impulse vs Temperature

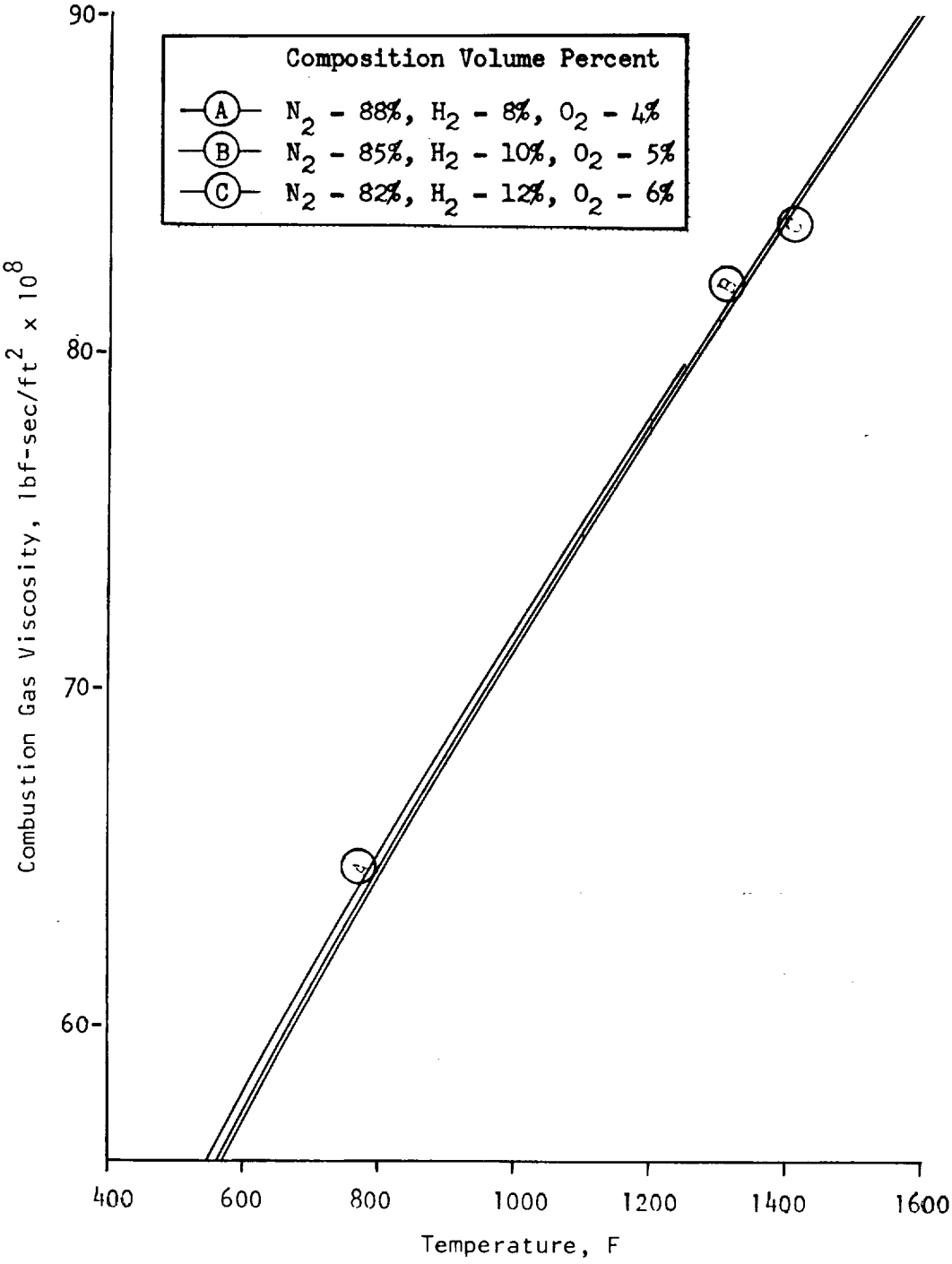

Figure 50. Viscosity of Tridyne Combustion Products vs Temperature

constant within the temperature range of 70 to 1500 F with a low ΔP system as the chamber mass flowrate decreases as the exit temperature increases. This characteristic is discussed more fully in the following paragraphs.

Delivered Performance

For microthrust nozzles, the boundary layer effects are significant and substantially reduce nozzle throat effective areas. Although experimental data on discharge coefficients in the low Reynolds numbers range are somewhat limited, recent analysis of the effects of approach velocity and the boundary layer profile has resulted in remarkably good agreement between various references. A correlation developed by Rocketdyne personnel is shown in Fig. 51 distributed over a Reynolds number range of 50 to 100,000. The range of interest on the Tridyne program is from 1000 to 8000. The values shown are estimated to be within 1 percent of actual.

Superimposed on the Fig. 51 curves are data acquired from calibration of the sonic venturi used for measuring thruster flowrates. Both nitrogen and helium were flowed over a pressure range of 10 to 50 psig and flow versus time was measured by a Beckman positive-displacement flowmeter. The venturi throat diameter was 0.01395 inch with an error margin of less than 0.00005 inch. The wall/throat radius ratio was 3:1. Calibration data show no apparent coefficient change due to the difference in specific heat ratios of helium and nitrogen (1.66 and 1.40, respectively).

The thrust developed by the chamber is determined by the product of the mass flowrate and the delivered specific impulse. The mass flowrate change with temperature at a constant inlet pressure is shown in Fig. 52. The mass flowrate equation is presented in the experimental evaluation section for venturi flow analysis. Two parameters used in the equation, $\dot{m}$ and P/P_T, are shown in Fig. 53 and 54, respectively, plotted as functions of temperature. It should be noted that a chamber pressure increase with

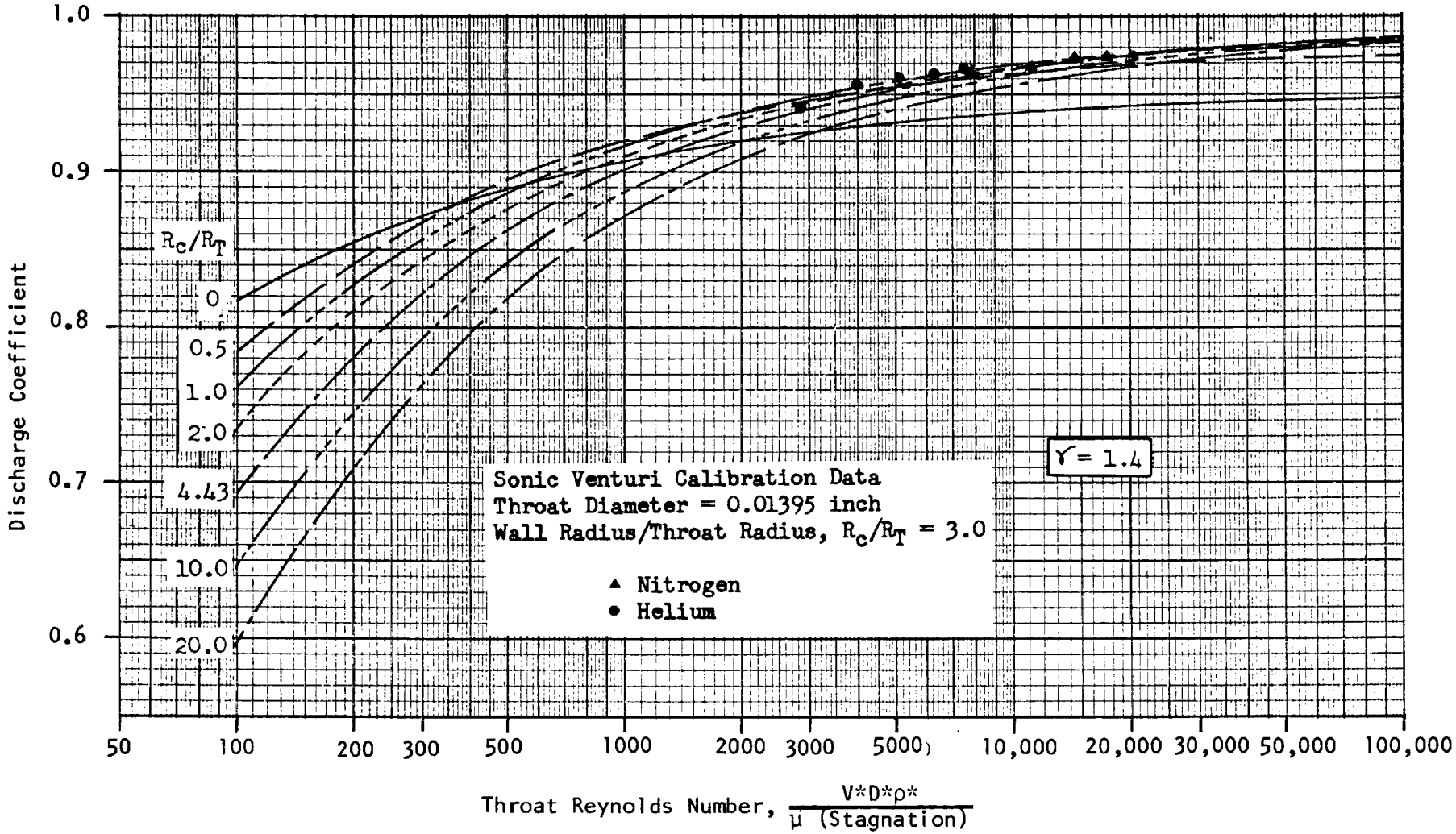

Figure 51. Predicted Values of Discharge Coefficient for Sonic Nozzles

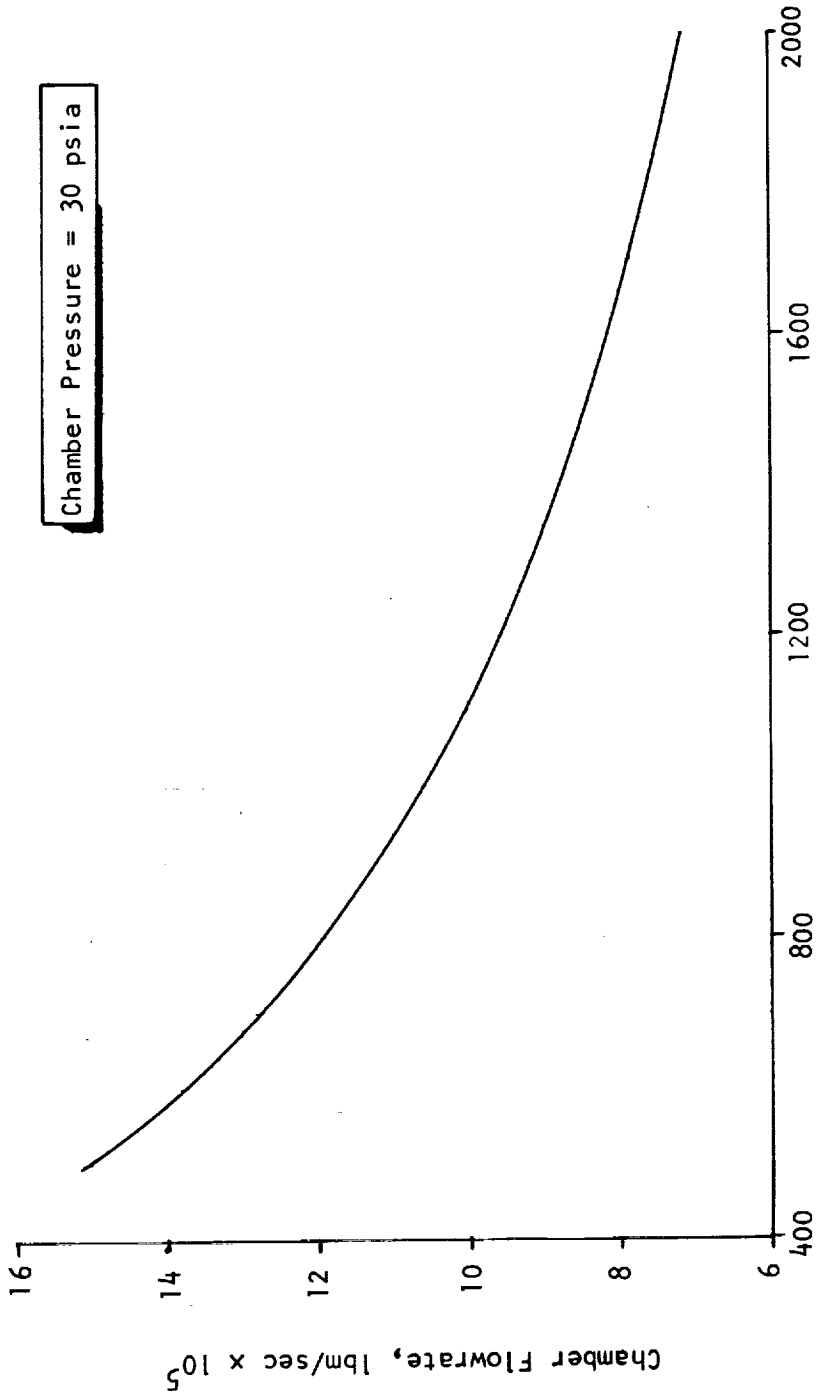

Figure 52. Chamber Mass Flowrate vs Exit Temperature for Tridyne

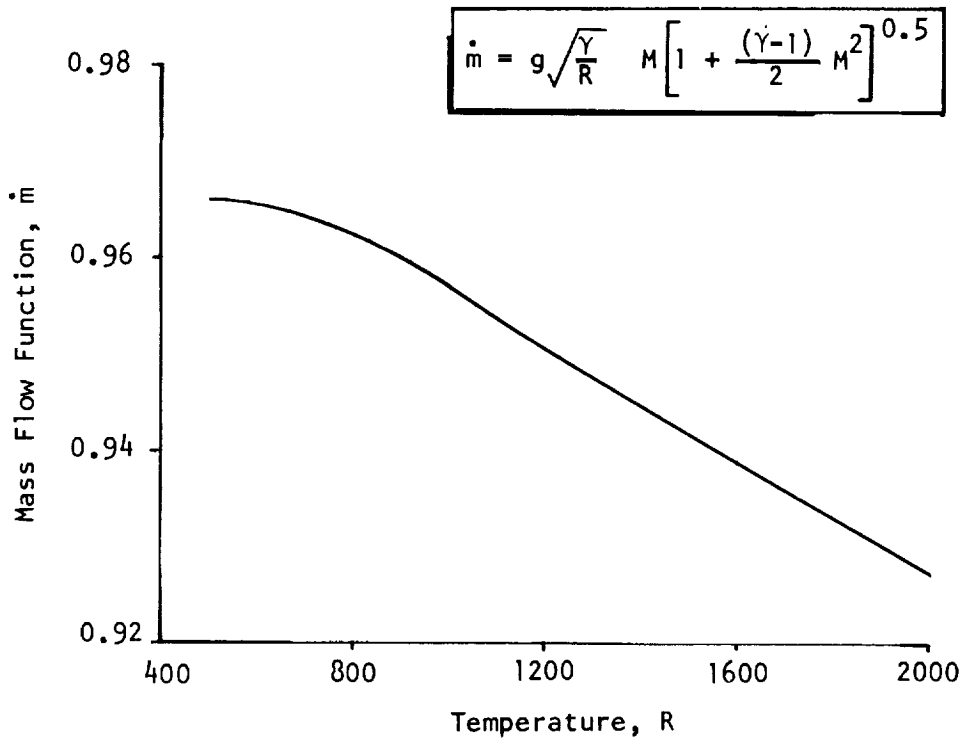

Figure 53. Mass Flow Functions vs Temperature

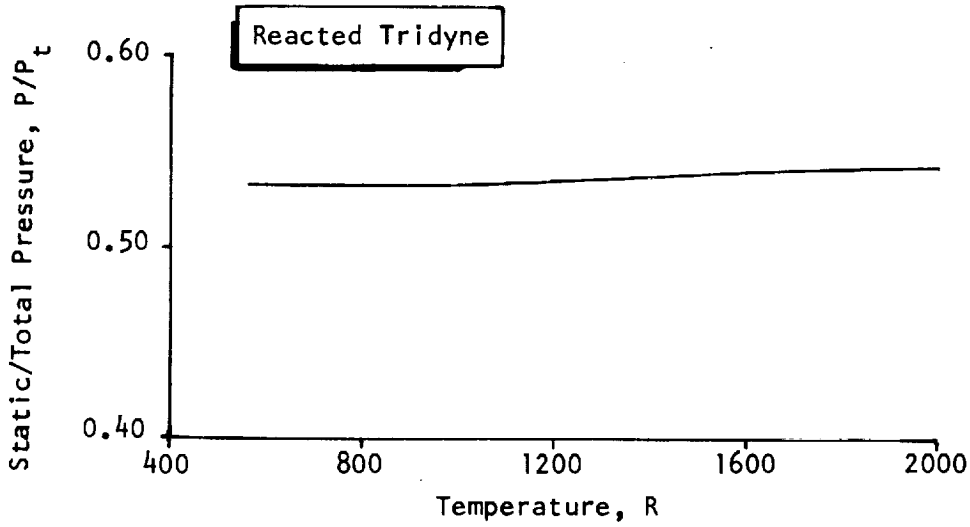

Figure 54. Sonic Static to Total Pressure Ratio vs Temperature

temperature would produce a higher thrust. The constant pressure thrust variation with temperature is shown in Fig. 55 which indicates a slight increase with decreasing temperatures. This may be partially compensated for by a slight chamber pressure decrease at lower pressure. It is also quite possible that the viscous losses predicted at high temperatures by Rocketdyne's performance program are conservatively computed. The program is well substantiated at thrust levels about 1-pound thrust. However, few substantiating data are available for reference in the range of 0.01 pound thrust. This is an area warranting study and further experimental evaluation.

Because of frequent reference to Reynolds number effects on the discharge coefficient during the program, a parametric range of numbers were computed for both unreacted Tridyne at ambient temperature (70 F) and the combustion products over a temperature range of 100 to 1500 F. These are shown in Fig. 56 and 57, respectively. A crossplot of Fig. 56 data showing the exit nozzle Reynolds number variation with temperature is shown in Fig. 58 permitting the discharge coefficient temperature variance to be determined by reference to Fig. 51. This is also plotted in Fig. 59.

THERMAL ANALYSIS

An analysis was made of the flightweight thruster tests to determine heat loss factors and to provide criteria for spacecraft module designs. The test installation is shown in Fig. 12. An ultra-miniature thermocouple is shown positioned downstream of the catalyst bed in the cavity formed between the aft screen and the chamber nozzle. The thermocouple juncture is approximately 0.020 inch from the chamber wall and the thermocouple is electroformed integrally within the wall. The couple is formed of two 0.5-mil platinum alloy leads encased within a thin-wall, 8-mil-diameter sheath. Insulation of magnesium oxide is provided in the 2-mil nominal gaps separating the wires from each other and from the casing, and the sheath closure is a high-temperature refractory bead.

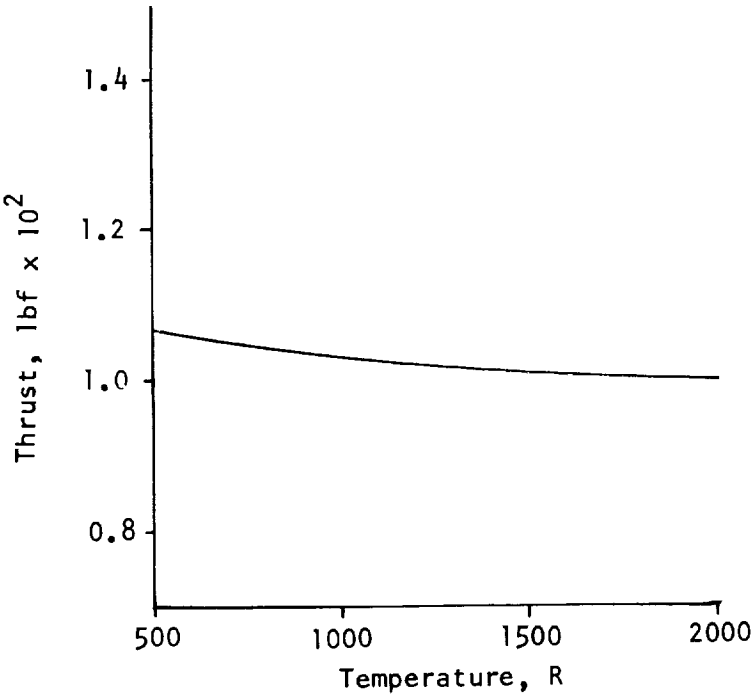

Figure 55. Thrust Variation With Temperature

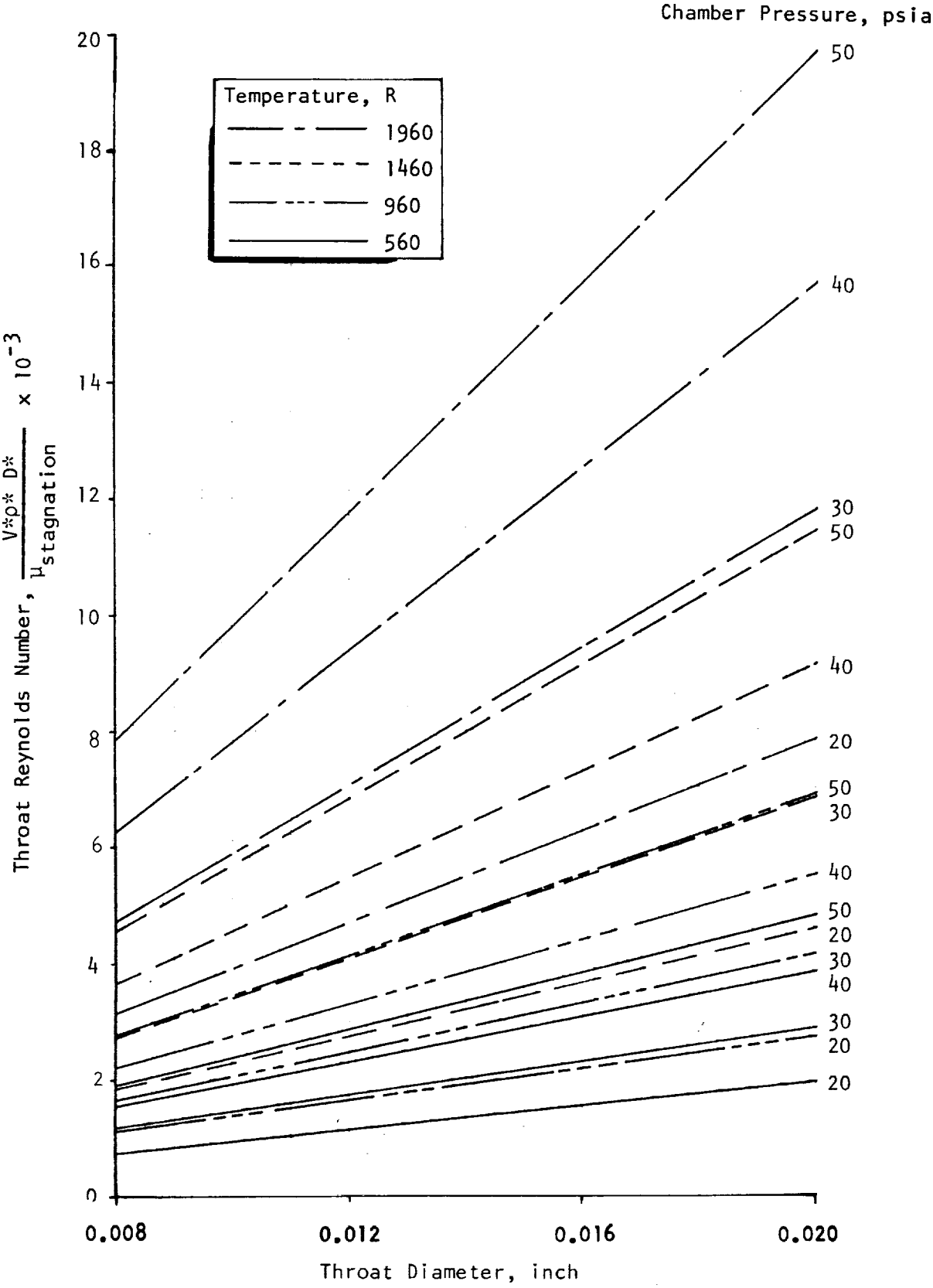

Figure 56. Throat Reynolds Number vs Throat Diameter (Molecular Weight of Reacted Tridyne = 27.0)

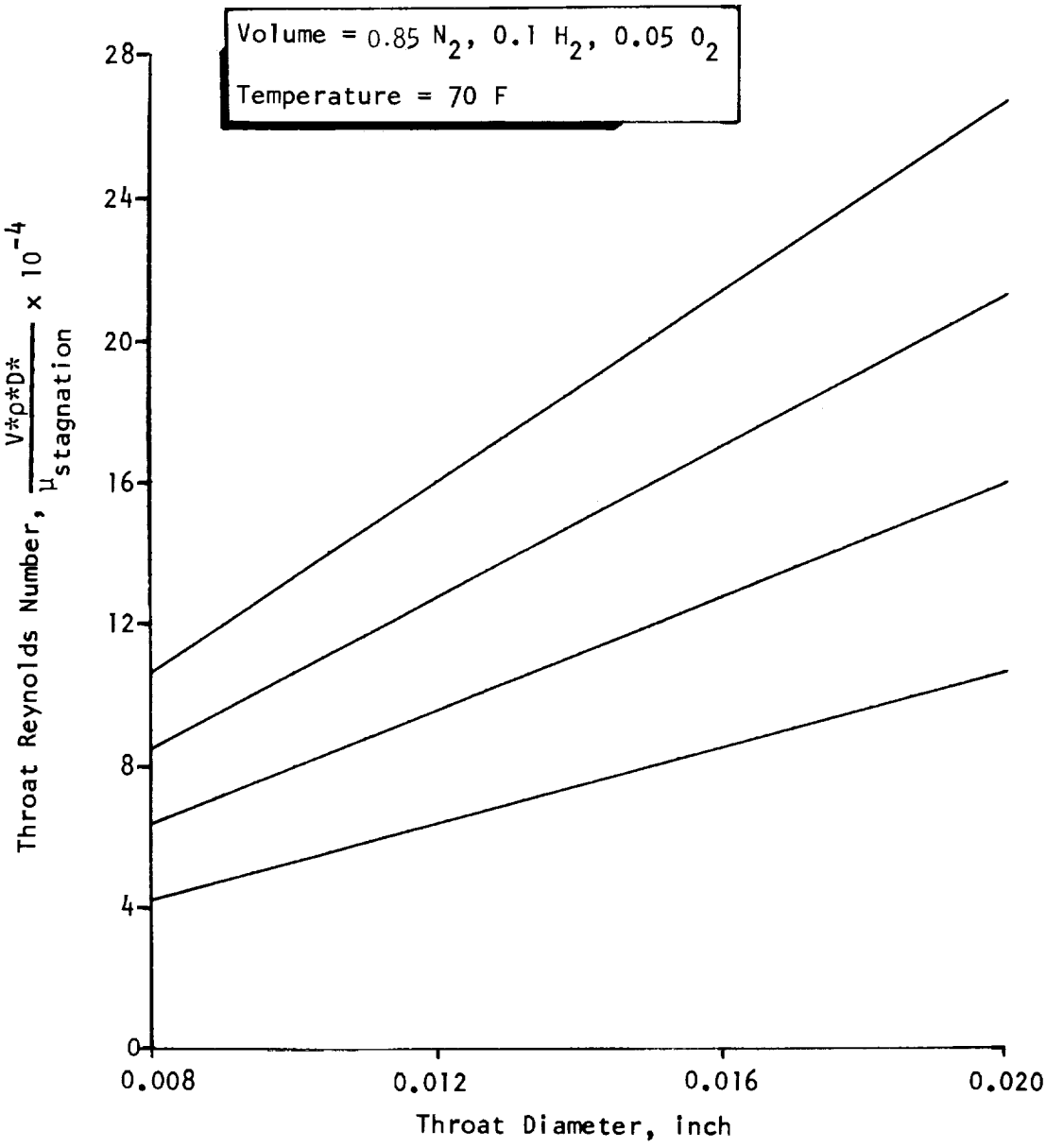

Figure 57. Throat Reynolds Numbers vs Throat Diameter (Molecular Weight of Tridyne Gas = 25.61)

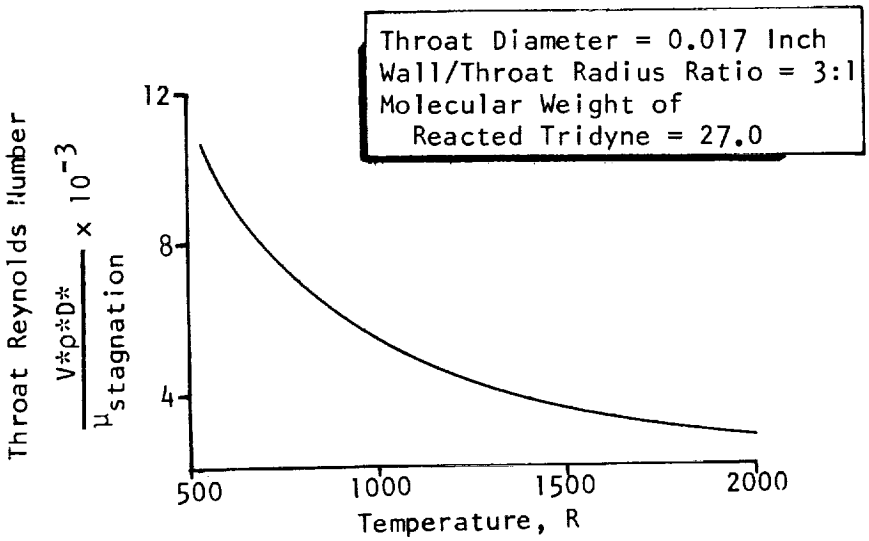

Figure 58. Throat Reynolds Number Variation With Temperature

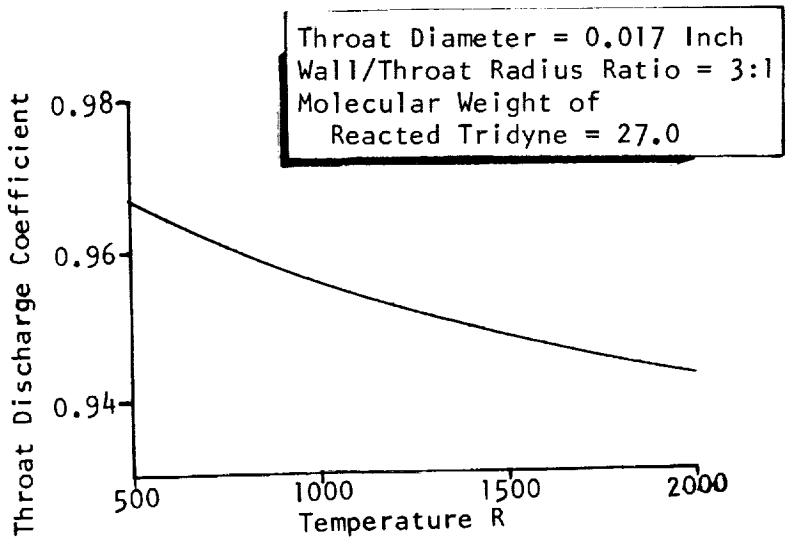

Figure 59. Throat Discharge Coefficient vs Gas Temperature

Those thruster thermal characteristics of interest in the analysis are summarized briefly. The chamber body is of electroformed nickel and weighs 0.16 gram. The chamber contains nominally 0.02 gram of catalyst which is formed by the disperson of noble metals over aluminum oxide pellets. The catalyst pellets have single-point contact with the chamber although some also contact the retaining screens. The screens are virtually free floating and contact the chamber wall in approximately four local areas at the outer peripheries. Consequently, the screens were assumed to approach gas stream temperature.

The inlet line is the primary heat loss path. It consists of nickel tubing 0.04 inch ID, 0.10 inch OD, and 0.15 inch in length. Mounting material for the inlet line is assumed to be an infinite heat sink as the mass is two or three orders of magnitude larger than the thruster. The inlet line admittances were lumped to that of an equivalent solid line of 15.7×10^{-4} sq in. area and 0.21 inch length.

TEST CONDITIONS

The thrust chamber was operated at design conditions (30-psia chamber pressure) and found to equilibrate at near 1000 F as recorded by the chamber thermocouple described above. The Tridyne mixture is designed to provide 1500 F reaction temperature. Consequently, a study was performed to determine thermal losses and provide data on the engine thermal efficiency.

The thermocouple output (millivolts) was recorded on an oscilloscope (Fig. 60) during the temperature decay transient from peak temperature. Figure 61 depicts pressure traces and thermocouple voltage during a pulse of about 15 milliseconds duration. The thermocouple response during the pressure buildup is initially very sharp, and shows a temperature response rate of 14.2 F/ms. The rate decreases to 0.4 F/ms after 15 milliseconds of operation and at chamber shutdown declines at the initial rate of 2 F/ms. Since

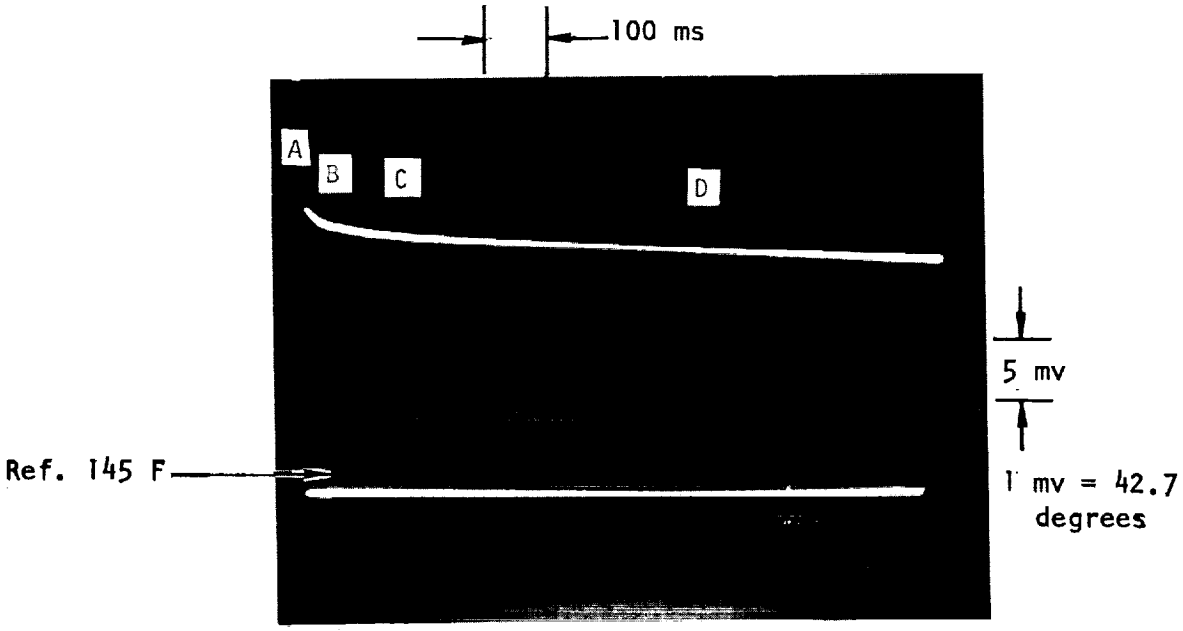

Figure 60. Oscilloscope Recording of Thermocouple Transient

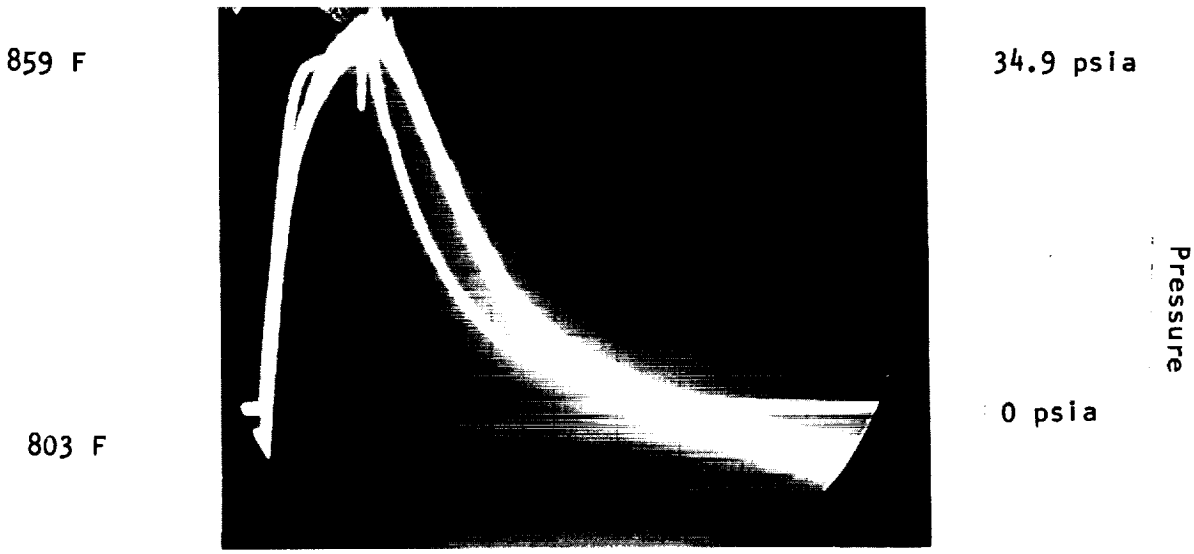

Figure 61. Rapid Thermal Transient (ΔT = 56 F/20 ms)

the decay rate is almost completely caused by conduction from the juncture into the chamber wall, it becomes evident that the thermocouple does not record peak gas temperatures because of the high energy loss from the thermocouple juncture. However, with no gas flow the thermocouple should provide an accurate chamber temperature-time history.

Referring again to Fig. 60, the maximum steady-state chamber temperature is 940 F (point B following thermocouple-chamber equilibration). The slope of the curve at this point indicates a heat loss rate from the chamber of 1.85×10^{-2} Btu/sec. At points C and D the loss rates are 1.23×10^{-2} and 0.5×10^{-2} Btu/sec, respectively. These rates are based on the thermal capacitance of the thruster outer shell. The potential energy loss of the Tridyne is shown, by the product of the enthalpy difference between the temperatures of 1500 and 1000 F (Fig. 62) of 145.8 Btu/lbm and the thruster flowrate of 7.9×10^{-5} lbm/sec at 1000 F to be 1.15×10^{-2} Btu/sec. Based on this theoretical loss, the highest loss rate (point B) is 1.60 times as large as the theoretical potential loss. This indicates that the thermocouple is reading very close to the actual chamber temperature instead of fully responding to gas temperatures. In addition, it is evident there is a large axial flow of heat from the nozzle end of the chamber to the injector end. Point D, 550 milliseconds after chamber shutdown, shows a loss rate about one-half the theoretical loss with little change in the slope for the rest of the recorded interval. The assumption that this rate approximates the actual conduction heat loss from the chamber during steady-state operation would account for 50 percent of the theoretical energy loss.

Thermal Analysis

Radiation losses were analyzed using the Stefan-Boltzmann equation with emissivity (ε) values assigned by comparison with tabulated reference materials. Using ε values of 0.3 for the chamber body and nozzle exterior, 0.9 for the nozzle interior, and a 0.95 form factor results in a computed radiation loss value of 9.7×10^{-4} Btu/sec at a chamber temperature of 940 F. This is equivalent to 8.5 percent of the estimated theoretical loss.

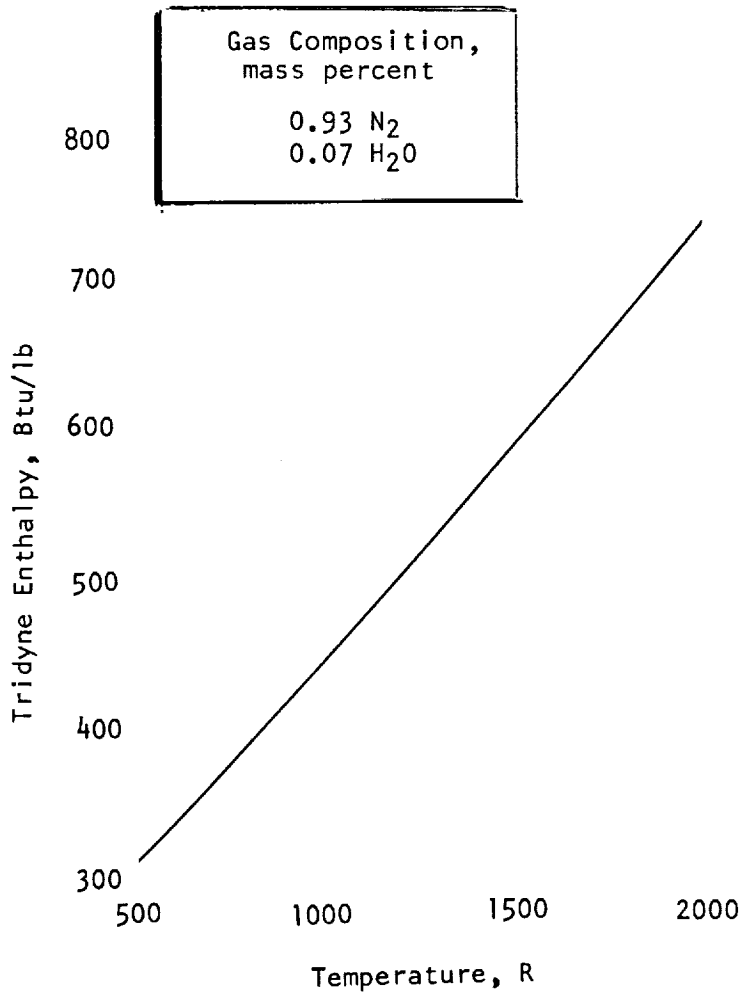

Figure 62. Tridyne Enthalpy Versus Temperature

The actual gas temperature in the chamber can be computed by using the thermal loss rates, a heat transfer coefficient, the effective chamber area, and the driving potential.

The Bartz equation for convective heat transfer coefficient estimation in the region of the nozzle is as follows:

$$h_g = \left[\frac{0.026}{D_*^{0.2}} \left(\frac{\mu^{0.2} C_p}{Pr^{0.6}}\right)\left(\frac{P_c g_c}{c^*}\right)^{0.8} \left(\frac{D_*}{R_c}\right)^{0.1}\right]\left(\frac{A_*}{A}\right)^{0.9} \sigma$$

where

h_g = heat transfer coefficient, Btu/in.^{2}-sec, F

D = throat diameter, inch

μ = gas viscosity, lbm/in.-sec

C_p = gas specific heat, Btu/lbm-F

Pr = Prandtl number, $\mu C_p/k$

g_c = gravitational acceleration, 32.174 ft/sec^2

c* = characteristic velocity, ft/sec

R_c = nozzle wall radius of curvature, inch

A_* = throat area, in.^{2}

A = area of reference, in.^{2}

σ = boundary layer factor, dimensionless (value of 1.0 used for small wall-gas gradient)

Computing h_g for conditions in the chamber at the thermocouple station results in a value of 1.88×10^{-4} Btu/in.^{2}-sec-F. Assuming this value applies over the thruster internal wall area and using the measured conductive and radiation losses results in a computed temperature difference of 175 F between the gas stream temperature and the wall temperature. The calculated gas temperature is 1115 F. With allowance for the thermal losses, this is consistent with virtually complete Tridyne energy conversion.

A thermocouple was placed in the exit nozzle in an effort to record the gas stream temperature directly. The thermocouple response was found to be intolerably slow due to the low gas density (at a 6:1 expansion ratio the gas density is 5 percent of that in the chamber). An alternate installation was tried (Fig. 12) in which the thermocouple was inserted in a tube in the aft chamber section with a braze attachment at the tube's outer end 0.25 inch from the chamber wall. This method resulted in thermocouple damage from the braze process. It is an attractive approach, however, as it would permit the thermocouple bead and sheath to approach gas stream temperature.

TRIDYNE MODULE PERFORMANCE

An important phase of the program was the projection of test data and thruster performance to conditions of spacecraft operation. The module design presented in the Design section (Fig. 4) is the basis of the thermal analysis to establish heat loss rates from a three-chamber cluster (pitch, yaw, and roll control) and to determine heater requirements to maintain the module at a reference temperature. The design features of the module are discussed in the Design section.

A thermal analog network of the rocket engine assemblies in the three-chamber module configuration was constructed for input to the Rocketdyne Differential Equation Analyzer Program (DEAP-1). One-third of the Tridyne module analog network formulated is illustrated in Fig. 63. The analog uses a three-node nozzle and three-node combustion chamber thermal representation with convective heating from the combustion gases, radiation to space, and conduction through attachments to the shield. Radiation is considered from the thrust chamber to the shield. A two-node representation of the propellant lines is assumed to connect the thrust chambers to the propellant valves.

Heat losses for the three-chamber module are shown in parametric form for application to various mounting conditions. The base reference assumes an

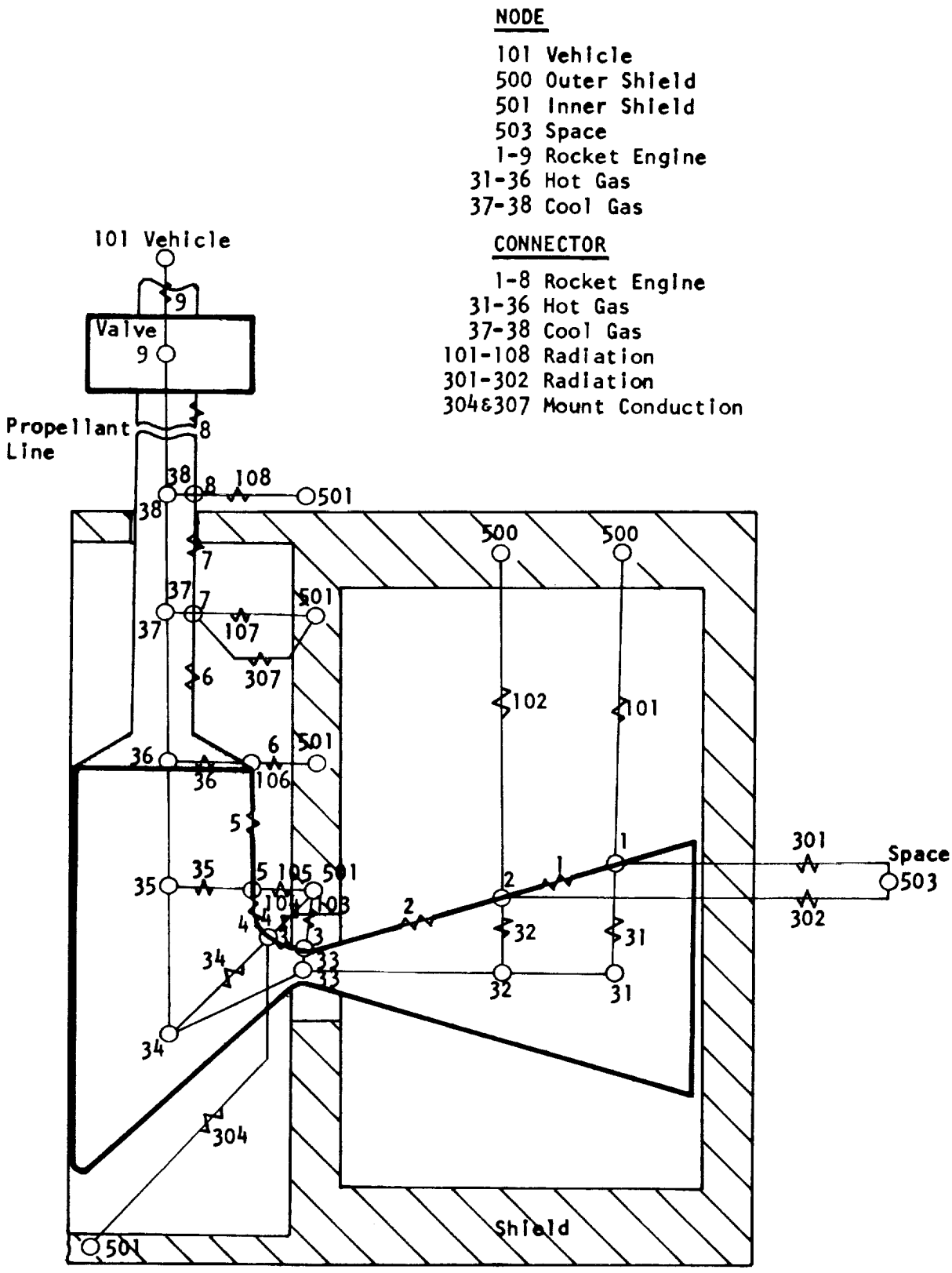

Figure 63. Tridyne Thermal Model

environmental temperature of 175 F as might occur at the end of a solar panel deployed in space. Heat losses for conditions other than the reference can be estimated by using appropriate ratios.

Heat losses for the thrust chambers forward mounts and rear mounts are shown in Fig. 64 and 65 as functions of thruster temperature. Figure 66 shows inlet line conduction losses versus line length for various thruster temperatures, and radiation losses versus thruster temperature are presented in Fig. 67. Total heat loss is shown in Fig. 68 over a thruster temperature range for the conditions noted on the curve.

The temperature losses occurring at maximum chamber wall temperature (estimated to be 1300 F) would be 2.6 watts which represents an enthalpy loss of 8.4 percent. If no heat were supplied to the module, the equilibrium temperature would be 1850 R and the chamber mass flow would be 103 percent of the minimum (1960 R mass flow is 7.3×10^{-5} lbm/sec).

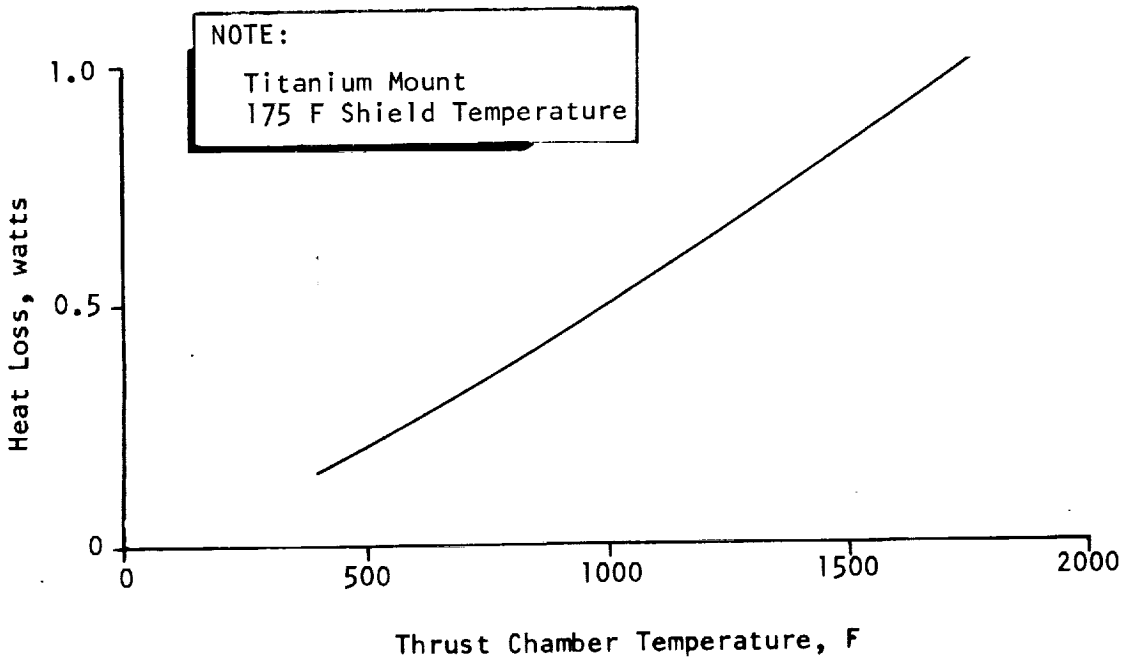

Figure 64. Tridyne Module Thrust Chamber Forward Mount Heat Loss

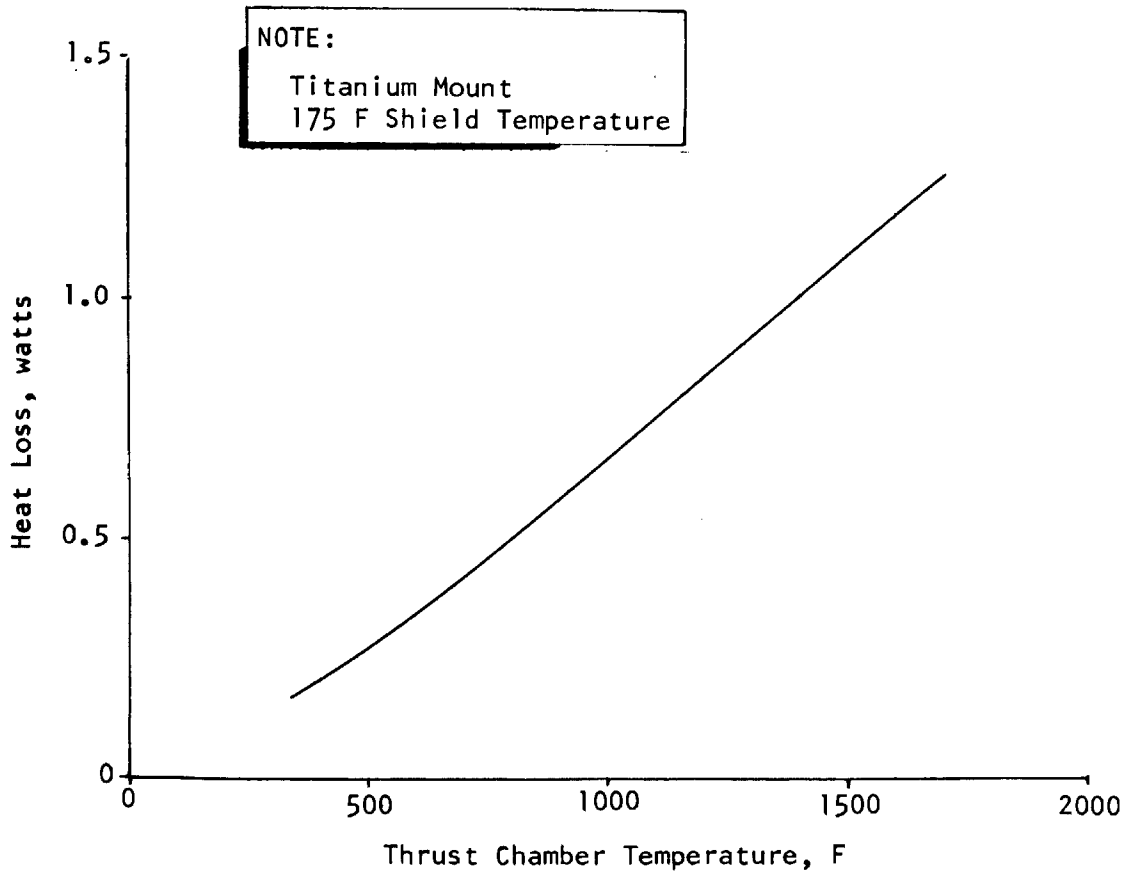

Figure 65. Tridyne Module Thrust Chamber Rear Mount Heat Loss

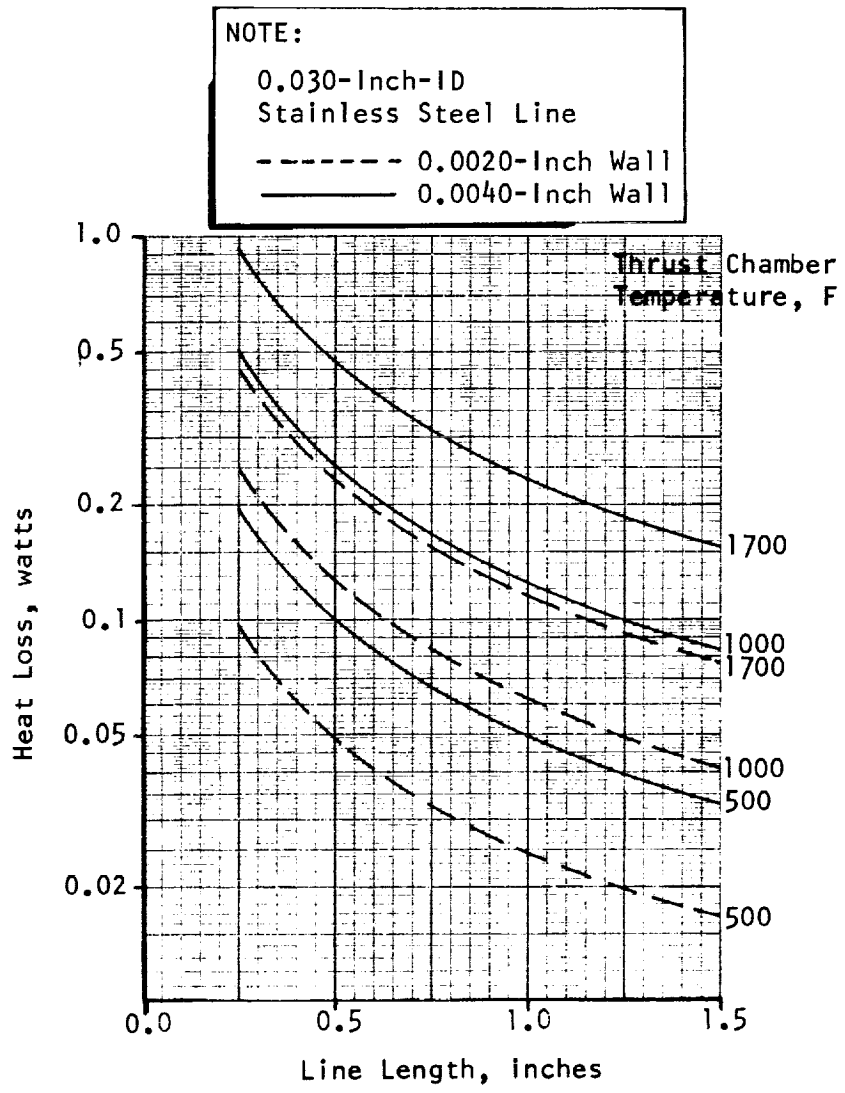

Figure 66. Tridyne Thruster Module Propellant Line Heat Loss vs Line Length

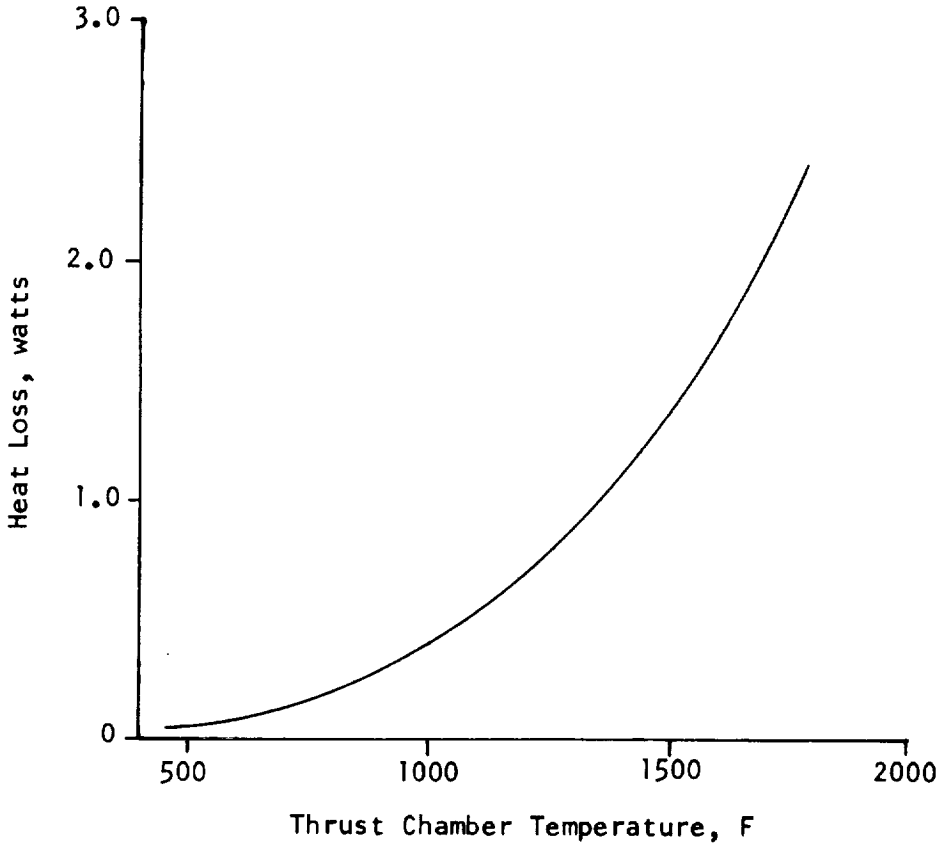

Figure 67. Tridyne Module Thrust Chamber Radiation Heat Loss

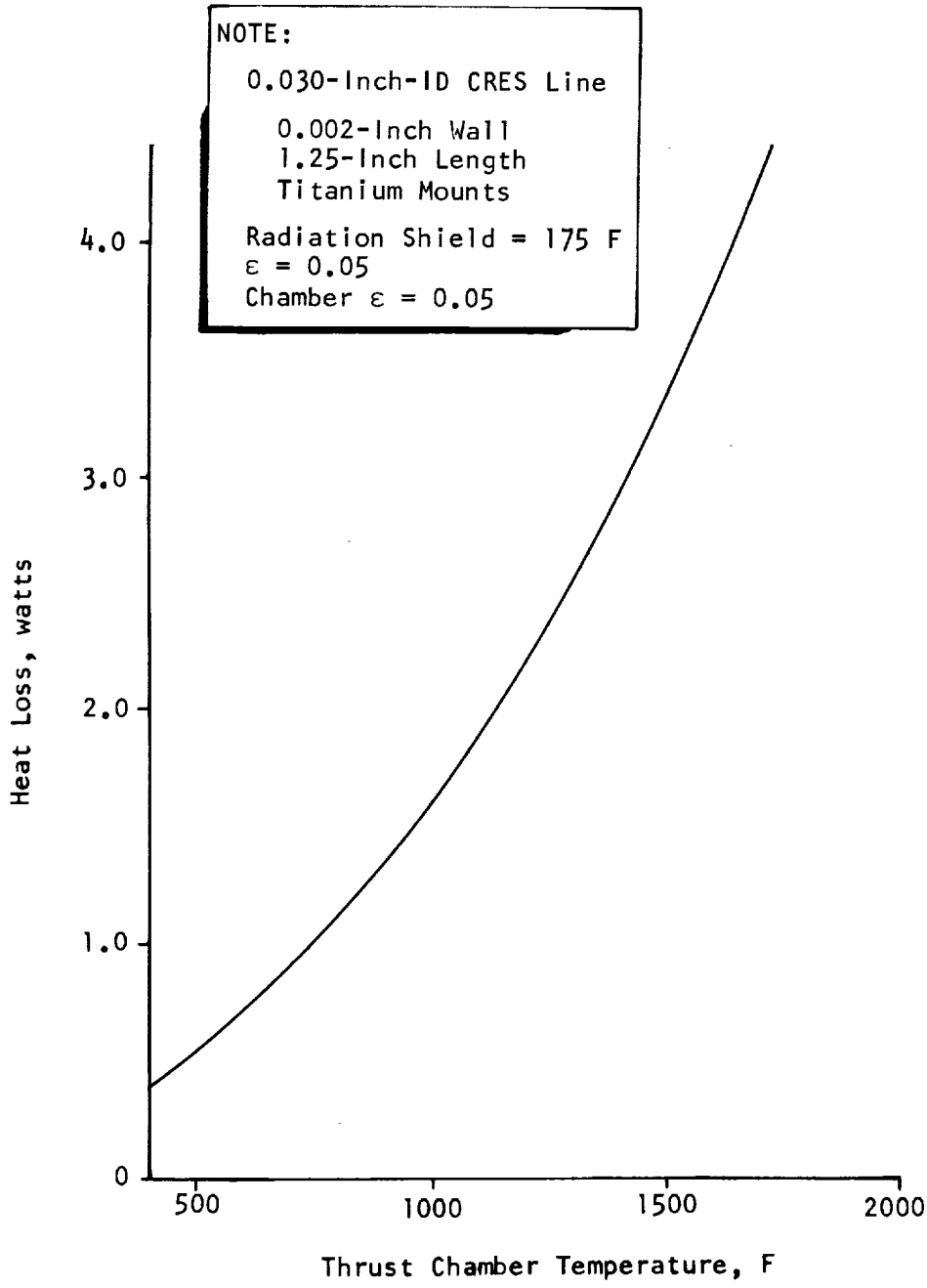

Figure 68. Tridyne Module Thrust Chamber Total Heat Loss Conduction and Radiation

PROJECTED PERFORMANCE

A projection of the thermal response for a Tridyne thruster incorporating design refinements is shown in Fig. 69. The major changes include small catalyst pellets (0.002-inch-OD), reduced catalyst mass (0.14 gram), thin retaining screens (0.004 inch), and minor changes to the thruster contour to permit use of thinner walls (0.0025 inch) in the chamber body. Previously presented modular installation features of reflective insulation and low-conductivity inlet lines are included in the projection thermal analysis.

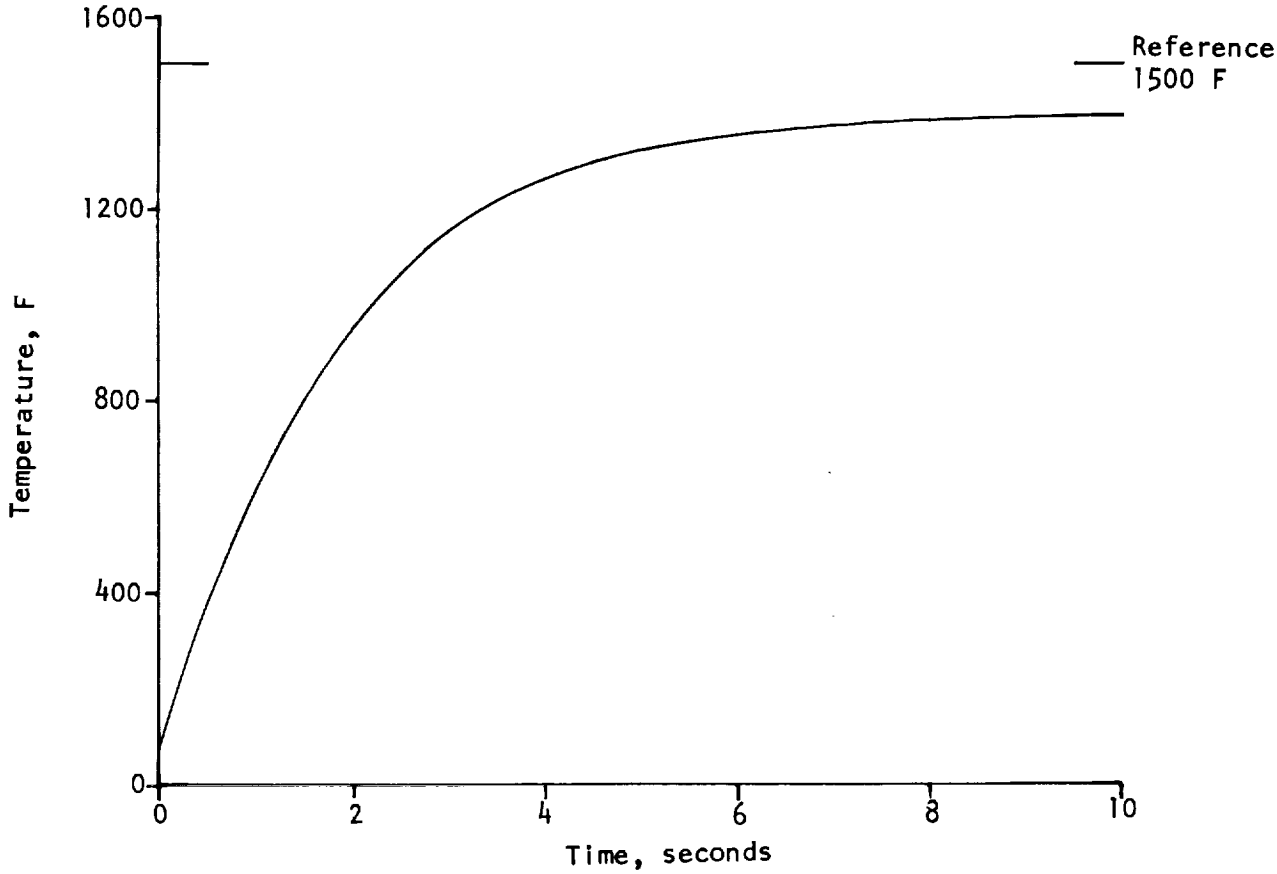

Figure 69. Projected Thermal Response for Advanced Tridyne Thruster

CONCLUSIONS AND RECOMMENDATIONS

The program demonstrated the feasibility of using Tridyne in attitude control thrusters in the 0.01-pound-thrust class. Criteria were also provided for catalyst selection, thruster module designs, and thruster fabrication methods. Operational characteristics of the thruster were documented over a range of initial temperatures from ambient to equilibrium, and the thermal characteristics were measured.

The flightweight thrusters can be fabricated and assembled to standards normally used for spacecraft hardware. Dimensional tolerances are controllable to 0.0001 inch on critical dimensions, which permits a high degree of control on the thrust level of the thrusters.

Several areas are noted in which performance improvements are possible. A smaller catalyst pellet would permit a reduction in the catalyst mass as well as the chamber size and mass, thus improving thermal response. A separate internal catalyst compartment isolated from the thruster body and a moderate chamber redesign to permit use of a thinner wall would also decrease the chamber thermal inertia.

Some of the instrumentation installations could be improved by minor exchanges for better adaptation to the small scale of the test hardware. Thermocouples, in particular, could be made more responsive to gas temperature by extending the juncture and leads a short distance (about 0.015 inch) beyond the end of the shield. The installation should then be calibrated to reference gas temperatures in the range of interest. Both temperature response rate and error magnitude should be measured.

Representative pressure response measurements are feasible on Tridyne thrusters by use of prototype mockup chambers duplicating the flightweight thruster void volumes. This approach would more closely approximate the actual pressure response by permitting low-void-volume, close-coupled transducers to be used.

Thruster temperature characteristics could also be more precisely determined by providing better thermal isolation in the form of long, thin-wall inlet lines and reflective shielding for radiation losses.

A logical extension of the program effort should include the demonstration of a representative real-time, long-duration space mission duty cycle with a three-chamber module. Data of interest are thermal behavior, impulse repeatability, valve leakage effects, and general component durability in a vacuum environment for prolonged periods.

REFERENCES

1. AFRPL-TR-66-278, Advanced Pressurization Systems Technology Program, Final Report, H. E. Barber, Rocketdyne, a Division of North American Rockwell Corporation, Canoga Park, California, 15 November 1966, CONFIDENTIAL.

2. RR 64-2, Hydrogen/Oxygen Catalytic Ignition Studies for Application in the J-2 Engine, R. W. Roberts, Rocketdyne, a Division of North American Rockwell Corporation, Canoga Park, California, January 1964.

3. NASA-CR-72176, Evaluation and Demonstration of the Use of Cryogenic Propellants (O_2/H_2) for Reaction Control Systems, Volume I; Experimental Evaluations and Demonstration, N. Rodewald, G. Falkenstein, P. Herr, and E. Prono, NASA, June 1967.

4. NASA-CR-72244, Evaluation and Demonstration of the Use of Cryogenic Propellants (O_2/H_2) for Reaction Control Systems, Volume II: Experimental Evaluations and Demonstrations, N. Rodewald, G. Falkenstein, P. Herr, and E. Prono, NASA, June 1968.

5. Tridyne Tank Gun Scavenger Systems (Report in Process), C. Buell and R. Gurnitz, Rocketdyne, a Division of North American Rockwell Corporation, Canoga Park, California, 1969.

APPENDIX A

TEST SUMMARIES FOR TASKS I AND IV

The test summaries for the experimental evaluation of Tasks I and IV are included within the following pages of this report.

Qualifying information relative to the Task I tests is briefly presented. Tests 1-61 were conducted with the purpose to determine the catalyst quantities for representative chambers. The pressure data in Runs 31-43 are slightly in error due to zero shifts in the pressure transducers. Temperature response information is presented in tests 44-81 for the purpose of comparing experimental results with theoretically predicted results. The chambers used in tests 61-81 were wound with heaters. These tests provide information concerning catalyst temperature preconditioning.

Table A-1 presents data for Task I and Table A-2 lists Task IV data.

TABLE A-1

TASK I TEST SUMMARY

Test Number	Chamber Type ID, inch/material	Heater	Catalyst Type	Catalyst Size, mesh	Catalyst Mass, grams	$\frac{A^*, in.^2}{D, in.}$	Time, seconds	$T_{chamber}$, F	$P_{chamber}$, psia	P_{line}, psia	$\dot{\omega}_{exp}$, sci/sec	$\frac{\dot{\omega}_I}{\dot{\omega}_E}$	τ, seconds	$M_c\left(\frac{P_c}{\dot{\omega}}\right)_{exp}$	T_{ss}/T_o	Remarks
01	0.225/SS	No	MFSA	16	0.0795	$\frac{2.433}{0.0176}$	0	165	14.0	31.8						
							20	804	27.6	30.0	3.57	0.0642		0.616		
02							NG				---	---		---		
03							NG				---	---		---		
04					0.1082		0	117	14.4	31.6						
							~17	892	28.8	30.4	3.28	0.702		0.952		
05					0.1082		0	117	0.8	31.6						
							12	926	29.2	30.0	2.90	0.795		1.09		
06			*	0.5 mil	0.032		0	53	0.8	31.6						
							~17	53	29.6	30.4	---	---		---		
07			MFSA	16	0.123		0	260	1.2	31.4						
							~17	894	29.8	30.4	2.14	1.112		1.71		
08					0.1304		0	206	14.4	31.8						
							~10	903	29.4	30.2	2.44	0.903		1.57		
09			Shell		0.0308		0	126	14.0	31.8						
							7	126	28.8	30.0	3.78	0.807		0.616		No ignition
10					0.3508		0	111	14.2	31.2						
							8	111	29.2	29.8	3.46	0.990		2.96		No ignition
11					0.3382		0	150	13.0	31.6						
							15	981	27.0	29.8	3.22	0.643		2.84		
12			MFSA	30	0.1111		0	181	14.0	31.6						
							~16	1025	30.0	30.2	2.09	1.091		1.59		
13				30	0.1111		0	223	14.8	31.0						
							29	763	29.0	29.8	---	---		---		
14	0.150/SS		Shell	16	0.1802	$\frac{1.767}{0.015}$	0	150	14.0	30.6						
							28	996	29.0	29.8	2.38	0.715		2.20		
15				30	0.1938		0	142	14.0	31.0						
							28	987	28.6	29.8	3.64	0.449		1.52		
16				60	0.1999		NG				---	---		---		
17					0.1999		0	375	14.0	31.2						
							17.1	975	29.0	30.2	1.79	0.932		3.24		

*Platinum-rhodium (Pt-Rh) wire

TABLE A-1

(Continued)

Test Number	Chamber Type ID, Inch/material	Heater	Catalyst Type	Catalyst Size, mesh	Catalyst Mass, grams	$\frac{A^*, in.^2}{D, in.}$	Time, seconds	$T_{chamber}$, F	$P_{chamber}$, psia	P_{line}, psia	$\dot{\omega}_{exp}$, sci/sec	$\frac{\dot{\omega}_I}{\dot{\omega}_E}$	τ, seconds	$M_c\left(\frac{P_c}{\dot{\omega}}\right)_{exp}$	T_{ss}/T_o	Remarks
18	0.150/SS	No	MFSA	30	0.1105	1.767 / 0.015	0	150	14.0	30.6						
							20	949	28.4	29.6	4.76	0.441		0.835		
19	0.225/SS		Shell	16	0.1802	2.433 / 0.0176	0	165	14.0	30.8						
							9	703	29.4	30.2	2.10	1.206		2.53		
20				30	0.1938		0	221	14.0	31.0						
							23.7	1097	29.6	30.0	2.13	1.040		2.70		
21				60	0.1999		0	391	14.0	31.0						
							19.3	1030	29.6	30.0	2.08	1.084		2.85		
22			MFSA	30	0.1105		0	205	14.0	31.0						
							27.2	1017	29.6	30.0	2.04	1.106		1.60		
23			Shell	16	0.3612		0	142	14.0	31.0						
							30	725	26.0	29.0	Leak	--		--		
24			MFSA	16	0.0848		0	189	14.0	31.2						
							34.6	928	29.0	30.0	2.09	1.079		1.18		
25				16	0.0848		0	157	14.0	32.0						
							21.5	996	29.8	30.8	2.06	0.814		1.22		
26				16	0.0848		0	173	14.0	31.8						
							23.2	729	29.8	30.6	2.31	1.09		1.09		
27			Shell	30	0.1938		0	173	14.0	31.8						
							23.3	945	29.8	31.0	2.15	1.072		2.69		
28			MFSA	30	0.1105		0	181	14.0	31.8						
							21.3	987	29.8	31.0	2.14	1.061		1.54		
29			Shell	60	0.1999		0	173	14.0	31.8						
							23.0	992	29.6	31.0	2.09	1.070		2.83		
30				16	0.1802		0	173	14.0	31.7						
							23.5	852	29.6	30.8	2.25	1.064		2.37		
31	0.150/SS			30	0.1938	1.767 / 0.015	0	173	13.7	30.2						
							24.0	801	30.1	29.0	3.19	0.549		1.83		Error in pressure readings
32			MFSA	16	0.0848		0	173	13.7	30.4						
							21.0	630	30.5	28.6	3.58	0.510		0.72		Error in pressure readings

TABLE A-1

(Continued)

Test Number	Chamber Type ID, inch/material	Heater	Catalyst Type	Catalyst Size, mesh	Catalyst Mass, grams	$\frac{A^*, in.^2}{D_2, in.}$	Time, seconds	$T_{chamber}$, F	$P_{chamber}$, psia	P_{line}, psia	$\dot{\omega}_{exp}$, sci/sec	$\frac{\dot{\omega}_I}{\dot{\omega}_E}$	τ, seconds	$M_c\left(\frac{P_c}{\dot{\omega}}\right)_{exp}$	T_{ss}/T_o	Remarks
33	0.150/SS	No	Shell	16	0.1802	1.767 / 0.015	0	173	13.7	30.2						Error in pressure readings
							27.6	825	30.6	29.0	3.08	0.524		1.79		
34			MFSA	30	0.1105		0	173	13.7	30.2						
							21.0	772	30.9	29.0	2.26	1.778		1.51		
35			Shell	60	0.1999		0	173	13.7	30.0						
							24.7	987	30.1	29.0	1.88	0.856		3.20		
36			MFSA	30	0.0368		0	197	13.7	30.2						
							22.4	928	30.9	28.8	1.97	0.859		0.58		
37			MFSA	16	0.0447		0	181	13.7	30.2						
							21.5	890	31.1	29.0	2.13	0.993		0.65		
38			Shell	30	0.0648		0	173	13.7	30.0						
							21.3	1004	31.1	29.0	2.04	0.791		0.99		
39			Shell	16	0.0701		0	181	14.1	30.2						
							24.0	708	31.1	28.8	2.12	0.838		1.03		
40			Shell	16	0.0370*		0	120	13.7	30.9						
							22.2	111	28.9	29.3	3.24	0.789		0.320		No ignition
41			Shell	30	0.0302		0	341	13.7	30.7						
							23.5	852	29.5	29.3	2.46	0.724		0.362		
42			MFSA	16	0.0217*		0	181	13.7	30.7						
							21.5	384	29.7	29.5	1.82	1.225		0.354		
43				30	0.0133		0.	236	13.7	29.9						
							24.1	725	29.7	29.5	1.67	1.129		0.237		
44	0.10/LAV				0.0246	2.270 / 0.017	0	~150	~0	--						
							5	873	30.5	31.1						Extrapolation to
							30	941	30.6	31.2	3.53	0.861	~0.87	0.213		time = 0
45					0.0246		0	~150	~0	--						
							30	911	18.6	19.3	2.00	0.699	~1.48	0.229		
46					0.0112		0	~153	~0	--						
							30	780	19.1	19.4	1.91	0.794	~1.00	0.112		

*Catalyst dried with GN_2 at 1000 F for 1 hour

TABLE A-1

(Continued)

Test Number	Chamber Type ID, inch/material	Heater	Catalyst Type	Catalyst Size, mesh	Catalyst Mass, grams	$\frac{A^*, in.^2}{D, in.}$	Time, seconds	$T_{chamber}$, F	$P_{chamber}$, psia	P_{line}, psia	$\dot{\omega}_{exp}$, sci/sec	$\frac{\dot{\omega}_I}{\dot{\omega}_E}$	τ, seconds	$M_c\left(\frac{P_c}{\dot{\omega}}\right)_{exp}$	T_{ss}/T_o	Remarks
47	0.10/LAV	No	MFSA	30	0.0112	$\frac{2.270}{0.017}$	0	~150	~0	--						Extrapolation to time = 0
							30	835	30.6	31.0	3.00	0.792	~0.72	0.114		
48					0.0112		0	171	0	17.5						
							5	774	15.8	16.7						
							30	844	16.0	16.7	1.54	0.807	0.97	0.116		
49					0.0112		0	241	0.4	31.9						
							5	840	30.2	31.1						
							30	899	30.6	31.3	2.09	0.993	0.71	0.164		
50					0.0475		0	232	13.6	32.0						Catalyst not in proper position
							5	482	30.6	31.2						
							30	613	30.6	31.1	2.52	---	4.015	0.527		
51					0.0475		0	---	13.6	---						Catalyst stuck in throat
							5	298	18.7	19.0						
							30	366	18.6	18.9	0.41	*		2.16		
52			Shell		0.0448		0	---	13.6	---						No temperature data at time = 0
							5	596	16.3	16.7		*				
							30	720	16.3	16.7	0.93	1.44	---	0.785		
53					0.0448		0	249	13.6	32.0						
							5	932	30.0	30.7						
							30	1068	30.2	30.7	2.9	0.746	1.625	0.466		
54					0.0720		0	241	13.6	32.0						
							5	720	29.9	30.8						
							30	890	30.2	30.8	2.65	0.869	2.48	0.810		
55					0.0720		0	249	13.6	18.1						
							5	447	16.6	17.1		*				
							30	587	16.7	17.1	1.00	1.45	5.7	1.20		
56			MFSA		0.0612		0	232	13.6	18.1						
							5	495	16.7	17.2		*				
							30	613	16.6	17.1	1.07	1.327	2.68	0.950		
57					0.0612		0	241	13.6	32.4						
							5	789	30.1	31.3						
							30	979	30.4	31.3	2.62	0.853	2.01	0.712		

*Unchoked

TABLE A-1

(Continued)

Test Number	Chamber Type ID, inch/material	Heater	Catalyst Type	Catalyst Size, mesh	Catalyst Mass, grams	$\frac{A^*, in.^2}{D, in.}$	Time, seconds	$T_{chamber}$, F	$P_{chamber}$, psia	P_{line}, psia	$\dot{\omega}_{exp}$, sci/sec	$\frac{\dot{\omega}_I}{\dot{\omega}_E}$	τ, seconds	$M_c\left(\frac{P_c}{\dot{\omega}}\right)_{exp}$	T_{ss}/T_o	Remarks
58	0.10/LAV	No	MFSA	1/16 in.	0.0449	2.270 / 0.017	0									
							30	176	30.4	31.2	3.89	---	---	0.352		No ignition
59			Shell	1/16 in.	0.0866		0									
							30	176	30.4	31.2	3.80	---	---	0.695		No ignition
60				30	0.0302	2.270 / 0.017	0	223	13.6	32.6						
							5	703	30.8	31.3						
							30	793	31.1	31.4	3.16	0.780	1.26	0.297	---	
61					0.0302		0	223	13.6	17.9						
							5	647	16.8	17.1						
							30	729	16.8	17.1	1.13	*	1.79	0.449	---	
62	0.15/SS (flange)	Yes	MFSA		0.0214	3.906 / 0.0233	0	141	0	17.0						
							5	695	16.0	17.2						
							30	916	16.2	17.2	2.36	0.891	4.19	0.147	0.436	(See p. 37)
63		Yes					0	469	0	18.0						
							5	975	15.8	16.8						No flow measurement
							30	1068	16,0	16.8						
64							0	478	0	18.0						
							5	975	15.8	16.6						
		**					30	1068	16.0	16.8	2.16	0.909	1.83	0.159	0.612	
65		Yes					0	557	0.6	31.2						
							5	907	28.4	29.6						
							30	916	28.6	29.6	4.02	0.921	1.39	0.152	0.739	
66							0	210	0	31.2						
							5	754	28.2	29.6						
							30	840	28.2	29.4	3.72	1.006	1.25	0.162	0.515	
67							0	486	0	31.0						
							5	924	28.2	29.4						
							30	941	28.6	29.6	3.65	1.006	0.99	0.168	0.675	
68							0	780	0.8	31.0						
							3	1186	28.2	29.6						
							30	1254	28.6	29.6	3.33	1.034	0.99	0.184	0.723	
69							0	814	1.4	17.6						
							5	1220	17.2	17.6						
							30	1314	17.4	17.6	1.76	1.128	2.09	0.212	0.719	

*Unchoked
**Heater rewound

TABLE A-1

(Concluded)

Test Number	Chamber Type ID, inch/material	Heater	Catalyst Type	Catalyst Size, mesh	Catalyst Mass, grams	$\frac{A^*, in.^2}{D, in.}$	Time, seconds	$T_{chamber}$, F	$P_{chamber}$, psia	P_{line}, psia	$\dot{\omega}_{exp}$, sci/sec	$\frac{\dot{\omega}_I}{\dot{\omega}_E}$	τ, seconds	$M_c\left(\frac{P_c}{\dot{\omega}}\right)_{exp}$	T_{ss}/T_o	Remarks
70	0.15/SS (flange)	Yes	MFSA	30	0.0214	3.906 / 0.0223	0	966	1.8	18.8						
							3	1271	17.2	17.2						
							30	1375	17.6	17.2	1.70	1.162	1.08	0.222	0.778	
71						3.926 / 0.0223	0	949	2.4	31.0	~0.1					
							3	1314	29.4	29.6	---					
							30	1357	29.8	29.6	3.21	1.047	0.91	0.197	0.775	
72	0.15/SS (tube inlet)	Yes (0 watts)	Shell		0.053	2.217 / 0.0168	0	184	0.8	31.6	~0.1					
							30	712	30.0	29.6	2.21	1.110	>5.0	0.720	---	
73		Yes (0.98 watts)					0	609	2.0	31.6	~0.1					
							30	797	30.2	29.4	1.98	1.206	>5.0	0.810	---	
74		Yes (4.67 watts)					0	1093	2.4	31.6	~0.1					
							30	1059	30.4	29.4	1.8	1.209	>5.0	0.895	---	
75		Yes (10.9 watts)					0	1594	2.4	31.0	~0.1					
							5	1621	30.0	29.6	1.61	1.145	0.42	0.985	---	
76		Yes (10.9 watts)					0	1567	2.8	31.8	~0.1					
							4	1594	30.0	29.4	1.61	1.148	0.31	0.985	---	
77		Yes (10.9 watts)					0	1585	2.8	17.6	~0.1					
							30	1567	16.2	15.0	0.78	1.288	>5.0	1.10	---	
78		Yes (4.67 watts)					0	1084	3.0	18.0	~0.1					
							30	1160	16.0	14.8	0.88	1.260	>5.0	0.965	---	
79		Yes (1.20 watts)					0	600	2.8	18.0	~0.1					
							23.9 (end)	857	16.0	14.8	0.88	1.450	>5.0	0.965	---	
80		Yes (1.20 watts)					0	617	2.8	18.0	~0.1					
							30	865	16.0	14.8	0.87	1.516	>5.0	0.968	---	
81		Yes (0 watts)					0	353	2.4	17.6	~0.1					
							30	712	16.0	14.8	1.02	1.282	>5.0	0.830		

TABLE A-2

TASK IV TEST SUMMARY OF STEADY-STATE TEST RESULTS

Test Number	P_{line}, psia	$P_{venturi}$, psia	P_c, psia	T_c, F	$\dot{\nu}_a$ (rotameter), sci/sec	$\dot{\nu}_v = f(P_v)$, sci/sec	$\tau_{thermal}$	P_v/P_c	T_{ss}	Comments
Engine I (A_o = 2.01 x 10^{-4} in.^{2})										GN_2
26	24.5	24.3*	18.6	77	1.82	1.92*				
27	34.4	31.8*	24.3	77	2.67	2.50*				Possible chamber leakage
29	24.5	24.3	18.6*	77	1.82	1.92				
30	34.4	34.1	26.1*	77	2.64	2.69				
Engine II (A_o = 2.20 x 10^{-4} in.^{2})										GN_2
78	23.9	23.4	--	77	1.74	1.86				
79	33.8	33.3	--	77	2.52	2.65				
80	48.4	47.9	--	77	3.57	3.81				
Engine II (A_o = 2.20 x 10^{-4} in.^{2})										Tridyne
57	23.8	23.1	20.0*		1.32	1.84	2.94	1.15*	955	Venturi unchoked
58	33.5	33.1	30.5*		2.01	2.64	2.07	1.09*	987	↓
59	48.1	47.7	43.2*		2.85	3.80	1.46	1.11*	991	↓
60	48.1	47.6	43.1*		2.82	3.79	1.46	1.10*	1012	↓
108	37.3	37.5	-- *		--	2.98	1.74	-- *	1289	Venturi unchoked, insulated chamber
109	38.2	37.9	-- *		2.35	3.02	1.85	-- *	1021	↓
110	38.2	37.5	-- *		2.35	2.98	1.74	-- *	1027	↓

Av = 1.535 x 10^{-4} in.^{2}

Tridyne: $P_c = \dot{\omega} r \sqrt{T_o}/0.518\ A_o$

*Values calculated from theoretical equations and measured parameters

APPENDIX B

DISTRIBUTION LIST

	Copies
NASA Pasadena Office 4800 Oak Grove Drive Pasadena, California 91103 Attn: Patents and Contracts Management	1
Jet Propulsion Laboratory 4800 Oak Grove Dr. Pasadena, California 91103 Attn: Philip I. Moynihan	10
Chief, Liquid Propulsion Technology RPL or Chief, Liquid Experimental Engineering, RPX Office of Advanced Research and Technology NASA Headquarters Washington, D. C. 20546	3
Director, Technology Utilization Division Office of Technology Utilization NASA Headquarters Washington, D.C. 20546	1
NASA Scientific and Technical Information Facility P.O. Box 33 College Park, Maryland 20740	10
Director, Launch Vehicles and Propulsion Office of Space Science and Applications NASA Headquarters Washington, D.C. 20546	1
Director, Advanced Manned Misions Office of Manned Space Flight NASA Headquarters Washington, D.C. 20546	1
Mission Analysis Division NASA AMES Research Center Moffett Field, California 24035	1

	Copies
Ames Research Center Moffett Field, California 94035 Attn: Hans M. Mark	2
Goddard Space Flight Center Greenbelt, Maryland 20771 Attn: Merland L. Moseson Code 620 Attn: Dr. R. E. Hunter Code 734	2
Jet Propulsion Laboratory California Institute of Technology 4800 Oak Grove Drive Pasadena, California 91103 Attn: Henry Burlage, Jr. Propulsion Div. 38	2
Langley Research Center Langley Station Hampton, Virginia 23365 Attn: Ed Cortwright, Director	2
Lewis Research Center 21000 Brookpark Road Cleveland, Ohio 44135 Attn: Dr. Abe Silverstein, Director	2
Marshall Space Flight Center Huntsville, Alabama 35812 Attn: Hans G. Paul Code R-P+VED	2
Manned Spacecraft Center Houston, Texas 77001 Attn: J. G. Thibodaux, Jr., Chief Propulsion Power Division	2
John F. Kennedy Space Center, NASA Cocoa Beach, Florida 32931 Attn: Dr. Kurt H. Debus	2
Aeronautical Systems Division Air Force Systems Command Wright-Patterson Air Force Base Dayton, Ohio 45433 Attn: D. L. Schmidt Code ASRCNC-2	1

	Copies
Air Force Missile Development Center Holloman Air Force Base, New Mexico 88330 Attn: Major R. F. Bracken	1
Air Force Missile Test Center Patrick Air Force Base, Florida Attn: L. J. Ullian	1
Space and Missile Systems Organization Air Force Unit Post Office Los Angeles, California 90045 Attn: Col. Clark, Technical Data Center	1
Arnold Engineering Development Center Arnold Air Force Station Tullahoma, Tennessee 37388 Attn: Dr. H. K. Doetsch	1
Bureau of Naval Weapons Department of the Navy Washington, D.C. 20546 Attn: J. Kay RTMS-41	1
Defense Documentation Center Headquarters Cameron Station, Building 5 5010 Duke Street Alexandria, Virginia 22314 Attn: TISIA	1
Headquarters USAF (AFRDDG) Pentagon Washington, D.C. 20330	1
Picatinny Arsenal Dover, New Jersey 07801 Attn: I. Forsten, Chief Liquid Propulsion Laboratory	1
Air Force Rocket Propulsion Laboratory Research and Technology Division Air Force Systems Command Edwards, California 93523 Attn: RPRPD/Mr. H. Main	2

	Copies
U.S. Army Missile Command Redstone Arsenal Alabama 35809 Attn: Walter Wharton	1
U.S. Naval Ordnance Test Station China Lake California 93557 Attn: Chief, Missile Propulsion Division Code 4562	1
Chemical Propulsion Information Agency Applied Physics Laboratory 8621 Georgia Avenue Silver Spring, Maryland 20910 Attn: Tom Reedy	1
Aerojet-General Corporation P.O. Box 296 Azusa, California 91703 Attn: W. L. Rogers	1
Aerojet-General Corporation P.O. Box 1947 Technical Library, Bldg. 2015, Dept. 2410 Sacramento, California 95809 Attn: R. Stiff	1
Space Division Aerojet-General Corporation 9200 East Flair Dr. El Monte, California 91734 Attn: S. Machlawski	1
Aerospace Corporation 2400 East El Segundo Boulevard P.O. Box 95085 Los Angeles, California 90045 Attn: John G. Wilder MS-2293	1
Astrosystems International, Inc. 1275 Bloomfield Avenue Fairfield, New Jersey 07007 Attn: A. Mendenhall	1
Atlantic Research Corporation Edsall Road and Shirley Highway Alexandria, Virginia 22314 Attn: Dr. Ray Friedman	1

	Copies
AVCO Systems Division Wilmington, Massachusetts Attn: Howard B. Winkler	1
Beech Aircraft Corporation Boulder Division Box 631 Boulder, Colorado Attn: J. H. Rodgers	1
Bell Aerosystems Company P.O. Box 1 Buffalo, New York 14240 Attn: W. M. Smith	1
BELLCOMM 955 L-Enfant Plaza, S.W. Washington, D.C. Attn: H. S. London	1
Bendix Systems Division Bendix Corporation 3300 Plymouth Road Ann Arbor, Michigan 48105 Attn: John M. Brueger	1
Boeing Company P.O. Box 3707 Seattle, Washington 98124 Attn: J. D. Alexander	1
Boeing Company 1625 K Street, N.W. Washington, D.C. 20006 Attn: Library	1
Boeing Company P.O. Box 1680 Huntsville, Alabama 35801 Attn: Ted Snow	1
Missile Division Chrysler Corporation P.O. Box 2628 Detroit, Michigan 48231 Attn: John Gates	1
Wright Aeronautical Division Curtiss-Wright Corporation Woodridge, New Jersey 07075 Attn: G. Kelley	1

	Copies
Research Center Fairchild-Hiller Corporation Germantown, Maryland Attn: Ralph Hall	1
Republic Aviation Corporation Fairchild-Hiller Corporation Farmingdale, Long Island, New York Attn: Library	1
General Dynamics, Convair Division Library and Information Services (128-00) P.O. Box 1128 Los Angels, California 90005 Attn: Frank Dore	1
Missile and Space Systems Center General Electric Company Valley Forge Space Technology Center P.O. Box 8555 Philadelphia, Pa. Attn: F. Mezger F. E. Schultz	1
Grumman Aircraft Engineering Corp. Bethpage, Long Island, New York 11714 Attn: Joseph Gavin	1
Honeywell, Inc. Aerospace Div. 2600 Ridgway Rd Minneapolis, Minn. Attn: Mr. Gordon Harms	1
Hughes Aircraft Co. Aerospace Group Centinela and Teale Streets Culver City, California 90230 Attn: E. H. Meier Vice President and Division Manager R&D Division	1
Walter Kidde and Company, Inc. Aerospace Operations 567 Main Street Belleville, New Jersey Attn: R. J. Hanville Dir. of Research Engr.	1

	Copies
Ling-Temco-Vought Corporation P.O. Box 5907 Dallas, Texas 75222 Attn: Warren G. Trent	1
Arthur D. Little, Inc. 20 Acorn Park Cambridge, Massachusetts 02140 Attn: Library	1
Lockheed Missiles and Space Co. Attn: J. Guill Technical Information Center Sunnyvale, California 94088	1
Lockheed Propulsion Company P.O. Box 111 Redlands, California 92374	1
The Marquardt Corporation Attn: R. C. Allen 16555 Saticoy Street Van Nuys, California 91409	1
Baltimore Division Martin Marietta Corporation Baltimore, Maryland 21203 Attn: J. Calathes (3214)	1
Denver Division Martin Marietta Corporation P. O. Box 179 Denver, Colorado 80201 Attn: Dr. Morganthaler A. J. Kullas	1
Orlando Division Martin Marietta Corporation Box 5837 Orlando, Florida Attn: J. Ferm	1
Astropower Laboratory McDonnell-Douglas Aircraft Company 2121 Paularino Newport Beach, California 92663 Attn: Dr. George Moc Director, Research	1

	Copies
McDonnell-Douglas Aircraft Corporation P.O. Box 516 Municipal Airport St. Louis, Missouri 63166 Attn: R. A. Herzmark	1
Missile and Space Systems Division McDonnell-Douglas Aircraft Company 3000 Ocean Park Boulevard Santa Monica, California 90406 Attn: R. W. Hallet, Chief Engineer Adv. Space Tech.	1
Space Systems Division North American Rockwell 12214 Lakewood Boulevard Downey, California 90241 Attn: Library	1
Rocketdyne ((Library 055-306) 6633 Canoga Avenue Canoga Park, California 91304 Attn: Dr. R. J. Thompson S. F. Iacobellis	1
Northrop Space Laboratories 3401 West Broadway Hawthorne, California 90250 Attn: Dr. W. Howard	1
Aeronutronic Division Philco Corporation Ford Road Newport Beach, California 92663 Attn: D. A. Garrison	1
Astro-Electronics Division Radio Corporation of America Princeton, New Jersey 08540 Attn: Y. Brill	1
Rocket Research Corporation 520 South Portland Street Seattle, Washington 98108 Attn: F. McCullough, Jr.	1

	Copies
Sunstrand Aviation 2421 11th Street Rockford, Illinois 61101 Attn: R. W. Reynolds	1
Stanford Research Institute 333 Ravenswood Avenue Menlo Park, California 94025 Attn: Dr. Gerald Marksman	1
TRW Systems Group TRW Incorporated One Space Park Redondo Beach, California 90278 Attn: G. W. Elverum	1
TAPCO Division TRW, Incorporated 23555 Euclid Avenue Cleveland, Ohio 44117 Attn: P. T. Angell	1
Reaction Motors Division Thiokol Chemical Corporation Denville, New Jersey 07832 Attn: Dwight Smith	1
Thiokol Chemical Corporation Huntsville Division Huntsville, Alabama 35807 Attn: John Goodloe	1
Research Laboratories United Aircraft Corporation 400 Main Street East Hartford, Conn. 06108 Attn: E. Martin	1
Hamilton Standard Division United Aircraft Corporation Windsor Locks, Conn. 06096 Attn: R. Hatch	1
United Technology Center 587 Methilda Avenue P.O. Box 358 Sunnyvale, California 94088 Attn: Dr. David Altman	1

	Copies
Florida Research and Development Pratt and Whitney Aircraft United Aircraft Corporation P.O. Box 2691 West Palm Beach, Florida 33402 Attn: R. J. Coar	1
Naval Research Laboratory Washington, D.C. Attn: P. Beal	1

UNCLASSIFIED

Security Classification

DOCUMENT CONTROL DATA - R & D

(Security classification of title, body of abstract and indexing annotation must be entered when the overall report is classified)

1. ORIGINATING ACTIVITY (Corporate author) Rocketdyne, a Division of North American Rockwell Corporation, 6633 Canoga Avenue, Canoga Park, California 91304	2a. REPORT SECURITY CLASSIFICATION UNCLASSIFIED 2b. GROUP

3. REPORT TITLE

TRIDYNE ATTITUDE CONTROL THRUSTER INVESTIGATION, FINAL REPORT

4. DESCRIPTIVE NOTES (Type of report and inclusive dates)

Final Report

5. AUTHOR(S) (First name, middle initial, last name)

Hartley E. Barber; C. H. Buell

6. REPORT DATE 3 April 1970	7a. TOTAL NO. OF PAGES 132	7b. NO. OF REFS 0
8a. CONTRACT OR GRANT NO. NAS7-719 b. PROJECT NO. c. d.	9a. ORIGINATOR'S REPORT NUMBER(S) R-8144 9b. OTHER REPORT NO(S) (Any other numbers that may be assigned this report)	

10. DISTRIBUTION STATEMENT

11. SUPPLEMENTARY NOTES	12. SPONSORING MILITARY ACTIVITY

13. ABSTRACT

The results of an experimental program to evaluate and demonstrate the feasibility of a Tridyne attitude control thruster are reported. Substantiating data are presented for catalyst selection and optimization. Criteria for the design of a Tridyne attitude control module with preconditioning heaters are described. The design, fabrication, and testing of a flightweight thruster is detailed.

DD FORM 1 NOV 65 1473

UNCLASSIFIED

Security Classification

14. KEY WORDS	LINK A		LINK B		LINK C	
	ROLE	WT	ROLE	WT	ROLE	WT
Tridyne						
Thrust Chamber Assembly						
Performance Analysis						
Thermal Analysis						
Venturi						
Catalyst Bed						
MFSA						
Shell-405						